Circularly polarized dual frequency feed stacked microstrip antenna for mobile communications

Cleven, L.J.

Award date:
1989

Eindhoven University of Technology

Department of Electrical Engineering
Professional Group Electromagnetism and Circuit Theory

Circularly Polarized Dual Frequency Feed Stacked Microstrip Antenna for Mobile Communications

by L.J. Cleven

ET-16-89

This study fulfills the the requirements as laid down by the Eindhoven University of Technology in order to obtain the degree of Master of Science (Ir.) and has been performed under supervision of Dr. M.E.J. Jeuken in the period February 1989 until October 1989.

Eindhoven, October 1989.

Summary.

In antenna design for mobile communication, microstrip antennas are likely to become increasingly important, especially in the lower frequency bands. The antenna has to be designed for L-band usage with circular polarization of the electric field. The specifications for mobile communication in the L-band as laid down by the INMARSAT and MSATX organizations have served as guideline for the design and the review of the results obtained.
The approach chosen in this research is that of stacking two microstrip antennas and to dedicate each for a specified frequency. By feeding the upper antenna through the lower antenna, a new antenna is necessary namely the ring patch microstrip antenna. This report provides a theoretical analysis and practical study of this ring patch antenna and the whole antenna.
Theoretical results show that the bandwidth is less in comparison with a circular microstrip antenna. Consequently it is impossible to cover the entire transmit or receive bandwidth by one element. Although it is possible to cover the individual frequency bands for land-, maritime- or aeronautical mobile communications.
For practical usage however, it is necessary to broaden the bandwidth of both patches.
A striking property of this ring patch element is the possibility of improving the axial ratio by varying the design parameters.
A single element cannot meet the gain requirements demanded; hence array techniques are applied. Circular polarization is obtained by composing the array of circularly polarized or sequentially rotated linearly polarized patches. For small element spacings, the directivity of both arrays is almost equal but when the spacing increases the directivity loss of a 4 x 4 array which is composed of linearly polarized patches, can exceed 6 dB.
A new technique to shape the axial ratio of an array composed of linearly polarized elements that it will meet the MSATX requirements is introduced .
Summarizing the results it may be said that the INMARSAT specifications cannot be met however by using this last technique the MSATX requirements can be met.

Contents

1 Introduction.

As worldwide demand for communication systems increases so will the interest in mobile (satellite) communications, therefore a frequency band in the L-band (1.5 GHz - 1.6 GHz) has been allocated for mobile satellite communications.
Mobile satellite communication is a generic term embracing land mobile, maritime mobile and aeronautical mobile satellite communications.
During the World Administrative Radio Conference (WARC) on Mobile Services in 1987, a subdivision of frequency allocations for the three mobile satellite communication services was made and will come into effect in October 1989 [1-1].

The aim of this research work is to design an antenna for land mobile satellite communication. This requires the development of an antenna which has appeal to users who emphasize aesthetic appearance or prefer to be inconspicuous.
It is obvious that the use of microstrip technology [1-2] and microstrip antenna technology [1-3] has of necessity become of great importance.
In mobile satellite communication services in particular the benefit of this type antenna is obvious, due to its light weight, relatively low cost, thin planar configuration and the possibility to mount the microstrip antenna system conformal to the vehicle.
The advantage of microstrip antenna technology becomes even more evident when the frequency used is rather low. For these relatively low frequencies conventional antennas, usually horn antennas, will be bulky and cumbersome.

Microstrip antenna technology is a relatively new technology. The history of the microstrip antenna starts at the end of the 1950's, with the introduction of microstrip transmission lines.
One of the undesirable properties of these circuits was the loss due to radiation and pointed to the use of this configuration as antenna. The development of integrated microwave circuits (MIC's) added a new impulse to this.

Apart from the before mentioned advantages, previous research [1-4,1-5] reports that the bandwidth requirement for mobile satellite communication in this frequency band is difficult to meet because a microstrip antenna is a narrow band device.
This problem can be solved either by developing inherent wide band microstrip antennas like stacked microstrip antennas [1-6], by changing the form of the patch [1-7,1-8] or by composing an antenna of several microstrip antenna elements and dedicating each antenna element to a certain frequency band.
Composed antennas can either consist of concentric annular patches [1-3] or of several stacked microstrip patches. [1-9,1-10]

The objective of the investigation described in this report is to apply this last method and to develop a circular (circularly polarized) microstrip antenna system having dual frequency feed suitable for the frequencies 1.5 GHz - 1.6 GHz.
The advantage of separate receive and transmit signals is the possibility of improving the antenna G/T-ratio and the E.I.R.P. independently. [1-11]

This report is organized as follows:
In chapter 2 more background information about the communications system in general is given and specifications for the antenna to be designed are listed.
The theoretical analyses of the new patch configuration, necessary for the dual frequency feed microstrip antenna, is presented in chapter 3.
Chapter 4 deals with methods for realizing circular polarization with a single microstrip antenna. To obtain circular polarization, a feeding network is needed. In order to maintain the specific advantages of microstrip antennas, microstrip technology this network should be made by using microstrip technology.
To meet the requirements stated in chapter 2 array techniques are discussed in chapter 5.
Experimental results are discussed in chapter 6. This is done by comparing theoretical and measured data of the design based on given specifications.

1.1 References.

[1-1] Goddard M.,
'Frequency Allocations for Mobile Satellite Systems and Satellite Navigation', Proceedings of the 4 th International Conference on Satellite Systems for Mobile Communications and Navigation, October 1988, IEE Conference Publication 294, p.10-14.

[1-2] Bahl I.J. and Bhartia P.,
'Microwave Solid State Circuit Design', 1988 John Wiley and Sons Inc.

[1-3] Bahl I.J. and Bhartia P.,
'Microstripantennas', 1980 Artech House Inc.

[1-4] Vrinten M.L.A.,
'A Wide Band Circularly Polarized Microstrip Antenna Array', Graduate Report, Professional Group Electromagnetism and Circuit Theory, Department of Electrical Engineering, Eindhoven University of Technology, Netherlands, 1988, ET-4-88.

[1-5] Visser H.J.,
'Circularly Polarized Microstrip Phased Array Antennas for Mobile Communications', Graduate Report, Professional Group Electromagnetism and Circuit Theory, Department of Electrical Engineering, Eindhoven University of Technology, Netherlands, 1988, ET-3-89.

[1-6] Zwemstra T.,
'Analysis of a Dual Stacked Rectangular Microstrip Antenna', Graduate Report, Professional Group Electromagnetism and Circuit Theory, Department of Electrical Engineering, Eindhoven University of Technology, Netherlands, 1989, ET-14-89.

[1-7] Smolders A.B.,
'Analysis of Microstrip Antennas in the Spectral Domain Using a Moment Method', Graduate Report, Professional Group Electromagnetism and Circuit Theory, Department of Electrical Engineering, Eindhoven University of Technology, Netherlands, 1989, ET-15-89.

[1-8] Chung H.H., Foy W., Schaffner G., Pagels W., Vagner M., Nelson J. and Peng S.Y.,
'MSAT-X Electronically Steered Phased Array Antenna System', Proceedings of the MSAT Conference, May 1988, p. 223-228.

[1-9] Goto N. and Kaneta K.,
'Ring Patch Antennas for Dual Frequency Use', AP-S International Symposium 1987, 1987 International Symposium Digest Antennas and Propagation, Vol. II, p.944-947.

[1-10] Yasunaga M., Wanatabe F. and Yamada M.,
'Phased Array Antennas for Aeronautical Satellite Communications', Fifth International Conference on Antennas and Propagation, ICAP 87, Part I, p. 47-50.

[1-11] Komuro K.,
'Low Cost Mobile Terminals and Services', Proceedings of the International Conference on Mobile Satellite Communications, INMARSAT, July 1989, p. 207-219.

2 Specifications.

The starting points of this report are the specifications for voice and data channels as laid down by the International Maritime Satellite Organization (INMARSAT) [2-1] and for the Mobile Satellite Experiment (MSATX) [2-2].
The ultimate goal being the design of a small circularly polarized microstrip antenna element that can be used as an element of an array and that can be positioned on a car or truck. Guideline for the design are the above mentioned specifications.

First the antenna parameters are discussed and afterwards the specifications for the communication link, of which the antenna forms part. Specifications of the communication link are stated by means of a so called link budget. This is done for the INMARSAT case. [2-3]

2.1 Antenna specifications.

The antenna specifications given here are for the mobile communication system proposed by INMARSAT and MSATX.
INMARSAT proposes a system for communication between a ground station and an aircraft enlisting a transponder in a satellite (see figure 2.1, [2-4]).

The antenna must be suitable for L-band communication at frequencies between 1.5 GHz and 1.6 GHz. Another important requirement is the need for a almost nearly hemispherical coverage of the antenna beam. Necessary because communication via the satellite must be possible over a wide range of degrees of latitude.

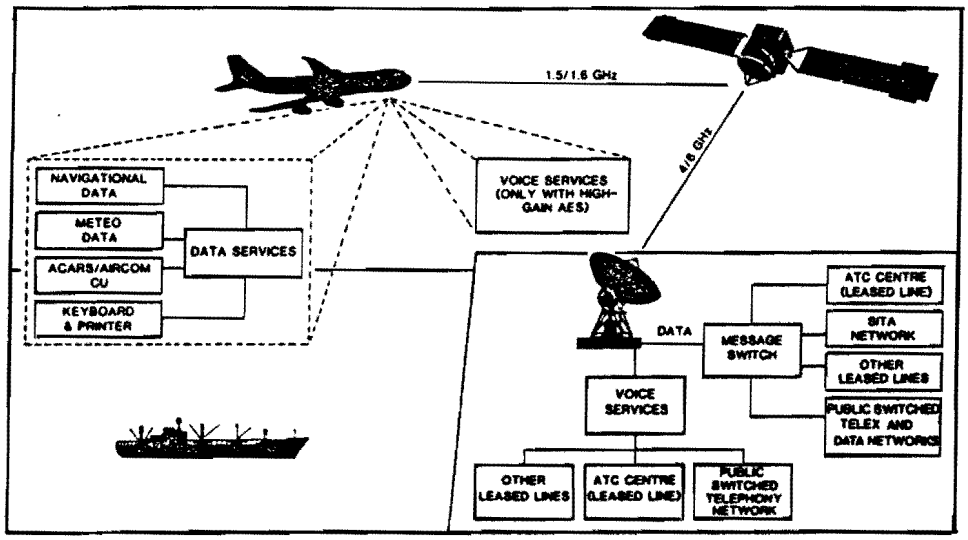

Fig 2.1 : Aeronautical satellite communications networks (INMARSAT)

Because vehicles are mobile circular polarization must be used. Looking in the direction of propagation and including the time dependence, the tip of the electric field vector traces out a circle and the polarization is called circular (CP). When the electric field vector rotates clockwise, polarization is called right hand circular (RHCP) otherwise it is called left hand circular (LHCP). In practice the wave is not perfectly circular polarized. The axial ratio (AR) indicates the maximum allowable aberration of circularity.

The antenna is fed by a transmission line, either coaxial cable or a microwave circuit. When the antenna input is not connected to a matched transmission line, reflections occur. To protect the transmitter from dissipating to much reflected power, the amplitude of the reflected wave must be limited.
The incident and reflected wave establish a standing wave.
A ratio that associates the maximum and minimum voltage of the standing wave is the voltage standing wave ratio. (VSWR)
Previous studies [2-5,2-6,2-7] show the bandwidth requirement being the most restrictive specification. One way to overcome this

bandwidth limitation is to do research into inherent wide band microstrip elements. Another possibility is to compose an antenna of several microstrip elements, each element assigned for a specified frequency.
This last point of view is the point of departure for this study and therefore a circular microstrip antenna system with dual frequency feed is chosen. Advantage of this construction is the flexibility in the system design; less complex transceiver required, ease of maintenance etc.
All the before mentioned considerations are summarized in table 2.1.

Table 2.1 : Antenna Specifications

Parameter	INMARSAT data	voice	MSATX
Frequency	1.5-1.6 GHz	1.5-1.6 GHz	1.5-1.6 GHz
Coverage			
elevation	5° - 90°	5° - 90°	20° - 60°
azimuth	360°	360°	360°
Gain			
(vehicle)	1 dB	12 dB	10 dB
Polarization	RHCP	RHCP	CP
Max. AR	2.5 dB	1 dB	4 dB
Max. VSWR	1.4	1.4	-

In figure 2.2 a detailed survey of frequencies assigned for land mobile, maritime mobile and aeronautical mobile communication is given [2-8].

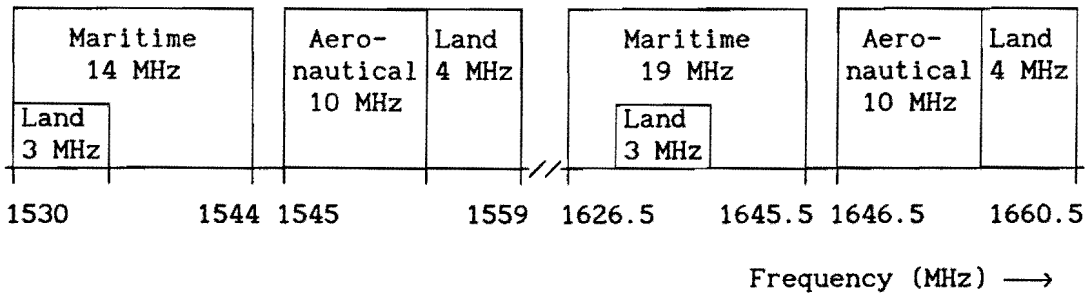

Fig. 2.2 : Mobile satellite communications frequency allocations

2.2 Link budget.

In a link budget the power balance, which describes the performance of a communication link, is given. The quality is described by the power received and is composed of the power transmitted plus all gains minus all losses. The antenna(s), phase shifters, power combiners/dividers and so on form the system, their losses lead to degradation of the antenna G/T and E.I.R.P., and form part of the link.

To give an impression, the link budgets for INMARSAT data and voice channels are stated on the next pages. [2-3]
These budgets for data and voice channels enclose the forward link, from earth station to satellite to mobile station (in this example an aircraft) and return link (from mobile station to satellite and back to earth station).
A few terms of these link budgets need some explanation; GES stands for Ground Earth Station and AES stands for Aircraft Earth Station.
It is simple to check these link budgets. General information about link budget calculations can be found in [2-9].

Table 2.1 : Link Budget for 600 bit/s Data Channels

Satellite MCS	Forward Link	Return Link
Link Requirement:		
Required C/N_0 (dBHz)	33.7	35.7
Uplink:		
	(GES to Satellite)	(AES to Satellite)
Frequency (GHz)	6.42	1.64
Elevation (deg)	5	5
EIRP (dBW)	62.0	13.5
Path Loss (dB)	201.3	189.4
G/T (dBK)	-14.0	-13.0
Uplink C/N_0 (dBHz)	75.3	39.7
Satellite:		
Satellite C/IM_0 (dBHz)	67.8	43.8
Downlink:		
	(Satellite to AES)	(Satellite to GES)
Frequency (GHz)	1.54	4.2
Elevation (deg)	20	5
EIRP (dBW)	22.4	-25.0
Path Loss (dB)	188.2	197.6
G/T (dBK)	-26.0	32.0
Downlink C/N_0 (dBHz)	36.8	38.0
Link Performance:		
Achieved C/N_0 (dBHz)	36.8	35.1
Margin (dB)	3.1	-0.4

Table 2.2 : Link Budget for 21000 bit/s Voice Channels

Satellite MCS	Forward Link	Return Link
Link Requirement:		
Required C/N_0 (dBHz)	47.9	47.9
Uplink:		
	(GES to Satellite)	(AES to Satellite)
Frequency (GHz)	6.42	1.64
Elevation (deg)	5	5
EIRP (dBW)	62.0	25.5
Path Loss (dB)	201.3	189.4
G/T (dBK)	-14.0	-13.0
Uplink C/N_0 (dBHz)	75.3	51.7
Satellite:		
Satellite C/IM_0 (dBHz)	67.8	55.0
Downlink:		
	(Satellite to AES)	(Satellite to GES)
Frequency (GHz)	1.54	4.2
Elevation (deg)	5	5
EIRP (dBW)	22.0	-13.0
Path Loss (dB)	188.9	197.6
G/T (dBK)	-13.0	32.0
Downlink C/N_0 (dBHz)	48.7	50.0
Link Performance:		
Achieved C/N_0 (dBHz)	48.6	47.0
Margin (dB)	0.7	-0.9

2.3 References.

[2-1] INMARSAT,
'Request for Proposals Number 085, Aircraft Earth Stations, 9 May 1986.

[2-2] Huang J.,
'L-Band Phased Array Antennas for Mobile Satellite Communications', IEEE 37 th Vehicular Technology Conference, Tampa (Fl), June 1987, p. 113-117.

[2-3] Wood P.,
'INMARSAT's Aeronautical Satellite Communication System', Proceedings of the 4 th International Conference on Satellite Systems for Mobile Communications and Navigation, October 1988, IEE Conference Publication 294, p. 78-82.

[2-4] Mimis V.,
'INMARSAT's Future Aeronautical Satellite Communications System', Tydschrift van het Nederlands Elektronica- en Radiogenootschap, deel 51, nr. 4, p.127-131.

[2-5] Vrinten M.L.A.,
'A Wide band Circularly Polarized Microstrip Antenna Array', Master's Thesis, Professional Group Electromagnetism and Circuit Theory, Department of Electrical Engineering, Eindhoven University of Technology, Netherlands, 1988, ET-4-88.

[2-6] Visser H.J.,
'Circularly Polarized Microstrip Phased Array Antennas for Mobile Communications', Master's Thesis, Professional Group Electromagnetism and Circuit Theory, Department of Electrical Engineering, Eindhoven University of Technology, Netherlands, 1989, ET-3-89.

[2-7] Toom E.C. den,
'Microstripantenne voor de mobiele satelliet communicatie', Master's Thesis, Professional Group Electromagnetism and Circuit Theory ,Department of Electrical Engineering, Eindhoven University of Technology, Netherlands 1989, ET-8-89. (in Dutch)

[2-8] Goddard M.,
'Frequency Allocations for Mobile Satellite Systems and Satellite Navigation', Proceedings of the 4th International Conference on Satellite Systems for Mobile Communications and Navigation, October 1988, IEE Conference Publication 294, p. 10-14.

[2-9] Dalgleish D.I.,
'An Introduction to Satellite Communications', p. 93-135, Peter Peregrinus Ltd. ,1989.

3 The circular ring patch antenna.

The idea behind stacked (microstrip) antennas is to dedicate one antenna for transmitting and the other for receiving. The use of microstrip antenna technology is advantageous because of its relatively small dimensions thickness and agility. Thus the height of the stacked antenna can still be small.

The stacked microstrip antenna studied in this report is composed of two microstrip antennas: a circular microstrip antenna and a circular ring patch antenna; placing the circular microstrip upon the circular ring patch antenna, as shown in fig. 3.1. The circular antenna geometry comprises a thin, conducting circular patch on a dielectric substrate backed by a thin, conducting ground plane. Circular microstrip antennas have been studied extensively [3-1,3-2]

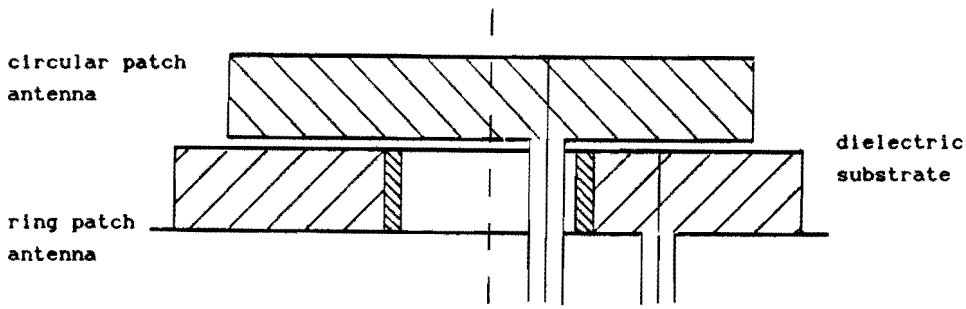

Fig. 3.1 : Stacked microstrip antenna

Circular ring patch antennas do have the same construction as a circular microstrip antenna except for the annular patch and the conducting ring between the annular conducting patch and the ground plane. This ring is placed in the centre of the annular patch and connects the patch and ground plane electrically.
An illustration and cross-section of a circular ring patch are given in fig. 3.2.

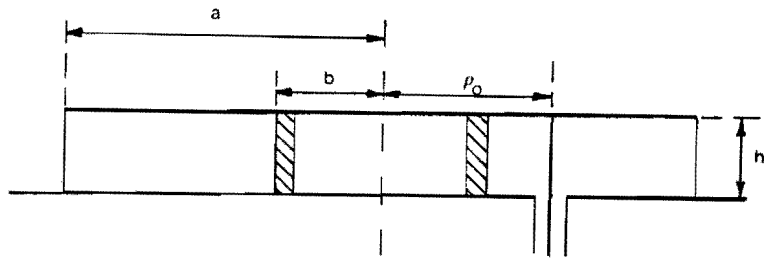

Fig. 3.2 : Circular ring patch microstrip antenna

Circular ring patch microstrip antennas have been reported recently. [3-3,3-4]

3.1 Choice of model.

Various models for the analyses of microstrip disk antennas are described in the literature. The cavity model is the least complex method and is expected to be accurate enough for predicting resonant frequency, radiation characteristics, input impedance etc. of circular shaped microstrip antennas. In this report, analyses of the circular ring patch microstrip antenna is based on the cavity model.

3.2 Fields in the circular ring patch microstrip antenna.

The cavity model's starting point is the assumption of a perfectly conducting annular patch, ring and ground plane. Because of the physical edge of the patch, the current normal to the edge must approach zero at the edge. These two starting points lead to the following boundary conditions for the circular ring patch antenna:

$$\bar{n} \times \bar{E} = \bar{0} \qquad \text{at : } \rho = b \text{ and } 0 \le z \le h$$
$$z = 0 \text{ and } b \le \rho \le a$$
$$z = h \text{ and } b \le \rho \le a \qquad (3.1)$$

$$\bar{n} \times \bar{H} = \bar{0} \qquad \text{at : } \rho = a \text{ and } 0 \le z \le h \qquad (3.2)$$

$\bar{n}$ is the unity vector normal to the surface considered.

Furthermore it is assumed that the thickness of the dielectric substrate (h) is small compared to the wavelength ($h \ll \lambda_o$). Working out eq. 3.1 and using the assumption just made shows that the electric field within the dielectric substrate, the cavity, has a z-component (E_z) only. By applying Maxwell's equations we show that the components of the magnetic field are H_ϕ and H_ρ.
The first result leads to the conclusion that only TM-modes appear in the the cavity while eq. 3.2 leads to the conclusion that $H_\phi(\rho=a)=0$.

Summarizing: the microstrip disk antenna can be modeled as an annular cavity, bounded by its top, ring and bottom by electric walls and on its perimeter by a magnetic wall.

Because of the flatness of the microstrip antenna ($h \ll \lambda_o$), the fields in the cavity do not vary along the z-direction.
So:

$$\frac{\partial}{\partial z}\left(\text{fields} \right) = 0 \qquad (3.3)$$

To obtain the internal fields, the cavity problem must be solved.
The wave equation for a cavity with no current sources is [Appendix A]:

$$\nabla^2 \bar{E} + k^2 \bar{E} = \bar{0} \qquad (3.4)$$

with : $k = \omega \sqrt{\varepsilon\mu}$
The general solution of the wave equation is:

$$E_z(\rho,\phi) = \left[A \cos(\nu\phi) + B \sin(\nu\phi) \right] \cdot \left[C\, J_\nu(k\rho) + D\, Y_\nu(k\rho) \right] \qquad (3.5)$$

Where $J_\nu(X)$ and $Y_\nu(X)$ are Bessel functions of the first and second kind and order ν. [3-5]
The magnetic field components can be found from:

$$\nabla \times \bar{E} = - j\omega\mu \bar{H} \qquad (3.6)$$

Which gives:

$$H_\rho = \frac{j}{\omega \mu \rho} \frac{\partial E_z}{\partial \phi} \tag{3.7}$$

$$H_\phi = - \frac{j}{\omega \mu} \frac{\partial E_z}{\partial \rho} \tag{3.8}$$

$$E_\phi = E_\rho = H_z = 0 \tag{3.9}$$

The fields must satisfy this wave equation and the boundary conditions. Applying these boundary conditions (eq. 3.1 and 3.2) gives the following result [Appendix A]:

$$E_z(\rho,\phi) = E_o \left[J_n(k\rho) - \frac{J_n(kb)}{Y_n(kb)} Y_n(k\rho) \right] \cos(n\phi) \tag{3.10}$$

And the magnetic fields become:

$$H_\rho(\rho,\phi) = - \frac{j\, n\, E_o}{\omega \mu \rho} \left[J_n(k\rho) - \frac{J_n(kb)}{Y_n(kb)} Y_n(k\rho) \right] \sin(n\phi) \tag{3.11}$$

$$H_\phi(\rho,\phi) = - \frac{j\, k}{\omega \mu} E_o \left[J_n'(k\rho) - \frac{J_n(kb)}{Y_n(kb)} Y_n'(k\rho) \right] \cos(n\phi) \tag{3.12}$$

3.3 Resonance frequency.

The magnetic fields inside the cavity give rise to induced electric currents. These currents flow in the top plate, ring and ground plane.

Surface currents on the patch can be determined from:

$$\begin{aligned} \bar{I} &= \bar{n} \times \bar{H} \\ &= - \hat{e}_z \times \bar{H} \\ &= H_\phi \hat{e}_\rho - H_\rho \hat{e}_\phi \end{aligned} \tag{3.13}$$

The currents on the ground plane are 180° out of phase with the currents on the patch because $\bar{H}$ is independent of z and the currents on the ground plane can be derived from :

$$\bar{I} = \bar{n} \times \bar{H}$$
$$= \hat{e}_z \times \bar{H} \qquad (3.14)$$

At the edge of the patch, the radial component of the surface current vanishes.
This implies:

$$K_\rho(\rho=a) = H_\phi(\rho=a) = 0 \qquad (3.15)$$

Therefore, with the preceding equation and eq. 3.12:

$$J_n'(k\rho) - \frac{J_n(kb)}{Y_n(kb)} Y_n'(k\rho) \Big|_{\rho=a} = 0 \qquad (3.16)$$

or with $\chi_{nm} = ka$ and $\beta = \frac{b}{a}$:

$$J_n'(\chi_{nm}) - \frac{J_n(\beta\chi_{nm})}{Y_n(\beta\chi_{nm})} Y_n'(\chi_{nm}) = 0 \qquad (3.17)$$

This equation has only discrete solutions, resonance will occur for frequencies (k) that match this condition. Therefore this equation is called the resonant condition.

For numerical calculations [3-6] it is better to write this equation as:

$$Y_n(\beta\chi_{nm})\, J_n'(\chi_{nm}) - J_n(\beta\chi_{nm})\, Y_n'(\chi_{nm}) = 0 \qquad (3.18)$$

to avoid singularities.
The resonant frequency of a patch antenna for the TM_{nm} mode can be evaluated from:

$$\chi_{nm} = ka = \frac{2\,\pi\, f_r \sqrt{\varepsilon_r}}{c_o}\, a \qquad (3.19)$$

Where χ_{nm} is the m-th zero of the resonant condition (eq. 3.17) and n is the order of the Besselfunctions. So the roots χ_{nm} of the resonant condition and β determine the inner and outer radius of circular ring patch microstrip antenna.
For some modes, a graph is plotted of χ_{nm} vs β.

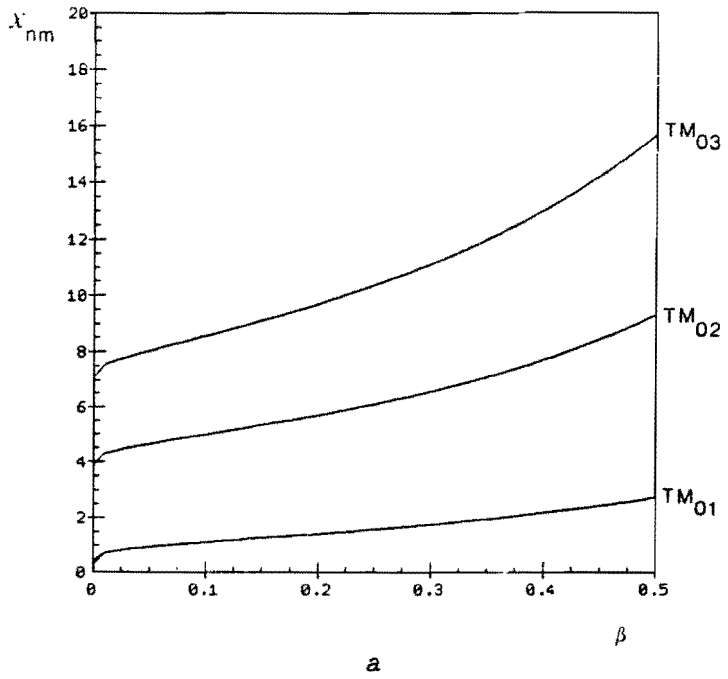

a

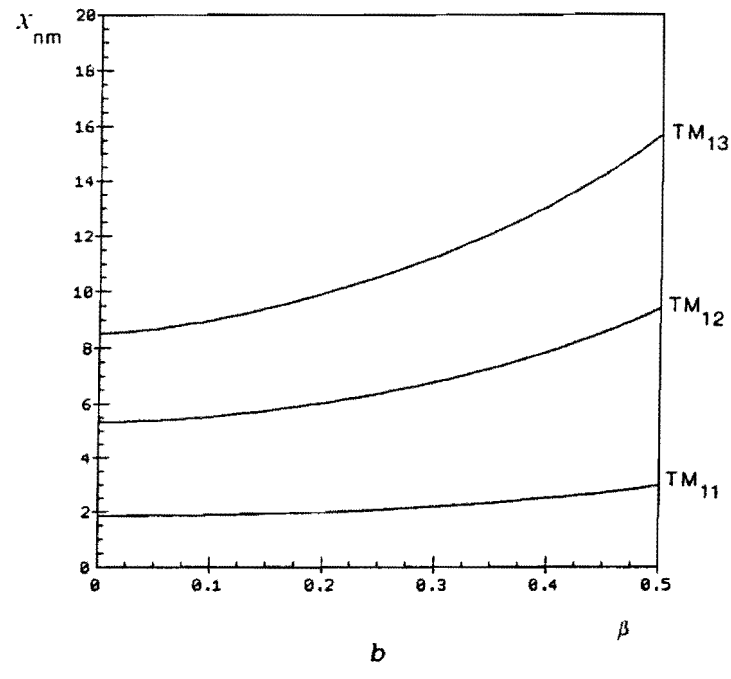

b

Fig. 3.3 : Roots of resonance condition χ_{nm} as function of β for a TM_{nm}-mode.

a) n=0 , m=1,2,3

b) n=1 , m=1,2,3

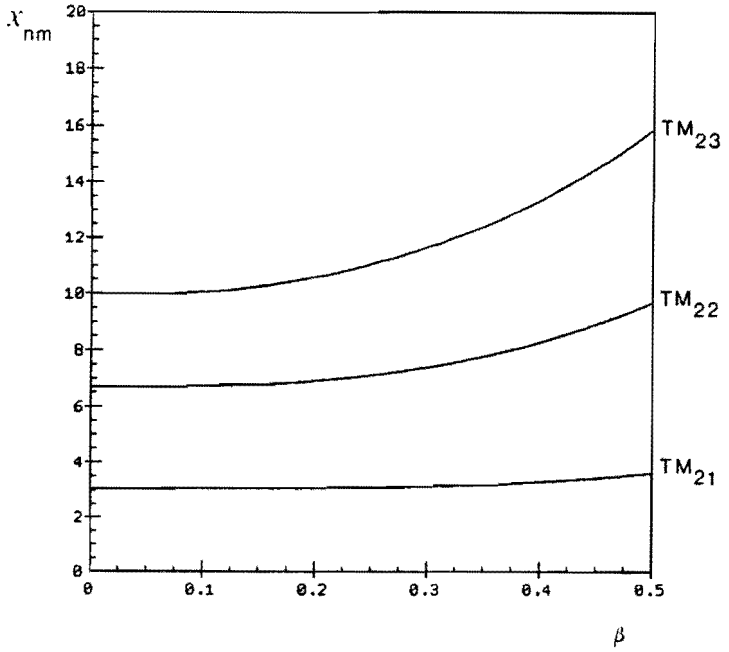

c

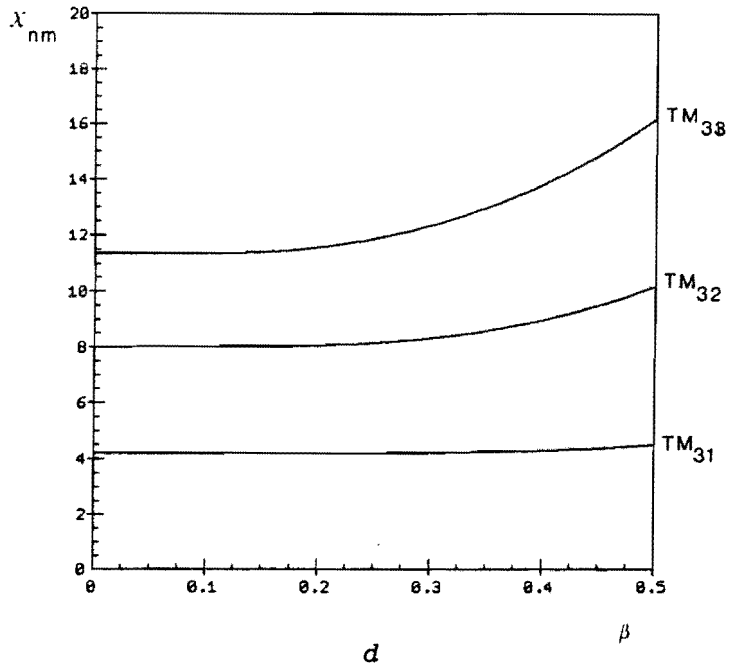

d

Fig. 3.3 : Roots of resonance condition χ_{nm} as function of β for

a TM_{nm}-mode

c) n=2 , m=1,2,3

d) n=3 , m=1,2,3

For a circular patch (β=0) the dominant mode is the TM_{11}-mode, the TM_{01}-mode (f=0, D.C. solution) left out of consideration.
However for $\beta \neq 0$, the solution of the resonant condition χ_{01} is smaller than χ_{11}. Notice that the curve for χ_{11} in fig. 3.3 b) is above the curve for χ_{01} (fig. 3.3 a)).
As a result, the TM_{01}-mode has, for $\beta \neq 0$, a lower cut of frequency and is thus now is the dominant mode.

Therefore not only the roots of the resonant condition can be calculated but also the currents on the patches can be calculated. Some current patterns on the top plate for various modes are shown in the figures below.

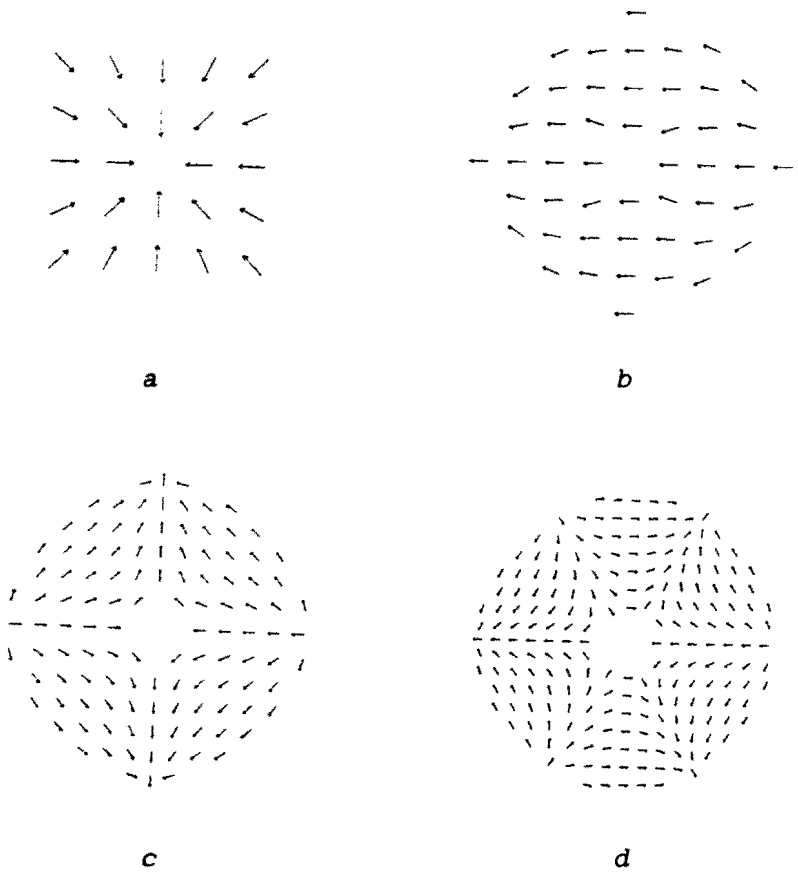

Fig. 3.4 : Currents on patch for TM_{nm}-modes: n=0 , n=1 , n=2 , n=3
β=0.2 , ε_r=2.2 , m=1
a) n=0 b) n=1 c) n=2 d) n=3

In the cavity model the absence of fringe fields along the edge of the resonator is assumed. In reality the (electric) fields extend outside the cavity and the physical radius a must be corrected for this effect.

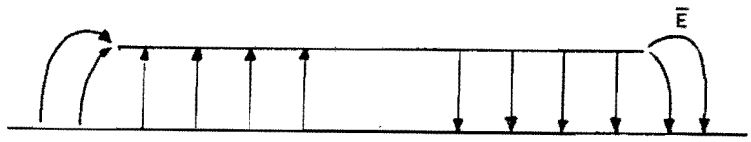

Fig. 3.5 : Fringe fields along edge of patch

This results in an effective radius a_e being introduced.
The resonant frequency can now be calculated from:

$$f_r = \frac{c_o \chi_{nm}}{2 \pi a_e \sqrt{\varepsilon_r}} \qquad (3.20)$$

And the relation between the physical radius (a) and the effective radius (a_e) is given by:

$$a_e = a \sqrt{1 + \frac{2h}{\pi a \varepsilon_r} \left[\ln\left(\frac{\pi a}{2h}\right) + 1.7726 \right]} \qquad (3.21)$$

In mobile satellite communication systems, the main beam is steerable. Therefore so called phased arrays are applied. In that case grating lobes should be avoided. To avoid grating lobes, the spacing between array elements has to be less than a wavelength. This condition implies that the radius of the antenna should be small.

In figure 3.6 the radius a is given as a function of β and f_r for various substrates.

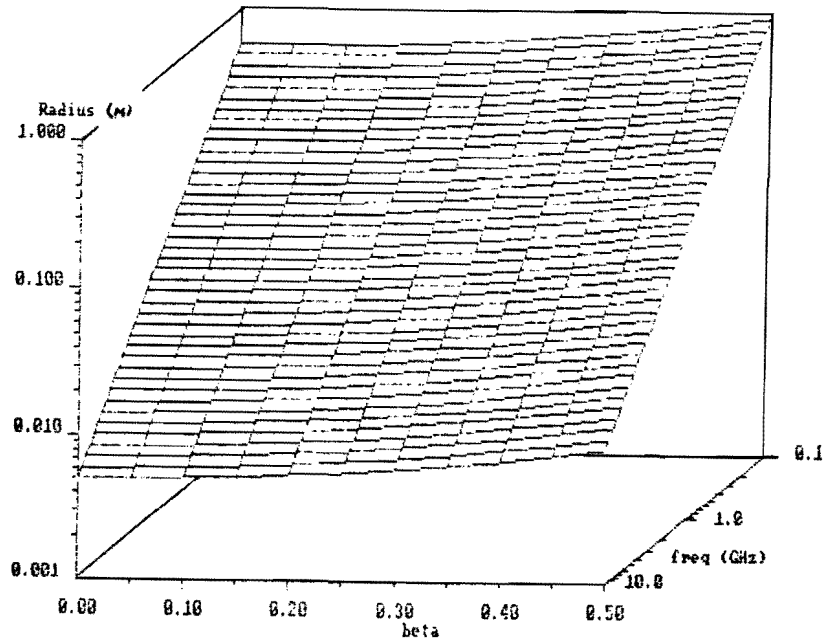

a

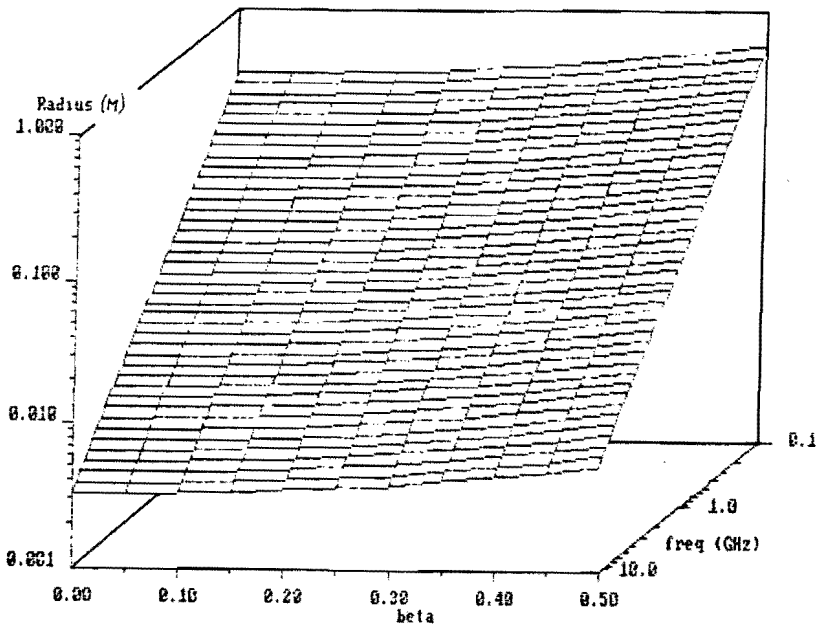

b

Fig. 3.6 : Calculated radius a (m) vs resonant frequency and β

a) ε_r*=2.2 , h=1.57 mm , tan(δ)=0.0009*

b) ε_r*=6.0 , h=1.91 mm , tan(δ)=0.0027*

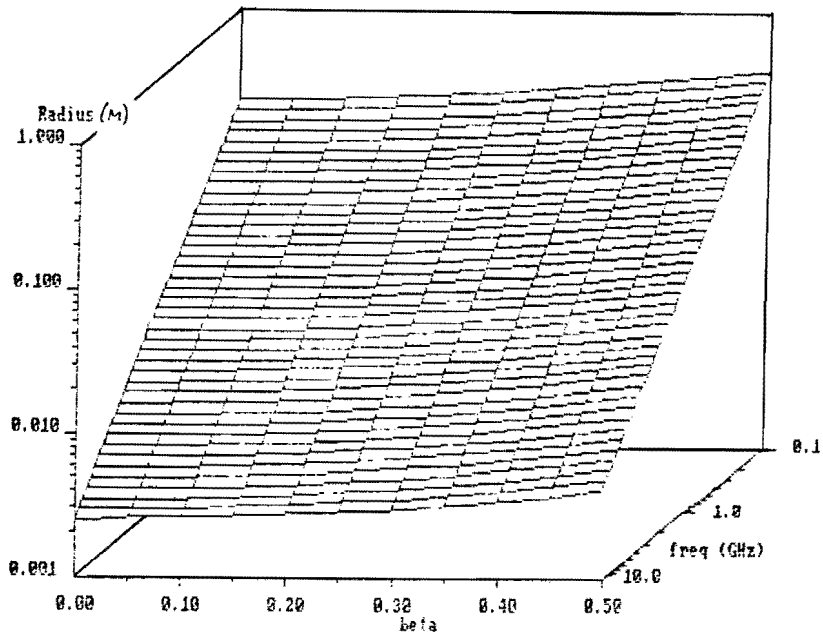

c

Fig. 3.6 : Calculated radius a (m) vs resonant frequency and β
c) ε_r=10.5 , h=1.91 mm , tan(δ)=0.0028

3.4 Far fields.

Far fields of the circular ring patch microstrip antenna are calculated from potential functions [3-7]. Either the field between the patch and ground plane at ρ=a (vector electric potentials) or the currents in the patch conductor, induced by the magnetic fields in the cavity, are used (vector magnetic potentials).
In this report, the vector electric potentials are employed. So the electric field inside the cavity is converted into an equivalent magnetic current on the side wall. Due to the infinitely large conducting ground plane, the source can be replaced by an equivalent magnetic current that is doubled. (Image theory) Hence the radiation mechanism in the upper half space of the microstrip antenna can be supposed as being caused by an equivalent magnetic current on the side wall:

$$\begin{aligned}\bar{M} &= 2\,\bar{E} \times \bar{n} \\ &= 2\,\bar{E} \times \hat{e}_{\rho} \\ &= 2\,E_z\,\hat{e}_{\phi}\end{aligned} \tag{3.22}$$

With this current, the vector electric potential can be determined:

$$\bar{A}_m(\bar{r}) = \frac{\varepsilon_o}{4\,\pi} \iiint_{V'} \bar{M}(\bar{r}') \; \frac{\exp\,(jk\,|\bar{r} - \bar{r}'|)}{|\bar{r} - \bar{r}'|}\; dV' \tag{3.23}$$

Where V' is the aperture of the magnetic current.

The far fields $\bar{E}$ and $\bar{H}$ can be calculated from:

$$\bar{E} = -\,\frac{1}{\varepsilon_o}\,\nabla \times \bar{A}_m \tag{3.24}$$

$$\bar{H} = \frac{1}{j\,\omega\,\varepsilon_o\,\mu_o}\,\nabla \times \nabla \times \bar{A}_m \tag{3.25}$$

The calculations of the far field are worked out in detail in appendix B, the results are (in spherical coordinates):

$$E_{\phi} = j^n\,\frac{e^{-jk_o r}}{2\,r}\,E_o\,a\,h\,k_o\,\cos(\vartheta)\,\sin(n\phi)$$

$$\left(\,J_n(ka) - \alpha\,Y_n(ka)\,\right)\cdot\left(\,J_{n-1}(X) + J_{n+1}(X)\,\right) \tag{3.26}$$

$$E_{\vartheta} = -\,j^n\,\frac{e^{-jk_o r}}{2\,r}\,E_0\,a\,h\,k_o\,\cos(n\phi)$$

$$\left(\,J_n(ka) - \alpha\,Y_n(ka)\,\right)\cdot\left(\,J_{n-1}(X) - J_{n+1}(X)\,\right) \tag{3.27}$$

And:

$$\alpha = \frac{J_n(kb)}{Y_n(kb)} \tag{3.28}$$

As mentioned before, these equations are only valid in the upper half space ($0 \leq \vartheta \leq \pi/2$). In the lower half space all field components are theoretically zero because of the infinitely large ground plane.

With this information the radiation characteristics of the antenna can be calculated. The power density in a given direction is defined as the power radiated from an antenna per unit solid angle. The power radiated is given by [3-8]

$$P(\vartheta,\phi) = \left| r^2 \, \bar{S}(\bar{r}) \right|$$

$$= \left| r^2 \, \frac{1}{2} \, Re \left(\bar{E} \times \bar{H}^* \right) \right|$$

$$= \frac{r^2}{2 Z_o} \left(|E_\vartheta|^2 + |E_\phi|^2 \right) \qquad (3.29)$$

Substituting eq. 3.26 and 3.27 in eq. 3.29 , the radiation patterns can be calculated. The radiation patterns for the TM_{01}, TM_{11}, TM_{21} and TM_{31} mode are shown in fig. 3.7.

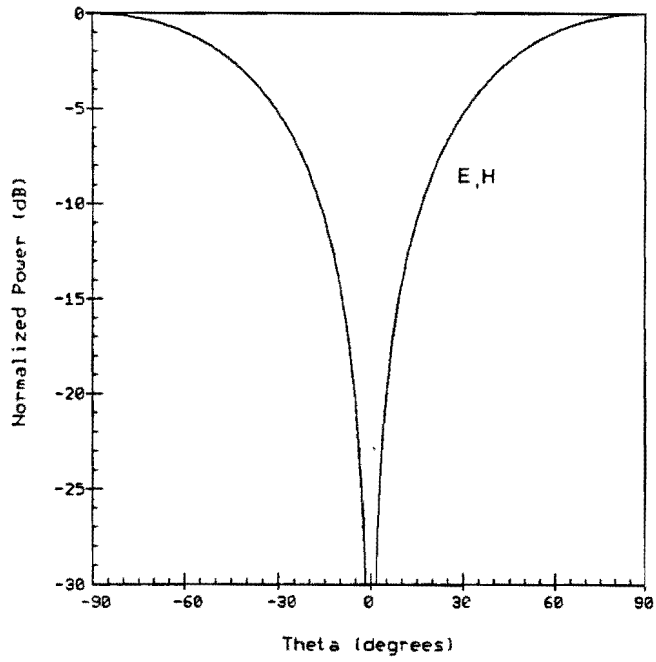

a : N = 0

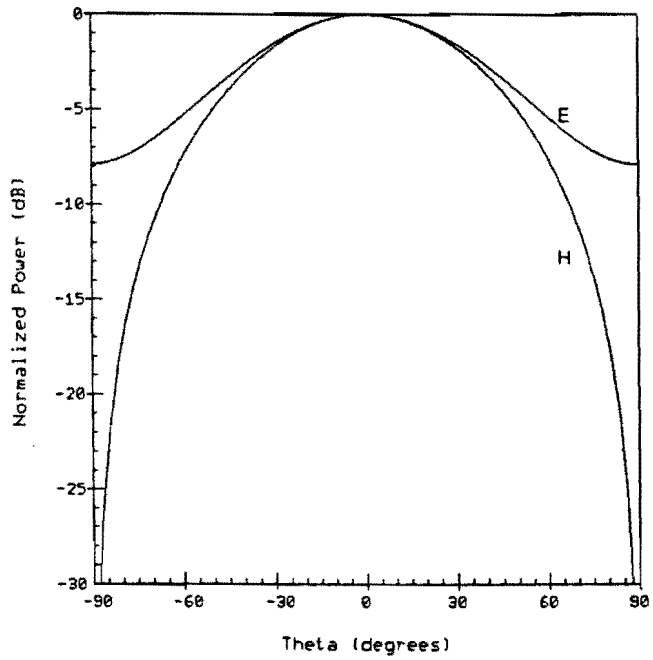

b : N = 1

Fig. 3.7 : Radiation pattern calculated in E-plane (ϕ=0°) and H-plane (ϕ=90°), β=0.2 , fr=1.6 GHz , ε_r=2.2

a) TM_{01}-mode

b) TM_{11}-mode

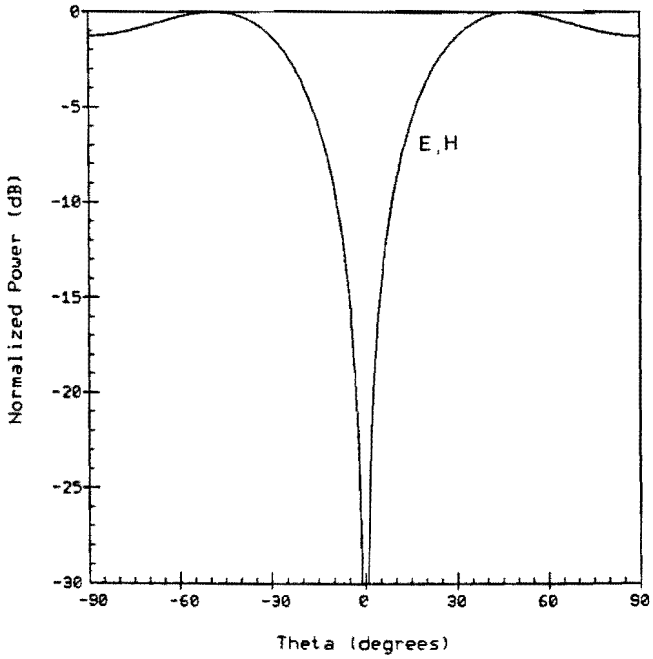

c: N = 2

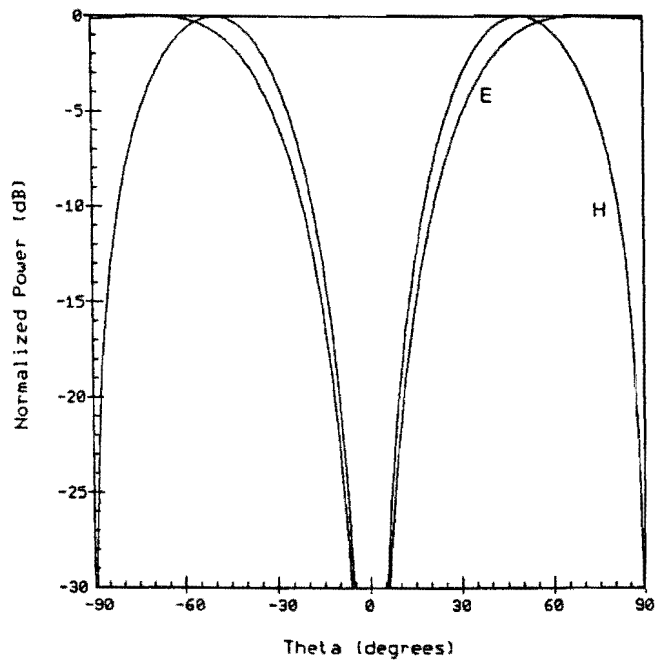

d : N = 3

Fig. 3.7 : Radiation pattern calculated in E-plane (ϕ=0°) and H-plane (ϕ=90°), β=0.2 , fr=1.6 GHz , ε =2.2

c) TM_{21}-mode

d) TM_{31}-mode

For n even the radiation characteristics are the same in E- and H-plane , and different in E- and H-plane for n odd.
These graphs show that the TM_{01} mode has a minimum in the radiation pattern broadside to the antenna ($\vartheta=0^{\circ}$). As a result of this minimum and the necessity of beam steering, the TM_{01} mode is not useful. The first mode that is suitable is the TM_{11} mode.
Henceforth the mode considered is the TM_{11} mode unless otherwise specified.

3.5 Losses in microstrip antennas.

The total power loss in a microstrip antenna is composed of four parts. The energy supplied to the microstrip antenna is either radiated as microwaves or converted in heat. Radiated power is divided into radiation, which is desired, and surface waves which are not. These surface waves give rise to end fire radiation which propagates into the substrate outside the microstrip patch.

Characteristic for surface waves is the attenuation in the transverse direction (normal to the antenna plane) and the real wave number in the direction of propagation [3-1]. In Collin's book [3-7] the solutions for these surface waves are investigated. The cut off frequencies for the surface modes are given by:

$$f_c = \frac{n\, c_o}{4\, h\, \sqrt{\varepsilon_r - 1}} \qquad (3.30)$$

For TE_n modes n = 1,3,5,... and for TM_n modes n = 2,4,6,... .
It should be noticed that the lowest order surface wave is a TM-mode with n=2. When the substrate is thin in comparison with the wavelength in vacuum ($h \ll \lambda_o$), the power transformed in surface waves is negligible.

Radiated power

By employing Poynting's theorem, the total power radiated can be calculated, namely:

$$P_r = \frac{1}{2}\frac{1}{2} \; Re \int\int_S \left(\bar{E} \times \bar{H}^* \right) \cdot \bar{n} \; dS \qquad (3.31)$$

Because the power is radiated through the upper half space only, the extra factor 1/2 is added. The surface S is a spherical surface at infinity and $\bar{n}$ is the vector normal to this surface.
After some mathematical calculations, the power radiated is:

$$P_r = \frac{\pi}{16\, Z_o} \left(ahk_o E_o \left[J_n(ka) - \alpha\, Y_n(ka) \right] \right)^2$$

$$\int_0^{\pi} \sin(\vartheta) \left(\left[J_{n+1}(k_o a \sin(\vartheta)) - J_{n-1}(k_o a \sin(\vartheta)) \right]^2 + \right.$$

$$\left. \cos^2(\vartheta) \left[J_{n+1}(k_o a \sin(\vartheta)) + J_{n-1}(k_o a \sin(\vartheta)) \right]^2 \right) d\vartheta \qquad (3.32)$$

For this last integral no analytical solution is known and this integral has to be calculated numerically. In appendix C eq. 3.32 is derived.

The remaining losses are the losses in the conductors and the dielectric substrate.

Losses in the conductor

Losses in the conductors are caused by the finite conductivity of the patch. If the surface resistivy of the conductors is R_s, the losses in the patch and ground plane can be calculated from:

$$P_c = 2\, \frac{R_s}{2} \int\int_S |\bar{I}|^2 \, dS \qquad (3.33)$$

Where S stands for the patch area and $\bar{I}$ is the induced surface current on the patch; $\bar{I} = \bar{n} \times \bar{H}$.

R_s is given by:

$$R_s = \sqrt{\frac{\pi \mu f}{\sigma}} \tag{3.34}$$

With σ the conductivity of the metallization.

So P_c becomes:

$$P_c = 2 \frac{R_s}{2} \iint_S \left(|K_\rho|^2 + |K_\phi|^2 \right) dS \tag{3.35}$$

Working out these integrals shows that [see appendix D]:

$$P_c = \frac{1}{8\sqrt{\pi \sigma \mu_o^3 f^3}} \left[\left(2 k a J_n'(ka) \left(-J_n(ka) + \alpha Y_n(ka) \right) + \left((k a)^2 - n^2 \right) \left(J_n(ka) - \alpha Y_n(ka) \right)^2 \right) - \left(2 k b J_n(kb) \left(J_n'(kb) - \alpha Y_n'(kb) \right) + (k b)^2 \left(J_n'(kb) - \alpha Y_n'(kb) \right)^2 \right) \right] \tag{3.36}$$

with:

$$\alpha = \frac{J_n(kb)}{Y_n(kb)} \tag{3.37}$$

Losses in the dielectric

The dielectric loss can be determined by integrating the electric field within the cavity over the volume V of the cavity.

$$P_d = \frac{\omega \varepsilon''}{2} \iiint_V |E|^2 \, dV \tag{3.38}$$

Where ε'' is the imaginary component of the permittivity ε.

$$P_d = \frac{\omega\, \varepsilon_o \varepsilon_r\, \tan(\delta)}{2} \int_0^h \int_b^a \int_0^{2\pi} |E|^2\, \rho\, d\rho\, d\phi\, dz$$

$$P_d = \frac{h\, \tan(\delta)}{8\, f\, \mu_o}$$

$$\left[\left(\left((ka)^2 - n^2 \right) \left(J_n(ka) - \alpha\, Y_n(ka) \right)^2 \right) - \left((kb)^2 \left(J_n'(kb) - \alpha\, Y_n'(kb) \right)^2 \right) \right] \qquad (3.39)$$

With:

$$\alpha = \frac{J_n(kb)}{Y_n(kb)} \qquad (3.40)$$

See appendix E for explanation of this result.

The next step is to carry out calculations concerning efficiency. Define the radiation efficiency as :

$$\eta_r = \frac{P_r}{P_T} \qquad (3.41)$$

Analogous, the conductivity efficiency (η_c) and dielectric efficiency (η_d) can be defined. Note there is a contradiction between radiation efficiency and conductivity and dielectric efficiency. Unlike radiation efficiency, which should approach 1, the conductivity and dielectric efficiency should approach 0. Some results are given in fig. 3.8.

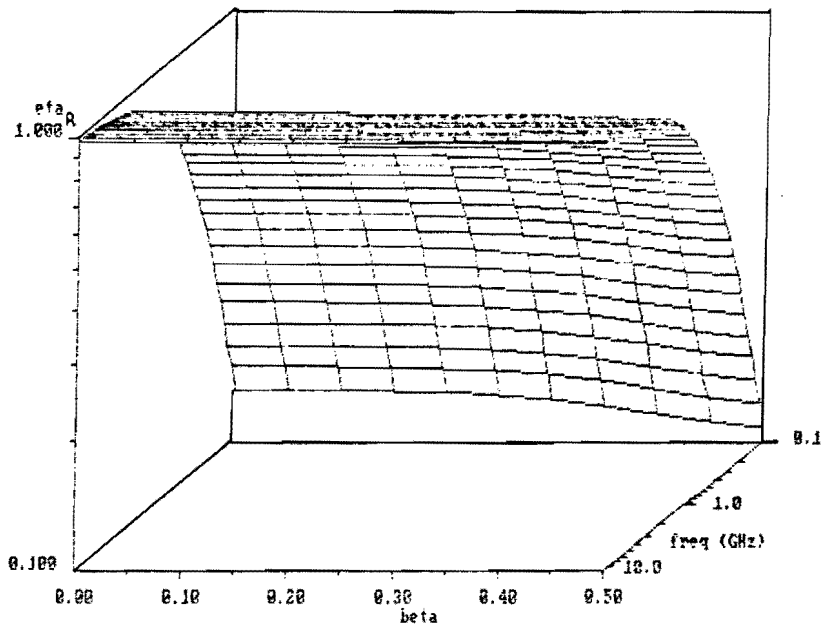

a

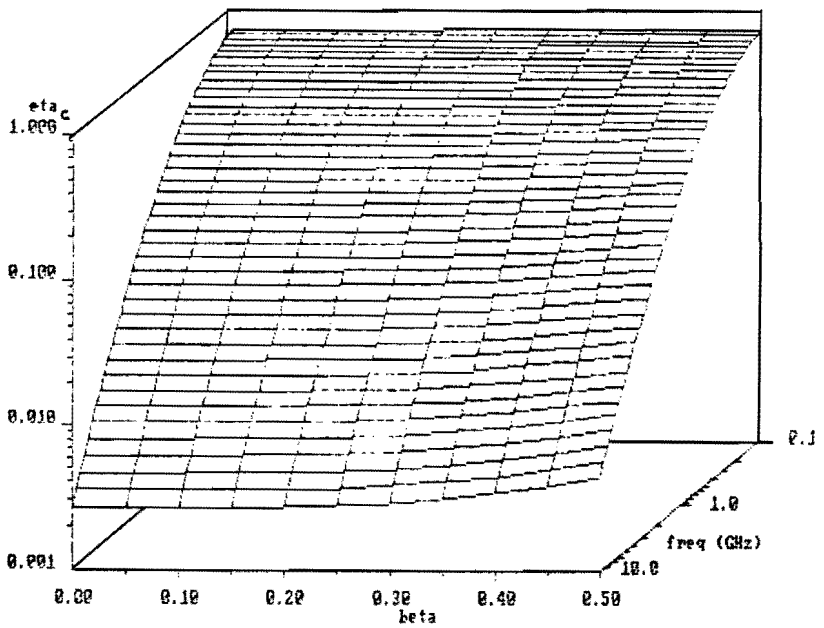

b

Fig. 3.8 : Radiation efficiency, dielectric and conductor efficiency vs frequency vs β

ε_r=2.2 , h=1.57 mm , tan(δ)=0.0009

a) radiation efficiency

b) conductitivity efficiency

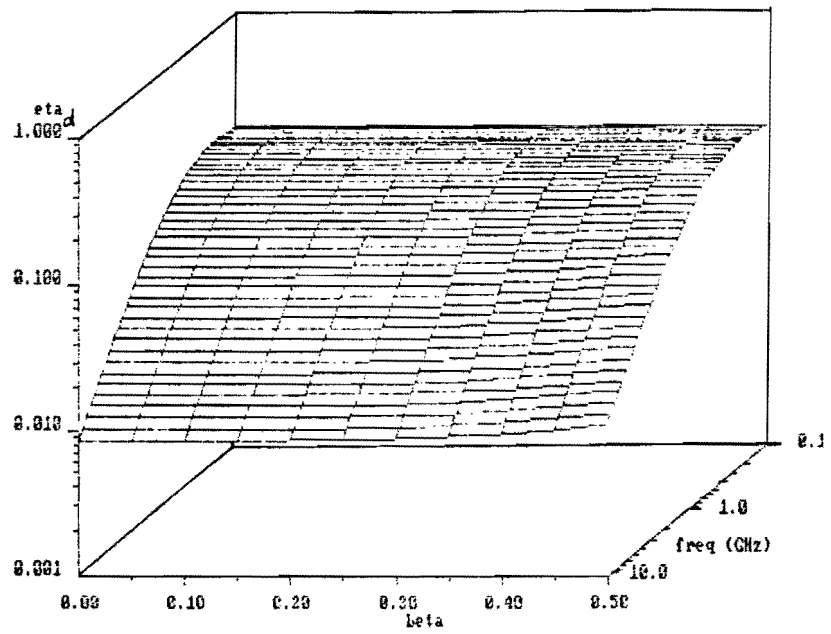

c

Fig. 3.8 : Radiation efficiency, dielectric and conductor efficiency vs frequency vs β
ε_r=2.2 , h=1.57 mm , tan(δ)=0.0009
c) dielectric efficiency

Graphs calculated show that radiation efficiency increases with increasing frequency and that the conductor and dielectric losses decrease with increasing frequency.

3.6 Input impedance.

Feed point location

Since all (microstrip) antennas have to be matched in respect of the feed, the input impedance calculation is particularly important.

Generally the input impedance can be written as:

$$Z_{in} = R_{in} + j X_{in} \qquad (3.42)$$

At resonance the input impedance of a microstrip antenna is real. The resonant resistance R can be calculated from the total power lost in the cavity P_T, using:

$$Z_{in} = R_{in} = R = \frac{V^2}{2\,P_T} \qquad (3.43)$$

And: $P_T = P_r + P_c + P_d$

If the patch is fed at an arbitrary point $(\rho_o, 0)$, the input voltage is :

$$V = \int E_z \, dh$$

$$= E_z(\rho_o, 0)\, h$$

$$= h\, E_o \left[J_n(k\rho_o) - \frac{J_n(kb)}{Y_n(kb)}\, Y_n(k\rho_o) \right] \qquad (3.44)$$

It is now possible to calculate the resonant resistance as function of the feed point location ρ_o , and find the position where the input impedance of the microstrip antenna matches the impedance of the feed.

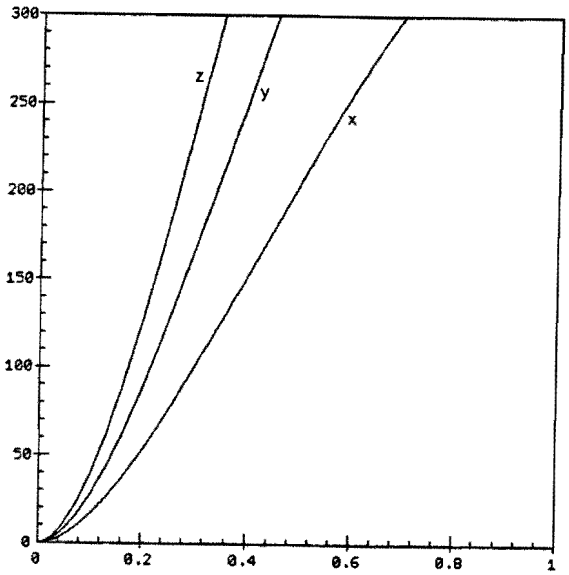

Fig 3.9 : R_{in} (Ω) as function of $(\rho_o - b)/(a-b)$
a: h=1.91 mm , tan(δ)=0.0009 , β=0.2 ,fr=1.6GHz
x: ε_r=2.2 , y: ε_r=6.0 , z: ε_r=10.5

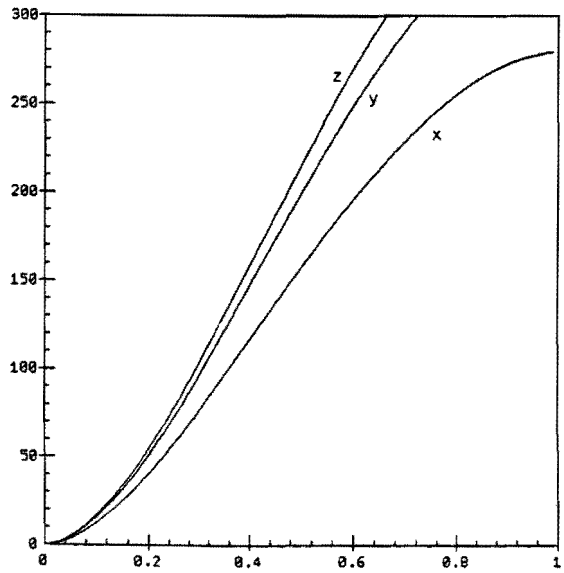

b

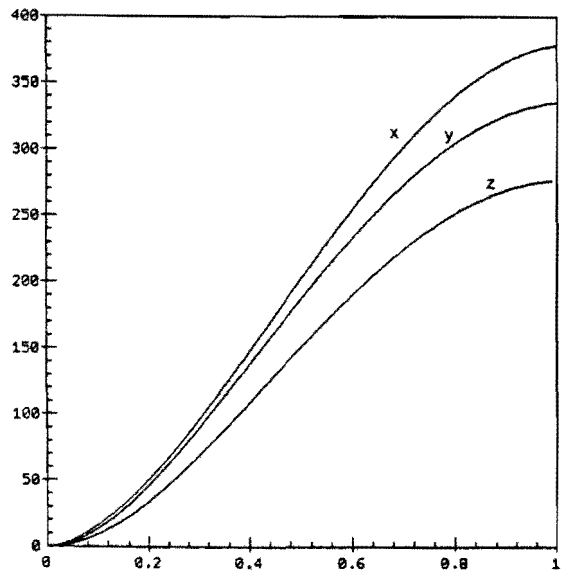

c

Fig. 3.9 : R_{in} (Ω) as function of $(\rho_o - b)/(a-b)$

b: ε_r=2.2 , tan(δ)=0.0009 , β=0.2 , fr=1.6 GHz

x: h=0.79 mm , y: h=1.57 mm , z: h=3.18 mm

c: ε =2.2 , h=1.57 , tan(δ)=0.0009 , fr=1.6 GHz

x: β=0.1 , y: β=0.3 , z: β=0.5

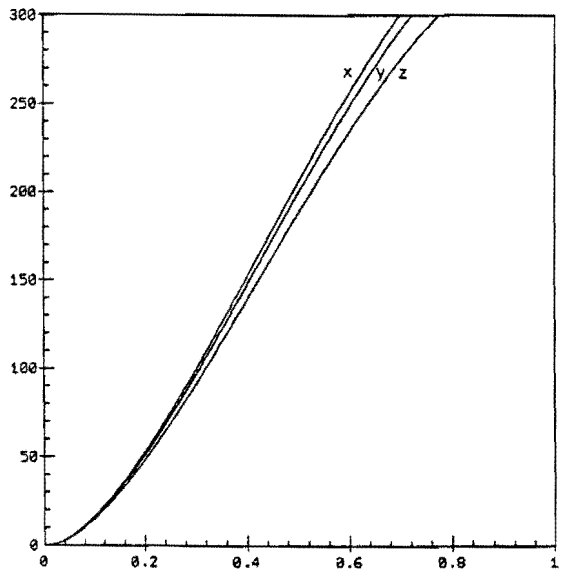

d

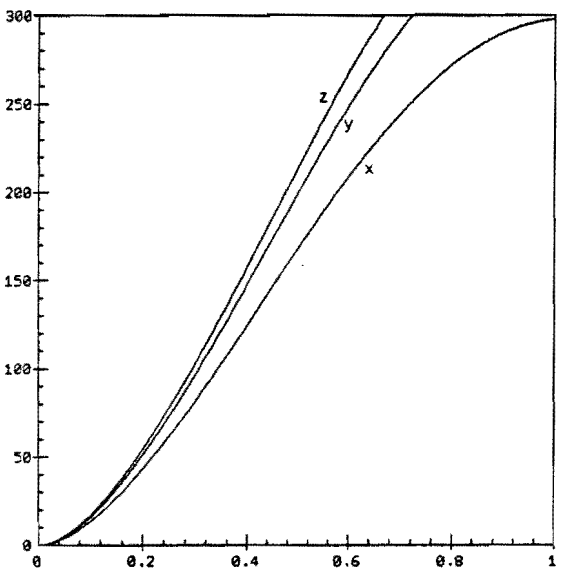

e

Fig. 3.9 : R_{in} (Ω) as function of $(\rho_o - b)/(a-b)$

d: ε_r=2.2 , h=1.57 mm , β=0.2 , fr=1.6 GHz

x: tan(δ)=0.00045 , y: tan(δ)=0.0009 , z: tan(δ)=0.0018

e: ε =2.2 , h=1.57 , tan(δ)=0.0009 , β=0.2

x: fr=0.8 GHz , y: fr=1.6 GHz , z: fr=3.2 GHz

The feed point location for a match:

-increases when h increases

-increases when ε_r increases

-increases when fr increases

-decreases when tan(δ) increases

-decreases when β increases

These above graphs show that it will be more difficult to position the feed when a substrate with a relatively high dielectric constant, a thick substrate or a small β is used; a small construction error will result in a larger mismatch.
A tan(δ) variation or frequency inaccuracy will not affect a serious mismatch.

Input impedance

The input impedance for frequencies near resonance, for thin substrates ($h \ll \lambda_o$) can be represented and calculated [3-10] by a simple RLC parallel resonant circuit.

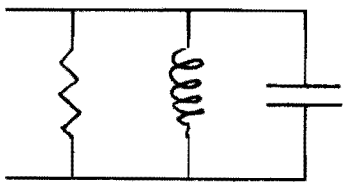

Fig. 3.10 : Input impedance modeled by a parallel RLC-circuit

The coaxial probe feed adds an inductive part to the impedance for thick substrates.
This inductance is given by [3-11]:

$$L_c = \frac{Z}{\omega} \tan\left(\frac{2\pi h \sqrt{\varepsilon_r}}{\lambda_o}\right) \qquad (3.45)$$

With:

$$Z = \frac{60}{\sqrt{\varepsilon_r}} \ln\left(\frac{d}{a}\right) \qquad (3.46)$$

and d the diameter of the coaxial probe and a the radius of the microstrip antenna.

The input impedance of a RLC parallel resonant circuit is:

$$Z_{in} = \frac{1}{\frac{1}{R} + \frac{1}{j\,\omega\,L} + j\,\omega\,C} \tag{3.47}$$

or

$$Z_{in} = \frac{R}{1 + jQ\left(\frac{\omega}{\omega_c} - \frac{\omega_c}{\omega}\right)} \tag{3.48}$$

With:

$$\omega_c = \frac{1}{\sqrt{LC}} \tag{3.49}$$

$$Q_T = \frac{R}{\sqrt{\frac{C}{L}}} \tag{3.50}$$

L and C are related to f_r and Q_T , by:

$$L = \frac{R}{2\,\pi\,f_r\,Q_t} \tag{3.51}$$

$$C = \frac{Q_t}{2\,\pi\,R\,f_r} \tag{3.52}$$

The quality factor Q_T necessary for calculating the input impedance at frequencies removed from resonance is defined as:

$$Q_T = \frac{\omega\,W_T}{P_T} \tag{3.53}$$

Where P_T is the total power attenuated and W_T the total stored energy. W_T is given by:

$$W_T = \frac{\varepsilon}{2} \iiint_V |E|^2\,dV \tag{3.54}$$

with V the volume of the cavity.
In appendix F calculations concerning the total stored energy are given.

Since it is possible to calculate the resonant frequency (f_r) and the quality factor (Q_T) from the design parameters (a,b,h,ε_r and tan(δ)), the input impedance can be determined.

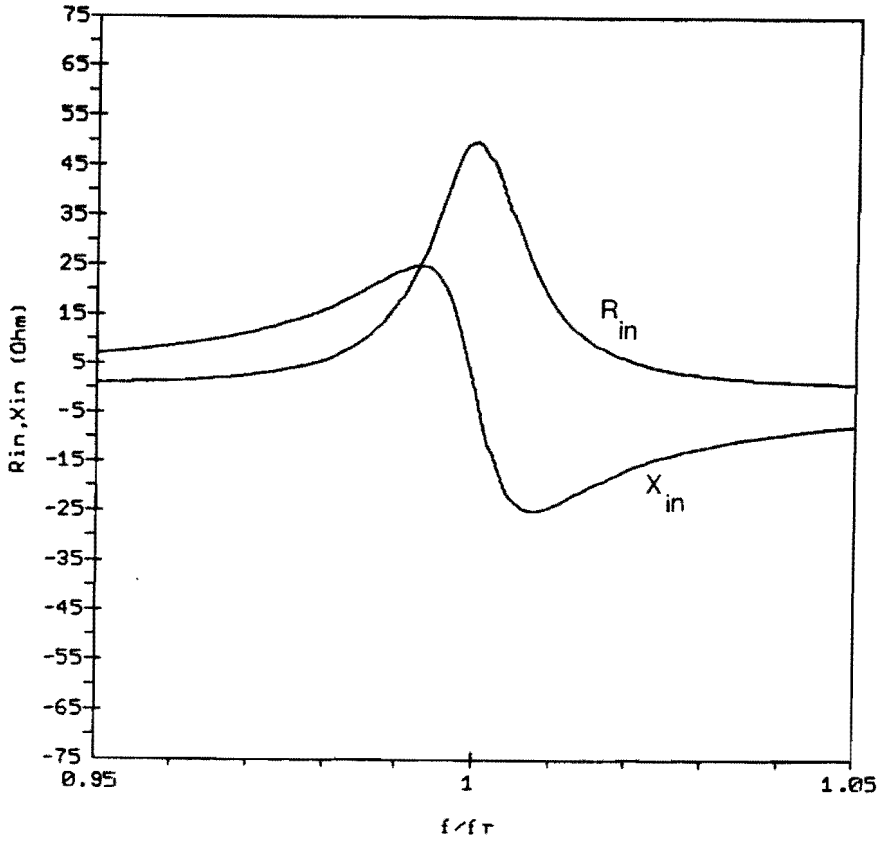

Fig. 3.11 : Typical plot of R_{in} and X_{in} (Ω) vs normalized frequency for a microstrip antenna
β=0.2 , ε_r=2.2 , h=1.57 , tan(δ)=0.0009 , f_r=1.6GHz

Representation of the input impedance by a parallel RLC-resonant circuit results in, for frequencies near resonance, a circle in the Smith chart.
The input admittance of the parallel RLC circuit is given by:

$$Y = G + j\left(\omega C - \frac{1}{\omega L}\right)$$

$$= G + j B_k \nu \qquad (3.55)$$

with :

$$B_k = \sqrt{\frac{C}{L}} \tag{3.56}$$

$$\nu = \frac{\omega}{\omega_r} - \frac{\omega_r}{\omega} \tag{3.57}$$

$$\omega_r = \frac{1}{\sqrt{LC}} \tag{3.58}$$

Normalizing this at the input admittance at resonance gives:

$$\frac{Y}{G} = 1 + j \frac{B_k}{G} \nu$$

$$= 1 + j\, Q\, \nu$$

$$= 1 + j\, V \tag{3.59}$$

The normalized input impedance then becomes:

$$z = \frac{Z}{R} = \frac{G}{Y} = \frac{1}{1 + j\, V} \tag{3.60}$$

This is the equation of a circle in the complex Z-plane. [3-12]

The reflection coefficient is defined as [3.13]:

$$\rho = \frac{Z_{in} - Z_o}{Z_{in} + Z_o} = \frac{Z_{in}/Z_o - 1}{Z_{in}/Z_o + 1} \equiv \frac{z - 1}{z + 1} \tag{3.61}$$

with Z_o the characteristic impedance of the transmission line. Because of the bilinear relation between the normalized input impedance and the reflection coefficient [3-13]

$$\rho = \frac{z-1}{z+1} \tag{3.62}$$

$\rho(\omega)$ is depicted as a circle in the Smith-chart.

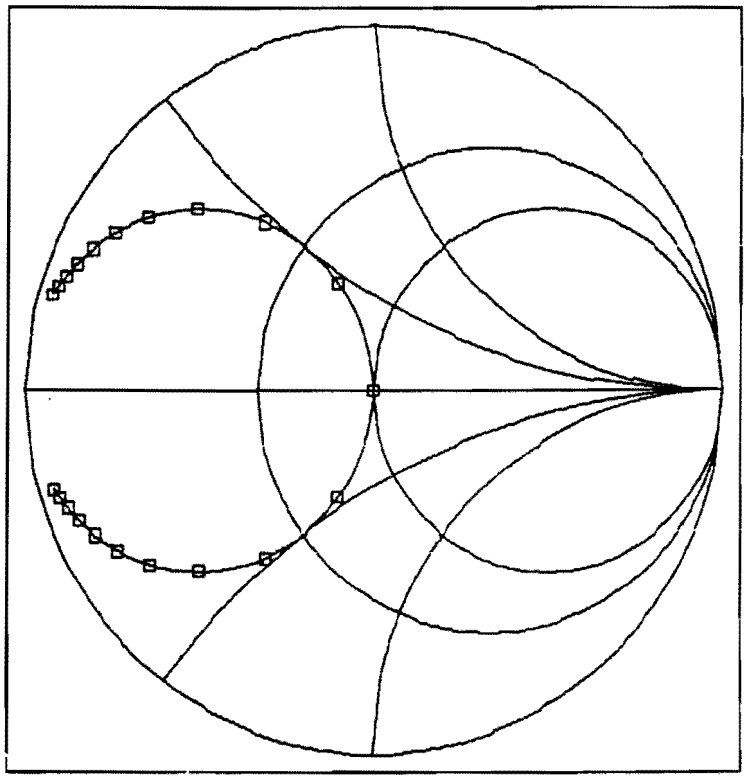

Fig. 3.12 : Typical plot of input impedance in Smith chart
β=0.2 , ε_r=2.2 , h=1.57 , tan(δ)=0.0009
f_r=1.6 GHz (ρ=0) , Δf=8 MHz

Another method to determine the reflection coefficient is by splitting the equation for Z_{in} into real and imaginary parts:

$$Z_{in} = \frac{1}{\frac{1}{R} + \frac{1}{j\,\omega\,L} + j\,\omega\,C} = A + j\,B \qquad (3.63)$$

with:

$$A = \frac{\omega^2 L^2 R}{(R - \omega^2 LRC)^2 + (\omega L)^2} \qquad (3.64)$$

$$B = \frac{\omega LR\,(R - \omega^2 LRC)}{(R - \omega^2 LRC)^2 + (\omega L)^2} \qquad (3.65)$$

The reflection coefficient then becomes:

$$|\rho|^2 = \frac{(A - Z_o)^2 + B^2}{(A + Z_o)^2 + B^2} \qquad (3.66)$$

This magnitude is called the return loss and is defined as:

$$\text{return loss} = -10 \log \left(|\rho|^2 \right)$$

$$= -20 \log \left(|\rho| \right) \qquad (3.67)$$

An example of the return loss in a frequency band near resonance is given in fig. 3.13.

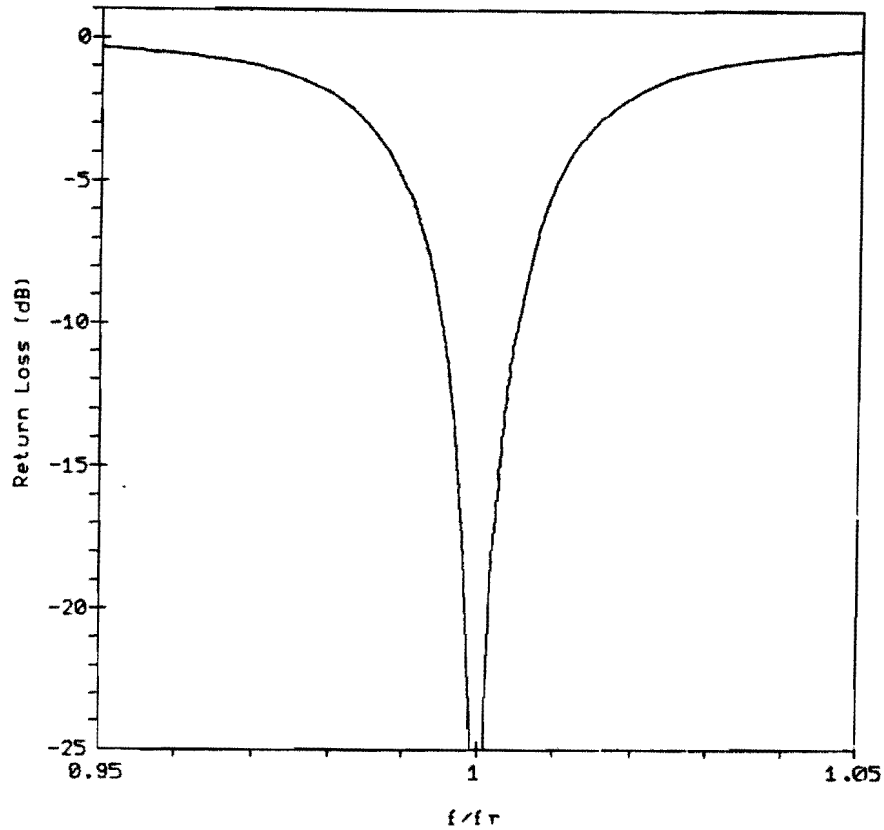

Fig. 3.13 : Return loss (dB) vs normalized frequency
β=0.2 , ε_r=2.2 , h=1.57 , tan(δ)=0.0009 , f_r=1.6GHz

Thus it is now possible to relate the VSWR to the design parameters. R, L and C are determined by P_r, P_c and P_d which are functions of the design parameters.

The VSWR, S, is defined as [3-13]:

$$S = \frac{1 + |\rho|}{1 - |\rho|} \tag{3.68}$$

The VSWR is calculated for different patches as a function of the frequency. The results are shown in fig. 3.14.

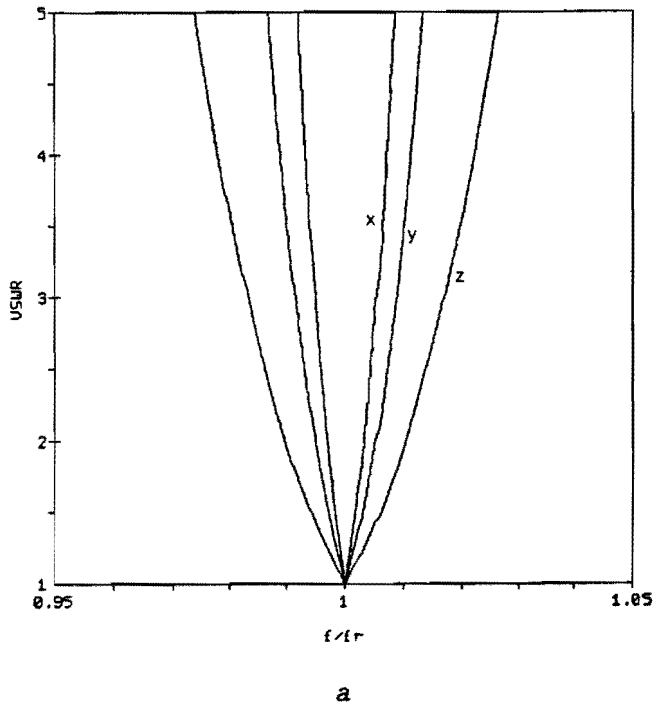

a

Fig. 3.14 : VSWR vs normalized frequency of a ring patch antenna
a: fr=1.6 GHz , β=0 , ε_r=2.2 , tan(δ)=0.0009
x: h=0.79 mm , y: h=1.57 mm , z: h=3.18 mm

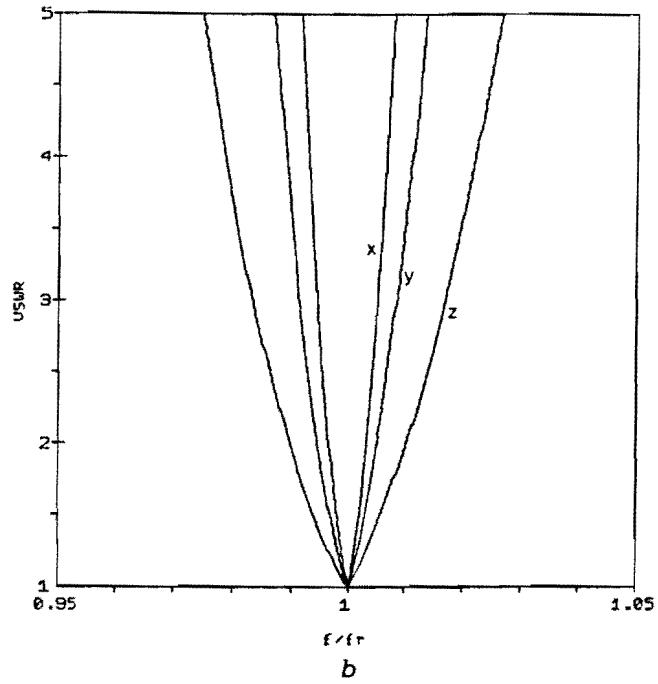

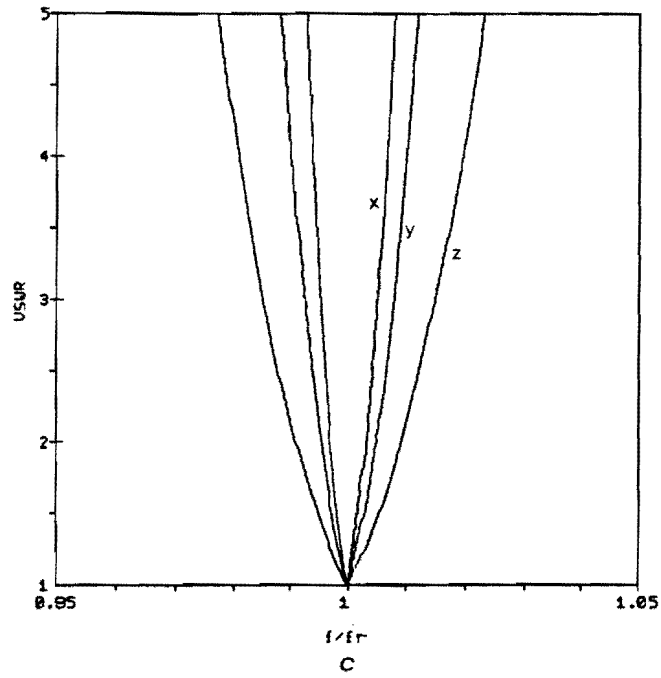

Fig. 3.14 : VSWR vs normalized frequency of a ring patch antenna
b: fr=1.6 GHz , β=0.2 , ε_r=2.2 , tan(δ)=0.0009
x: h=0.79 mm , y: h=1.57 mm , z: h=3.18 mm
c: fr=1.6 GHz , β=0.4 , ε_r=2.2 , tan(δ)=0.0009
x: h=0.79 mm , y: h=1.57 mm , z: h=3.18 mm

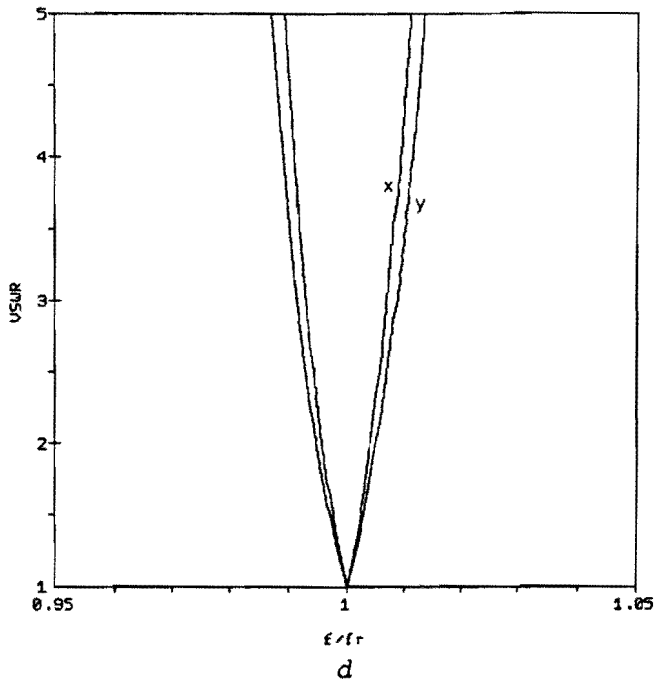

d

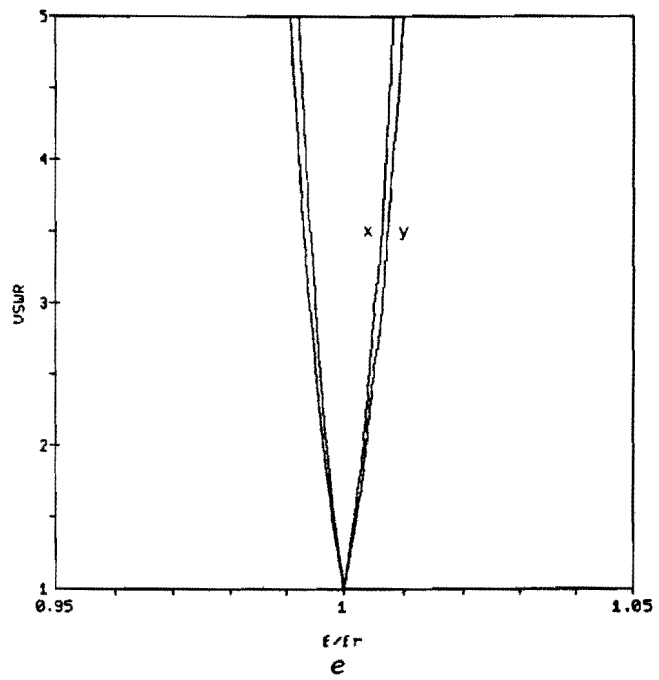

e

Fig. 3.14 : VSWR vs normalized frequency of a ring patch antenna

d: fr=1.6 GHz , β=0.2 , ε_r=6.0 , tan(δ)=0.0027

x: h=1.91 mm , y: h=2.54 mm

e: fr=1.6 GHz , β=0.2 , ε_r=10.5 , tan(δ)=0.0028

x: h=1.91 mm , y: h=2.54 mm

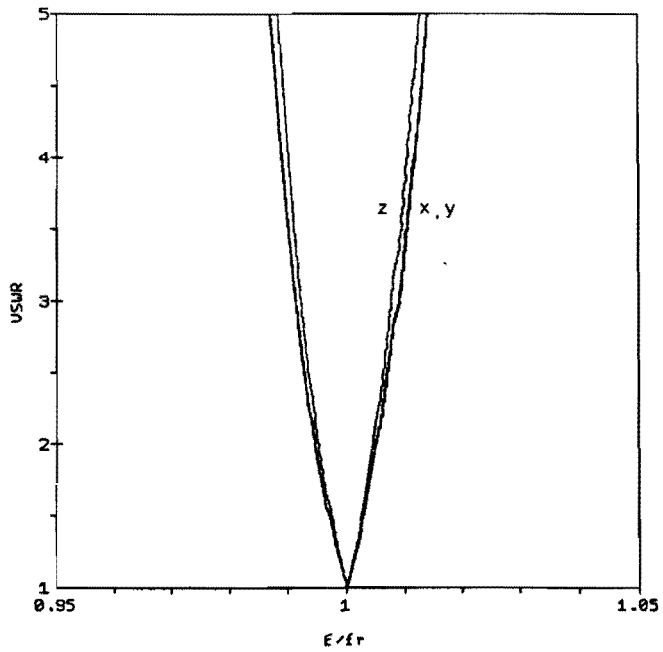

f

Fig. 3.14 : VSWR vs normalized frequency of a ring patch antenna
f: fr=1.6 GHz , ε_r=2.2 , h=1.57 mm , tan(δ)=0.0009
x: β=0.0 , y: β=0.2 , z: β=0.4

These graphs show that the VSWR bandwidth:
-increases with increasing h
-decreases with increasing ε_r
-decreases with increasing β
-is less affected by h variations when ε_r increases

Another important property is the bandwidth of the antenna. The bandwidth is defined as the frequency band where the VSWR is less than a certain specified value Sb.
Z_{in} represents the input impedance of the parallel RLC resonant circuit and can be written as [3-14,3-15]:

$$Z_{in} = \frac{R}{1 + jQ\left(\frac{\omega}{\omega_r} - \frac{\omega_r}{\omega}\right)}$$

$$= \frac{1}{1 + j\,Q\,\nu} \tag{3.69}$$

Substituting this in eq. 3.62 gives the following result:

$$|\rho|^2 = \frac{(T-1)^2 + (Q\nu)^2}{(T-1)^2 + (Q\nu)^2} \tag{3.70}$$

with:

$$T = \frac{R}{Z_o} \tag{3.71}$$

$$\nu = \frac{\omega}{\omega_c} - \frac{\omega_c}{\omega} \tag{3.72}$$

From eq. 3.68 and 3.69 [3-14,3-15] it follows:

$$\nu_i^2 = \frac{(T\,S_b - 1)\,(S_b - 1)}{Q^2\,S_b} \tag{3.73}$$

With:

$$\nu_i = \frac{\omega_i}{\omega_r} - \frac{\omega_r}{\omega_i} \tag{3.74}$$

$$\nu_1 = -\nu_2 \tag{3.75}$$

Using eq. 3.74 and 3.75 the following relation holds:

$$f_1\,f_2 = f_r^2 \tag{3.76}$$

The bandwidth can be calculated as follows:

$$\nu_1 = \frac{f_1}{f_r} - \frac{f_r}{f_1} \tag{3.77}$$

With eq. 3.76 this can be written as:

$$\nu_1 = \frac{f_1}{f_r} - \frac{f_2}{f_1}$$

$$= \frac{f_1\,f_r - f_2\,f_r}{f_r^2}$$

$$= \frac{f_1 - f_2}{f_r}$$

$$= \frac{\Delta f}{f_r} \tag{3.78}$$

On the other hand:

$$\nu_1 = \frac{1}{Q_T} \sqrt{\frac{(T S_b - 1)(S_b - 1)}{S_b}} \tag{3.79}$$

So the equation for the bandwidth in percents becomes:

$$BW = \frac{100}{Q_T} \sqrt{\frac{(T S_b - 1)(S_b - 1)}{S_b}} \tag{3.80}$$

For a ring patch, the quality factor and bandwidth as function of the frequency and β is calculated and plotted in fig. 3.15.

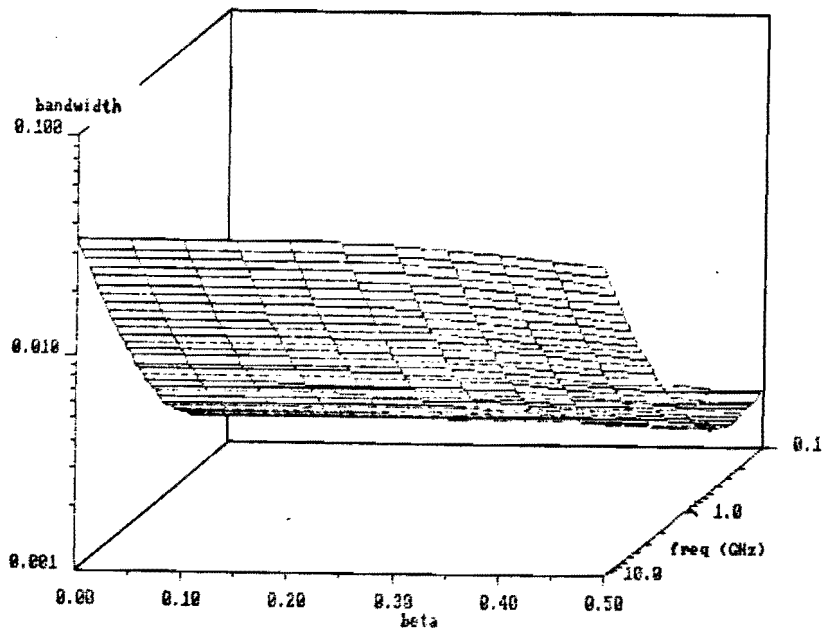

Fig. 3.15 : Bandwidth vs frequency vs β

ε_r=2.2 , h=1.57 mm , tan(δ)=0.0009

The optimum bandwidth is not achieved for T = 1, a perfect match, but for:

$$T_{opt} = \frac{S_b^2 + 1}{2\,S_b} \tag{3.81}$$

This gives just a slight improvement in comparison with T = 1 [3-14,3-15]. Using the approximation T =1, the well known expression for the bandwidth is obtained [3-1]:

$$BW = \frac{100}{Q_T}\,\frac{S - 1}{\sqrt{S}} \tag{3.82}$$

To meet the specifications as stated in fig. 2.1, a bandwidth of 30 MHz (=1.9 %) must be achieved. From fig. 3.14 and 3.15 it is clear that it is not possible to cover a whole transmitting or receiving band with one antenna unless thicker substrates or substrates with a lower dielectric constant are used.

3.7 Uncertainty analysis for circular microstrip antennas.

Deviations in effective electrical dimensions caused by variations in designed antenna dimensions, variations of the relative permittivity of the substrate material, or nonuniformity in the substrate thickness lead to discrepancies between the designed and actual resonant frequencies. This type of deviation of the designed microstrip characteristics is particularly significant because of the narrow bandwidth of such antennas.
In this section, the effects of fabrication uncertainties and manufacturer's tolerances on the resonance frequency will be considered. The uncertainty analysis used here is described in [3-16].

$$f_r = \frac{\chi_{nm}\,c_o}{2\,\pi\,a\,\sqrt{\varepsilon_r}} \tag{3.83}$$

Assuming that errors occur in calculating χ_{nm}, fabrication tolerances in the dielectric constant or because of inaccuracy in etching, the uncertainty then becomes:

$$|\Delta f_r| = \left[\left(\frac{\partial f_r}{\partial \chi_{nm}} \Delta \chi_{nm} \right)^2 + \left(\frac{\partial f_r}{\partial \varepsilon_r} \Delta \varepsilon_r \right)^2 + \left(\frac{\partial f_r}{\partial a} \Delta a \right)^2 \right]^{1/2} \qquad (3.84)$$

Carrying out the differentiations on eq. 3.83 and rewriting the result gives:

$$|\Delta f_r| = \left[\left(\frac{f_r}{\chi_{nm}} \Delta \chi_{nm} \right)^2 + \left(- \frac{f_r}{2 \varepsilon_r} \Delta \varepsilon_r \right)^2 + \left(- \frac{f_r}{a} \Delta a \right)^2 \right]^{1/2} \qquad (3.85)$$

Suppose χ_{nm} is calculated with an accuracy of 10^{-5} for β=0.2 (χ_{nm} = 1.99345) , the manufacturing tolerance of the dielectric substrate is ε_r = 2.2 ± 0.02 and etching tolerance is ± 0.05 mm.
When the resonance frequency is 1.6 GHz the maximum deviation of the resonant frequency is: ± 7.5 MHz or ± 0.5 %.
In conclusion we may state that the deviation of the resonance frequency is a significant part of the bandwidth. Hence this aspect of the design should be considered most carefully.

3.8 References.

[3-1] Bahl I.J. and Bhartia P.,
'Microstrip antennas',
Artech House Inc. 1980.

[3-2] James J.R., Hall P.S. and Wood C.,
'Microstrip Antenna: Theory and Design',
Peregrinus Ltd., 1981.

[3-3] Goto N. and Kaneta K.,
'Ring Patch Antennas for Dual Frequency Use'
Proceedings of the 1987 International Symposium on Antennas and Propagation, Blacksburg (Va), June 1987, Volume II, p. 944-947.

[3-4] Yasunaga M., Wanatabe F., Shiokawa T. and Yamada M.,
'Phased Array Antennas for Aeronautical Satellite Communications', Proceedings of the 5 th International Conference on Antennas and Propagation, 1987, IEE Conference Publication 274, p. 47-50.

[3-5] Abramowitz M. and Stengun I.A.,
'Handbook of Mathematical Functions',
Dover Publications Inc., New York, 1965.

[3-6] Press W.H., Flannery B.P., Teukolsky S.A., Vetterling W.T.,
'Numerical Recipes, the Art of Scientific Computing',
Cambridge University Press, 1986.

[3-7] Jeuken M.E.J.,
'Elektromagnetische Golven en Antennes',
Lecture Notes, Eindhoven University of Technology. (in Dutch)

[3-8] Collin R.E.,
'Field Theory of Guided Waves',
Mc. Graw-Hill Co., New York, 1960, p. 470-474.

[3-9] Balanis C.A.,
'Antenna Theory',
John Wiley And Sons, 1982.

[3-10] Long S.A. et al.,
'Impedance of a Circular Disc Printed Circuit Antenna'
Electronic Letters, Vol. 14, 1978, p. 684-686.

[3-11] Griffin J.M.,
'Broadband Circular Disc Microstrip Antenna',
Electronic Letters, Vol. 18, 1982, p. 266-269.

[3-12] Zinke O. and Vlcek A.,
'Lehrbuch der Hochfrequenztechnik',
Springer-Verlag, 1986, p.13 (in German).

[3-13] Versnel W.,
'Microgolftechniek',
Lecture Notes, Eindhoven University of Technology, 1985.
(in Dutch)

[3-14] Toom E.C. den,
'Microstripantenne voor de mobiele satelliet communicatie', Master's Thesis, Professional Group Electromagnetism and Circuit Theory, Department of Electrical Engineering, Eindhoven University of Technology, Netherlands, 1989, ET-8-89. (in Dutch)

[3-15] Pues H.,
'Studie van de bandbreedte van geintegreerde mikrogolfantennes: ontwikkeling van ontwerpmodellen voor breedbandige mikrostripantennes',
Proefschrift, Katholieke Universiteit Leuven, 1982-1983.
(in Dutch)

[3-16] Kline S.J. and McClintock F.A.,
'Describing Uncertainties in Single-Sample Experiments',
Mechanical Engineering, Vol. 75, 1953, p. 3-8.

4 Circular polarization with one microstrip antenna.

It has already been outlined that in mobile satellite communication circular polarization is required. In this chapter definitions of circular polarization and related quantities, like co- and cross polarization and axial ratio are given in the first part.
Subsequently several methods for generating a circular polarized field by a single microstrip antenna are discussed.
The performances of the circularly polarized antenna are viewed in the light of the specifications stated in chapter 2.
It will become apparent that a power divider and phase shifters are indispensable in order to generate circularly polarized waves. By constructing these networks in microstrip technology, the advantages of the microstrip antenna are maintained.

4.1 Circular polarization: definitions.

Consider an arbitrary antenna placed in the origin of the coordinate system. It is well known from antenna theory [4-1] that the radiation field can be written in complex phasor notation:

$$\bar{E}(r,\vartheta,\phi) = E_{\vartheta}(r,\vartheta,\phi)\ \hat{a}_{\vartheta} + E_{\phi}(r,\vartheta,\phi)\ \hat{a}_{\phi} \qquad (4.1)$$

$$\bar{H}(r,\vartheta,\phi) = H_{\vartheta}(r,\vartheta,\phi)\ \hat{a}_{\vartheta} + H_{\phi}(r,\vartheta,\phi)\ \hat{a}_{\phi} \qquad (4.2)$$

and the relation between $\bar{E}$ and $\bar{H}$ is given by:

$$Z_o\ \bar{H} = \hat{a}_r \times \bar{E} \qquad (4.3)$$

with Z_o the wave impedance in vacuum.
The complex $\bar{E}$-vector can be written as:

$$\begin{aligned}\bar{E}(r,\vartheta,\phi) &= E_{\vartheta}(r,\vartheta,\phi)\ \hat{a}_{\vartheta} + E_{\phi}(r,\vartheta,\phi)\ \hat{a}_{\phi} \\ &= |E_{\vartheta}(r,\vartheta,\phi)|\ \exp(j\psi_{\vartheta})\ \hat{a}_{\vartheta} + |E_{\phi}(r,\vartheta,\phi)|\ \exp(j\psi_{\phi})\ \hat{a}_{\phi}\end{aligned} \qquad (4.4)$$

Let $\bar{\mathcal{E}}(r,\vartheta,\phi,t)$ and $\bar{\mathcal{H}}(r,\vartheta,\phi,t)$ be the time dependant field components. These are determined by:

$$\bar{\mathcal{E}}(r,\vartheta,\phi,t) = Re\left(\bar{E}(r,\vartheta,\phi)\ \exp(j\omega t) \right) \tag{4.5}$$

Substituting eq. 4.4 in eq. 4.5 gives:

$$\bar{\mathcal{E}}(r,\vartheta,\phi,t) = |E_{\vartheta}(r,\vartheta,\phi)|\ \cos(\omega t+\psi_{\vartheta})\ \hat{a}_{\vartheta} + |E_{\phi}(r,\vartheta,\phi)|\ \cos(\omega t+\psi_{\phi})\ \hat{a}_{\phi} \tag{4.6}$$

By polarization of a wave is meant that property which describes the time varying direction and relative magnitude of the $\bar{\mathcal{E}}$- (and $\bar{\mathcal{H}}$-) vector in the time domain; in other words, the figure traced as a function of time by the extremity of the vector at a fixed location, and the manner in which it is traced as observed along the direction of propagation.
Equation 4.6 describes this figure.

When $\psi_{\vartheta} = \psi_{\phi} = \psi$, the $\bar{\mathcal{E}}$-vector is given by :

$$\bar{\mathcal{E}}(r,\vartheta,\phi,t) = \left(|E_{\vartheta}(r,\vartheta,\phi)|\ \hat{a}_{\vartheta} + |E_{\phi}(r,\vartheta,\phi)|\ \hat{a}_{\phi} \right) \cos(\omega t+\psi) \tag{4.7}$$

And the $\bar{\mathcal{E}}$-vector describes a straight line in space and time and the polarization is linear.

When however $\psi_{\vartheta} = \psi_{\phi} \pm \frac{\pi}{2}$ and $|E_{\vartheta}(r,\vartheta,\phi)| = |E_{\phi}(r,\vartheta,\phi)| = |E|$, the $\bar{\mathcal{E}}$-vector is written as:

$$\bar{\mathcal{E}}(r,\vartheta,\phi,t) = |E|\left(\cos(\omega t+\psi_{\vartheta})\ \hat{a}_{\vartheta} \pm \sin(\omega t+\psi_{\vartheta})\ \hat{a}_{\phi} \right) \tag{4.8}$$

The $\bar{\mathcal{E}}$-vector now describes a circle.
For the - sign, the electric field rotates counterclockwise and the polarization is left hand circular (LHC). When, on the other hand, the + sign is taken, the electric field then rotates clockwise and the polarization is right hand circular (RHC).

Generally this figure is an ellipse [4-2] in the (ϑ,ϕ) plane.
For the general case: $|E_{\vartheta}| \neq |E_{\phi}| \neq |E|$ and $\phi \neq 0$ or $\phi \neq \pm\pi/2$ the

locus of the terminus of the electric and magnetic field vector is, in each case, an ellipse for a given direction (ϑ,ϕ) as time progresses. This polarization ellipse, as depicted in figure 4.1 , can be considered as arising from the vectorial addition of two rotating vectors. One rotating clockwise (E_r) and the other rotating counterclockwise (E_l).

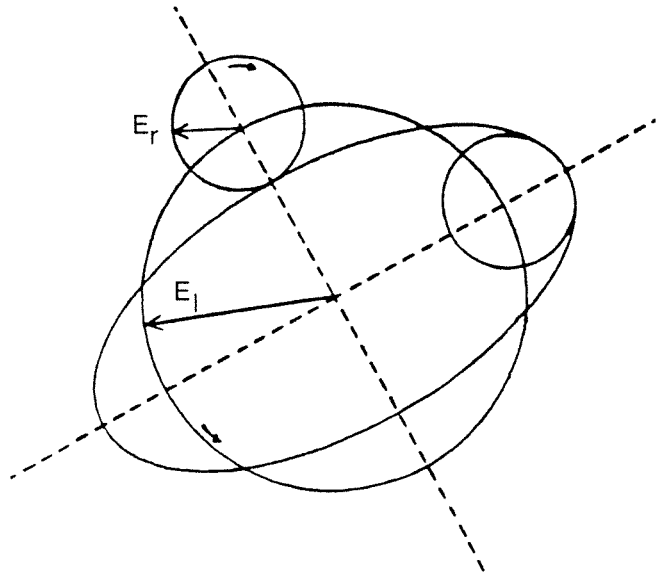

Fig. 4.1 : Polarization ellipse with RHC- and LHC-components
Direction of propagation of the wave is into the paper

Hence the electric field can be written as:

$$\bar{E}(r,\vartheta,\phi) = E_\vartheta(r,\vartheta,\phi)\,\hat{a}_\vartheta + E_\phi(r,\vartheta,\phi)\,\hat{a}_\phi$$

$$= E_l(r,\vartheta,\phi)\,\hat{a}_l + E_r(r,\vartheta,\phi)\,\hat{a}_r \qquad (4.9)$$

with complex unit vectors:

$$\hat{a}_l = \frac{1}{\sqrt{2}}\,(\,\hat{a}_\vartheta + j\,\hat{a}_\phi\,) \qquad (4.10)$$

$$\hat{a}_r = \frac{1}{\sqrt{2}}\,(\,\hat{a}_\vartheta - j\,\hat{a}_\phi\,) \qquad (4.11)$$

E_l and E_r represent the LHC- respectively RHC-component.
Writing out equation 4.11 gives:

$$E_l(r,\vartheta,\phi) = \frac{1}{\sqrt{2}}\left(\,E_\vartheta(r,\vartheta,\phi) - j\,E_\phi(r,\vartheta,\phi)\,\right) \qquad (4.12)$$

$$E_r(r,\vartheta,\phi) = \frac{1}{\sqrt{2}} \left(E_\vartheta(r,\vartheta,\phi) + j\, E_\phi(r,\vartheta,\phi) \right) \qquad (4.13)$$

A graphical representation is given in figure 4.1.

To express the circularity of the ellipse, the axial ratio is introduced. It is defined as:

$$AR = \frac{E_{max}}{E_{min}} \qquad (4.14)$$

From figure 4.1 it is obvious that the axial ratio represents the ratio of the major to the minor axis of the ellipse.

In a predominantly LHC-polarized wave the co- and cross-polarization and axial ratio are defined as:

$$|E_l|_{dB} = 20 \log \left(\frac{|E_l|}{|E_l|_{max}} \right) \qquad (4.15)$$

(co polarization)

$$|E_r|_{dB} = 20 \log \left(\frac{|E_r|}{|E_l|_{max}} \right) \qquad (4.16)$$

(cross polarization)

$$AR_{dB} = 20 \log \left(\frac{|E_l| + |E_r|}{|E_l| - |E_r|} \right) \qquad (4.17)$$

(axial ratio)

By interchanging the indexes l and r, the formulas for a predominantly RHC-polarized wave are obtained.

In general:

$$AR_{dB} = 20 \log \left(\left| \frac{|E_l| + |E_r|}{|E_l| - |E_r|} \right| \right) \qquad (4.18)$$

The axial ratio (in dB) varies between 0 dB, for a perfectly circularly polarized wave, and ∞ (dB) for a linearly polarized wave.

4.2 Circularly polarized microstrip antenna.

Circular polarization with a single microstrip patch is obtained when two orthogonal modes having equal amplitude and in-phase quadrature are excited within the cavity region.
There are two methods for creating circular polarization with a single microstrip patch: use of perturbation techniques and use of multiple feeds.

In the perturbation technique a single feed is used and the patch geometry is perturbed to excite two orthogonal modes. Examples of geometrical arrangements for circularly polarization having one feed are shown in figure 4.2.

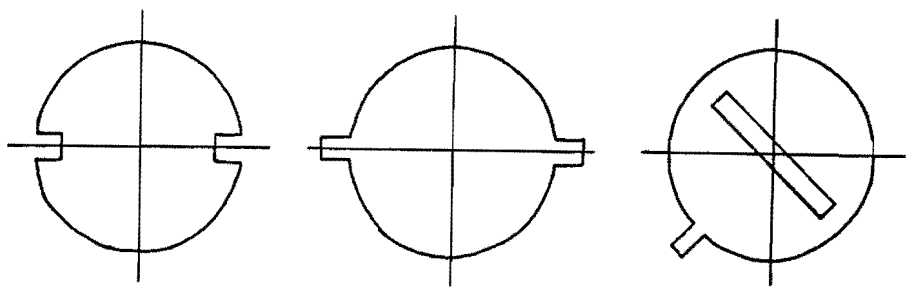

Fig. 4.2 : Examples of single feed circularly polarized asymmetrical microstrip patches

Although this type of patch has the advantage of only one feed, the great disadvantage is the lack of an adequate model. In this report no further attention is paid to this method for it is mainly one of trial and error.

A very well known approach for obtaining circular polarization is that of using two separate and spatial orthogonal radiators, excited with a relative phase shift of 90° . This configuration then provides two orthogonal linearly polarized waves which are in time phase quadrature.
It is easy to equip and excite a single microstrip antenna with two feeds in the way as described above. This is shown in figure 4.3.

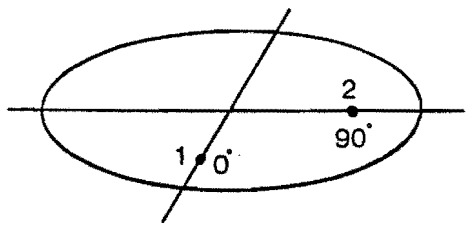

Fig. 4.3 : Circularly polarized circular microstrip patch

Consider an arbitrary antenna element located in the origin of the co-ordinate system, the radiation pattern of such an element can be written as:

$$\bar{E}(\vartheta,\phi) = - j\,k\,\frac{e^{-jkr}}{4\,\pi\,r}\left(f_{\vartheta}(\vartheta,\phi)\,\hat{a}_{\vartheta} + g_{\phi}(\vartheta,\phi)\,\hat{a}_{\phi} \right) \qquad (4.19)$$

This antenna is considered as a reference antenna. Rotating the antenna over angle ϕ_r in the xy-plane as depicted in fig. 4.4 leads to modification of eq. 4.19 as:

$$\bar{E}(\vartheta,\phi) = - j\,k\,\frac{e^{-jkr}}{4\,\pi\,r}\left(f_{\vartheta}(\vartheta,\phi-\phi_r)\,\hat{a}_{\vartheta} + g_{\phi}(\vartheta,\phi-\phi_r)\,\hat{a}_{\phi} \right) \qquad (4.20)$$

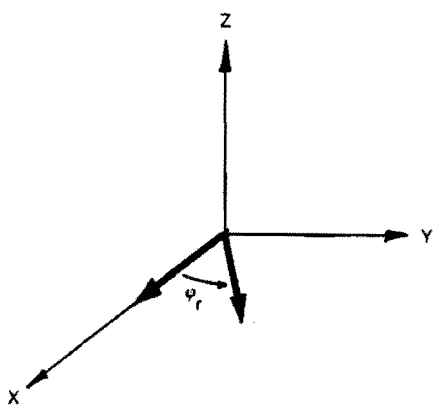

Fig. 4.4 : A representative antenna element in free space

Thus the far field components of the antenna in figure 4.3 are:

$$E_{\vartheta}(\vartheta,\phi) = \exp(j\ 0^{\circ})\ E_{\vartheta}(\vartheta,\phi) + \exp(j\ 90^{\circ})\ E_{\vartheta}(\vartheta,\phi-90^{\circ}) \qquad (4.21)$$

$$E_\phi(\vartheta,\phi) = \exp(j\ 0^\circ)\ E_\phi(\vartheta,\phi) + \exp(j\ 90^\circ)\ E_\phi(\vartheta,\phi-90^\circ) \tag{4.22}$$

Using the far field equations for a linearly polarized antenna with n=1 (eq. 3.26 and 3.27), the field components for the TM_{11}-mode can be written as:

$$E_\vartheta(r,\vartheta,\phi) = -\ j\ \frac{e^{-jk_o r}}{2r}\ E_o\ h\ a\ k_o\ \cos(\phi)$$

$$\left(J_1(ka) - \frac{J_1(kb)}{Y_1(kb)}\ Y_1(ka) \right) \left(J_0(X) - J_2(X) \right) \tag{4.23}$$

$$E_\phi(r,\vartheta,\phi) = j\ \frac{e^{-jk_o r}}{2r}\ E_o\ h\ a\ k_o\ \cos(\vartheta)\ \sin(\phi)$$

$$\left(J_1(ka) - \frac{J_1(kb)}{Y_1(kb)}\ Y_1(ka) \right) \left(J_0(X) + J_2(X) \right) \tag{4.24}$$

Defining the abbreviations:

$$A(r) = j\ \frac{e^{-jk_o r}}{2r}\ E_o\ h\ a\ k_o \left(J_1(ka) - \frac{J_1(kb)}{Y_1(kb)}\ Y_1(ka) \right) \tag{4.25}$$

$$F_1(\vartheta) = \left(J_0(X) - J_2(X) \right) \tag{4.26}$$

$$F_2(\vartheta) = \left(J_0(X) + J_2(X) \right) \tag{4.27}$$

with:

$$X = k_o a\ \sin(\vartheta)$$

This gives:

$$E_\vartheta(r,\vartheta,\phi) = -\ A(r)\ F_1(\vartheta)\ \cos(\phi) \tag{4.28}$$

$$E_\phi(r,\vartheta,\phi) = A(r)\ F_2(\vartheta)\ \cos(\vartheta)\ \sin(\phi) \tag{4.29}$$

Substituting these eq. in eq. 4.21 and 4.22 the far field components of a circularly polarized antenna are:

$$E_\vartheta(\vartheta,\phi) = - A(r)\, F_1(\vartheta)\, \cos(\phi) - j\, A(r)\, F_1(\vartheta)\, \cos(\phi - 90^\circ)$$

$$= - A(r)\, F_1(\vartheta)\, e^{j\phi} \qquad (4.30)$$

$$E_\phi(\vartheta,\phi) = A(r)\, F_2(\vartheta)\, \cos(\vartheta)\, \sin(\phi) + j\, A(r)\, F_2(\vartheta)\, \cos(\vartheta)\, \sin(\phi - 90^\circ)$$

$$= j\, A(r)\, F_2(\vartheta)\, \cos(\vartheta)\, e^{j\phi} \qquad (4.31)$$

With these equations and eq. 4.12 and 4.13 the left and right hand components of the electric field can now be calculated:

$$E_1(r,\vartheta,\phi) = \frac{1}{\sqrt{2}} \left(E_\vartheta(r,\vartheta,\phi) - j\, E_\phi(r,\vartheta,\phi) \right)$$

$$= \frac{1}{\sqrt{2}}\, A(r)\, \exp(j\,\phi) \left(F_1(\vartheta) - F_2(\vartheta)\, \cos(\vartheta) \right) \qquad (4.32)$$

$$E_r(r,\vartheta,\phi) = \frac{1}{\sqrt{2}} \left(E_\vartheta(r,\vartheta,\phi) + j\, E_\phi(r,\vartheta,\phi) \right)$$

$$= \frac{1}{\sqrt{2}}\, A(r)\, j\, \exp(j\,\phi) \left(F_1(\vartheta) + F_2(\vartheta)\, \cos(\vartheta) \right) \qquad (4.33)$$

And for the axial ratio is found:

$$AR = \left| \frac{|F_1(\vartheta) + F_2(\vartheta)\, \cos(\vartheta)| + |F_1(\vartheta) - F_2(\vartheta)\, \cos(\vartheta)|}{|F_1(\vartheta) + F_2(\vartheta)\, \cos(\vartheta)| - |F_1(\vartheta) - F_2(\vartheta)\, \cos(\vartheta)|} \right| \qquad (4.34)$$

This last equation is of utmost importance for considering the quality of a circularly polarized microstrip antenna.
Therefore on the next pages the axial ratio, co- and cross polarization and radiation patterns for various dielectric

substrates and various values of beta are calculated.

In fig. 4.5 the power in the co- and cross-polarization components of the electric field in a certain direction ϑ are calculated. The power radiated in a direction (ϑ,ϕ) is calculated using the Poynting vector $(\bar{S}(\bar{r}))$ and:

$$P(\vartheta,\phi) = \left| r^2 \, \bar{S}(\bar{r}) \right| \tag{4.35}$$

with:

$$\begin{aligned} \bar{S}(\bar{r}) &= \frac{1}{2} \, Re \, (\bar{E} \times \bar{H}^*) \\ &= \frac{1}{2} \, \frac{1}{Z_o} \, |\bar{E}|^2 \\ &= \frac{1}{2} \, \frac{1}{Z_o} \left(|E_\vartheta|^2 + |E_\phi|^2 \right) \\ &= \frac{1}{2} \, \frac{1}{Z_o} \left(|E_l|^2 + |E_r|^2 \right) \end{aligned} \tag{4.36}$$

Taking only the E_l (E_r)-component of a circularly polarized wave in eq. 4.36 the power radiated by the LHC (RHC) component of the electric field can be calculated.

If all the power is concentrated in the co-polarization component of the electric field, and thus the cross-polarization component does not exist, the wave is perfectly circularly polarized and the axial ratio is 0 dB. This can be easily verified by comparing the corresponding figures in fig. 4.5 and fig. 4.6. If however the the power is equally distributed over the co- and cross-polarization component, the wave is linearly polarized and the axial ratio is infinite. Because the quality of the circular polarized wave is specified by the axial ratio, fig. 4.6 is being used to discuss the properties of the antennas.

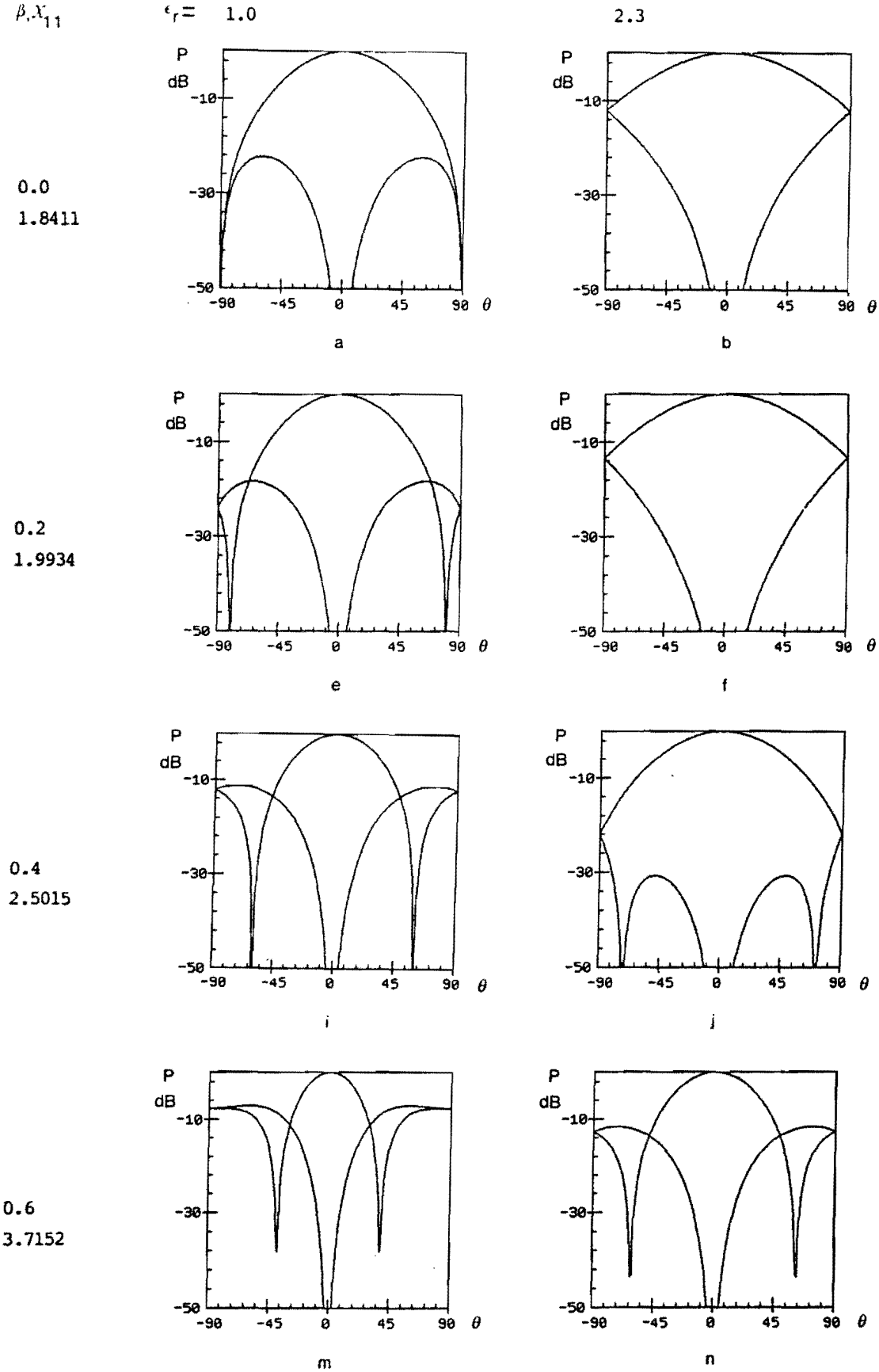

Figure 4.5 : Co- and Cross-polarization (dB) vs ϑ (degrees) as function of ε_r and β for the TM_{11}-mode

6.0

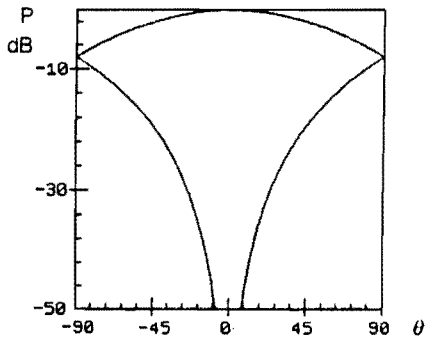

c

10.0

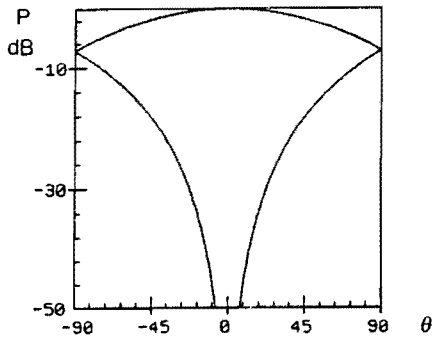

d

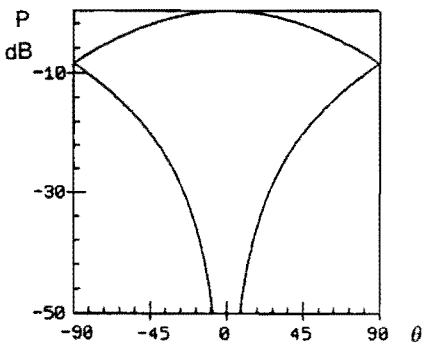

g

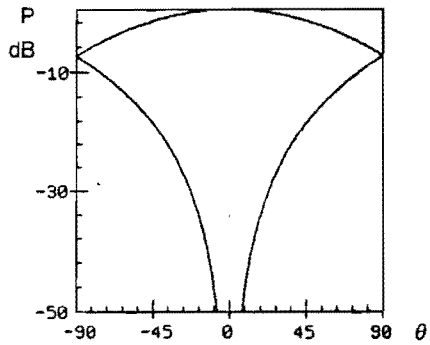

h

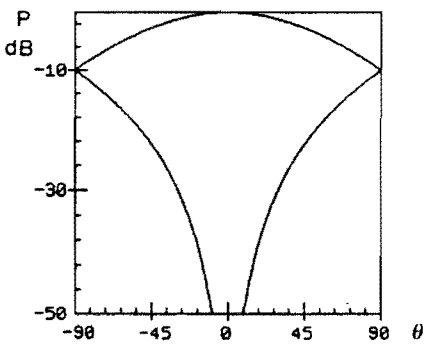

k

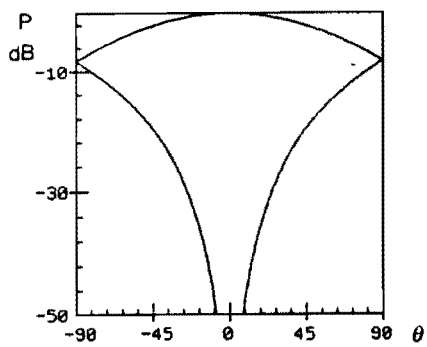

l

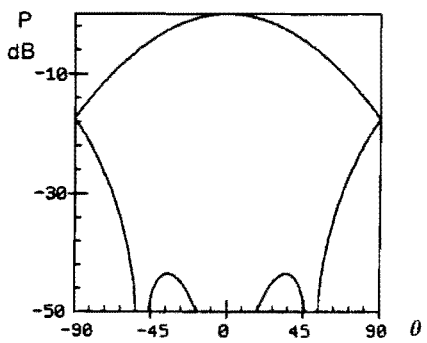

o

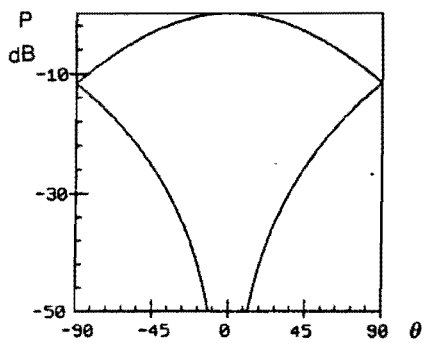

p

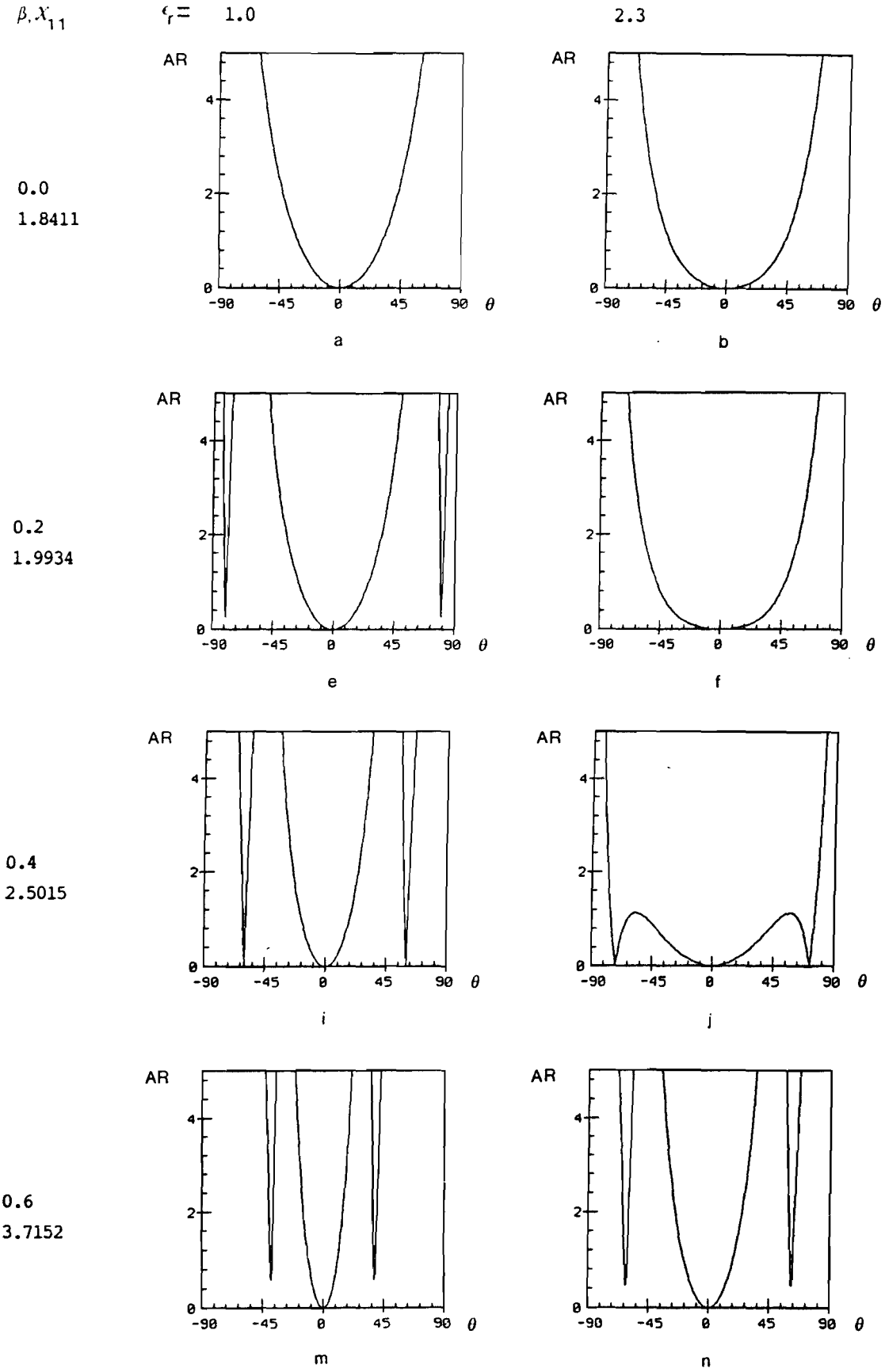

Figure 4.6 : Axial ratio (dB) vs ϑ (degrees) as function of ε_r and β for the TM_{11}-mode

6.0

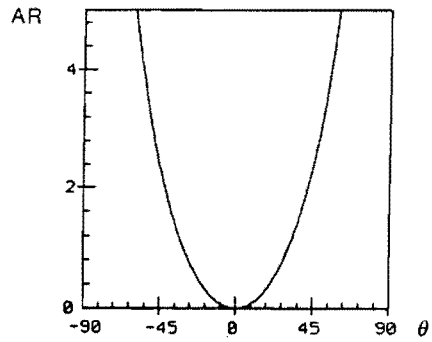

c

10.0

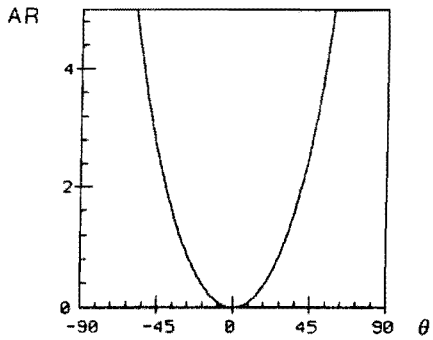

d

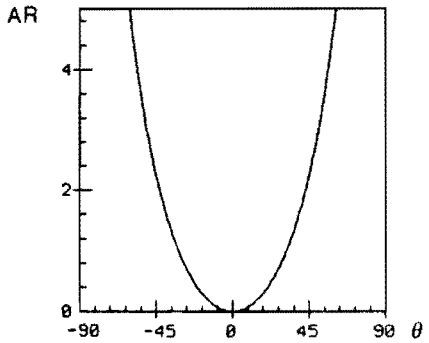

g

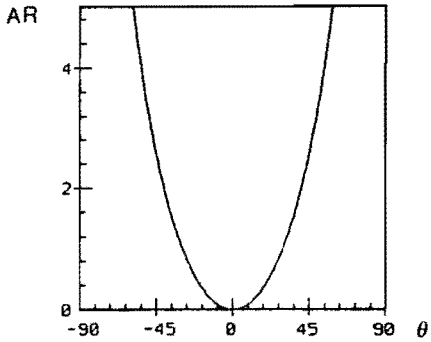

h

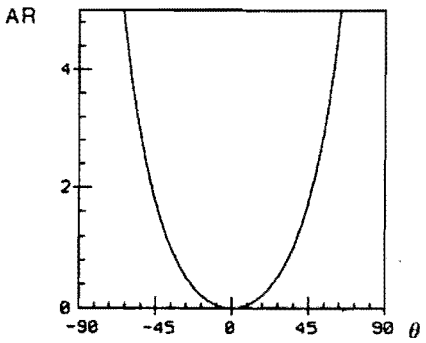

k

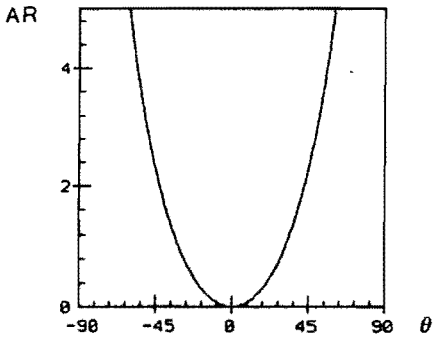

l

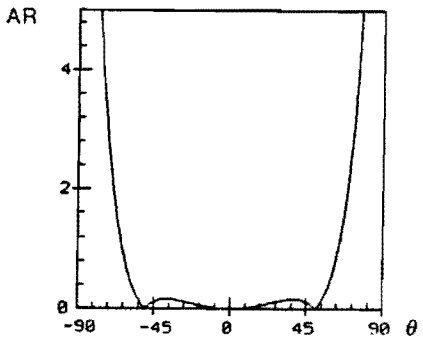

o

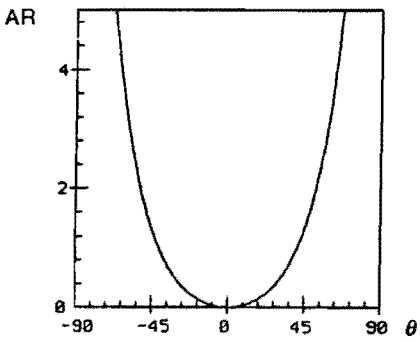

p

From fig. 4.6 the influence of β and ε_r on the axial ratio is apparent. On comparing the figures it can be seen that there is a correlation between β, ε_r and the axial ratio.
For a given β and increasing ε_r large values of the the axial ratio are suppressed thus improving the axial ratio (for example $\beta = 0.4$) over a wider range ϑ. When ε_r increases further the axial ratio gets worse.
On the other hand for a fixed value of ε_r and decreasing β the graphs exhibit similar properties. See for example graphs n,j,f,b. The pivot of this array of axial ratio plots with an optimum axial ratio, is the 'line' through the graphs a,j,o.

According to INMARSAT's specifications for voice channels, the maximum acceptable axial ratio is 1 dB.
Based on fig. 4.6 it can be said that it is impossible for the elevation angles requested ($5^\circ \leq \vartheta \leq 90^\circ$) to meet this specification. Only for discrete angles ϑ is the axial ratio 1 dB. The MSATX organization has laid down less strict specifications with regard to the axial ratio: 4 dB for $20^\circ \leq \vartheta \leq 60^\circ$. From the graphs it can be seen that many combinations are possible in order to meet this specification. Although an exact relationship is difficult to establish, the figures indicate that for each ε_r or β an optimum axial ratio can be achieved. Either a low value for β and ε_r must be chosen or as β increases ε_r must also increase and vice versa.

As far as the gain requirement is concerned, table 4.1 summarizes the results of gain calculations. From the data in this table it may be concluded that for a fixed β and decreasing ε_r the gain increases. A similar behaviour observed when ε_r has a fixed value and β increases. The correspondence in the characteristics just discussed is that the outer radius (a) increases. This can easily be verified using eq. 3.19.
This is in agreement with the general rule for antennas:-when the dimensions of the antenna increase, the gain increases.
It is also obvious from this table that the gain requirement can not be met by a single element, accordingly array techniques must be applied and these are discussed in the next chapter.

Table 4.1 : Gain of ring patch antenna (dB) as function of β and ε_r , f_r=1.6 GHz , h=1.91 mm , tan(δ)0.001

β , χ_{11}	ε_r:	2.2	6.0	10.5
0.0 , 1.8411		6.7	4.8	4.0
0.2 , 1.9934		7.1	5.0	4.2
0.4 , 2.5015		8.5	5.7	4.6
0.6 , 3.7152		9.9	7.6	5.9

Last point that has to be studied is the input resistance of a dual feed circularly polarized microstrip antenna. In order to gain insight into the feed point location (ρ_o) circuit theory is applied. The circular polarized microstrip antenna is fed at two points and may therefore be evaluated by a two port (figure 4.7) [4-4]

Fig. 4.7 : Two port representation of circularly polarized microstrip antenna for calculation of the input impedance.

The equations for a two port may be written in terms of impedance coefficients:

$$\begin{bmatrix} V_1 \\ V_2 \end{bmatrix} = \begin{bmatrix} Z_{11} & Z_{12} \\ Z_{21} & Z_{22} \end{bmatrix} \begin{bmatrix} I_1 \\ I_2 \end{bmatrix} \qquad (4.37)$$

Thus the input impedance of port 1 can be calculated from:

$(Z_{2,b} = - V_2 / I_2)$

$$Z_{in} = Z_{11} - \frac{Z_{12}^2}{Z_{22} + Z_{2,b}} \qquad (4.38)$$

With $Z_{2,b}$ the load impedance on port 2.

Coefficients Z_{11} and Z_{22} are the input impedances of a microstrip antenna with just one feed. For the parameters Z_{12} and Z_{21} the following equation holds:

$$Z_{i,j} = \left. \frac{V_i}{I_j} \right|_{I_i=0} \qquad (4.39)$$

V_i is given by eq. 3.33 :

$$V_i(\rho_i,\phi_i) = h\, E_o \left[J_n(k\rho_i) - \frac{J_n(kb)}{Y_n(kb)}\, Y_n(k\rho_i) \right] \cos(\phi_i - \phi_j) \qquad (4.40)$$

Because the angle between feed 1 and 2 is 90° , the coefficients Z_{12} and Z_{21} are zero. From the results of this calculation it follows that there is no coupling between the two feeds.

From the afore consideration it is concluded that the input impedance in case of two feeds is exactly the same as one feed. Thus the position of the feed point location (ρ_o) remains the same.

4.3 Feeding network.

In the preceding sections the necessity of circular polarization having to be employed in mobile communication has been pointed out. This circular polarization can be realized by two signals with equal amplitude and a relative phase shift of 90° . The microwave components that bring about these conditions are discussed in this paragraph.

To generate a phase difference between two signals two transmission lines of different length are used.

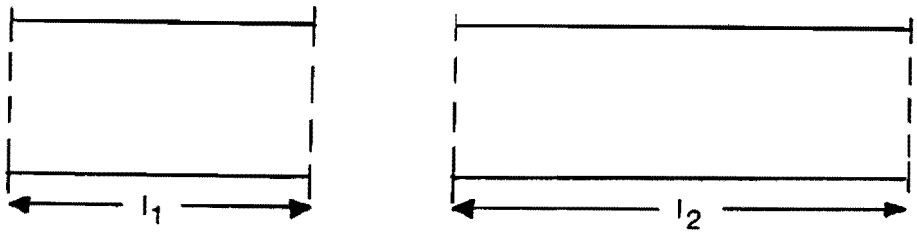

Fig. 4.9 : Phase difference caused by length difference of two transmission lines

Referring to figure 4.9 the phase difference at the end of the transmission lines is:

$$\Delta\phi = \frac{2\pi}{\lambda}\left[l_2 - l_1\right] = \frac{2\pi}{\lambda}\Delta l \qquad (4.41)$$

From this last formula it follows that this phase shifter is a frequency dependant element. A 90° phase difference between the two signals can be created when the difference in length is a quarter lambda.

These transmission lines must match the impedance of the antennas accordingly the design equations are therefore stated below.

The characteristic impedance (Z_o) of the transmission line is given by:

$$Z_o = \begin{cases} \dfrac{\eta}{2\pi\sqrt{\varepsilon_{r,eff}}}\ln\left(\dfrac{8h}{W} + \dfrac{4W}{h}\right) & W/h \le 1 \\ \dfrac{\eta}{\sqrt{\varepsilon_{r,eff}}}\left(\dfrac{W}{h} + 1.393 + 0.667\ln\left(\dfrac{W}{h} + 1.444\right)\right)^{-1} & W/h > 1 \end{cases} \qquad (4.42)$$

With $\eta = 120\pi$ (Ω), h the substrate thickness and W the width of the microstrip line. $\varepsilon_{r,eff}$ is the effective relative dielectric constant and can be calculated from:

$$\varepsilon_{r,eff} = \frac{\varepsilon_r + 1}{2} + \frac{\varepsilon_r - 1}{2} F(W/h) \qquad (4.43)$$

With:

$$F(W/h) = \begin{cases} \left(\sqrt{1 + 12 \frac{W}{h}} \right)^{-1} + 0.04 \left(1 - \frac{W}{h} \right)^2 & W/h \leq 1 \\ \left(\sqrt{1 + 12 \frac{W}{h}} \right)^{-1} & W/h < 1 \end{cases} \qquad (4.44)$$

Because the relative dielectric constant of the dielectric substrate differs from air, the wavelength in the substrate is given by:

$$\lambda_m = \frac{\lambda_o}{\sqrt{\varepsilon_{r,eff}}} \qquad (4.45)$$

The other element required for generating circular polarized waves is a power splitter. Various power splitters are known like T-splitter, Wilkinson splitter, hybrid branch line coupler, multi conductor coupler etc.. [4-5]
A Wilkinson-splitter is used in this report. Due to better isolation between the output ports, the choice for this type of splitter has been made.
In figure 4.10 the configuration of a Wilkinson-splitter is given.

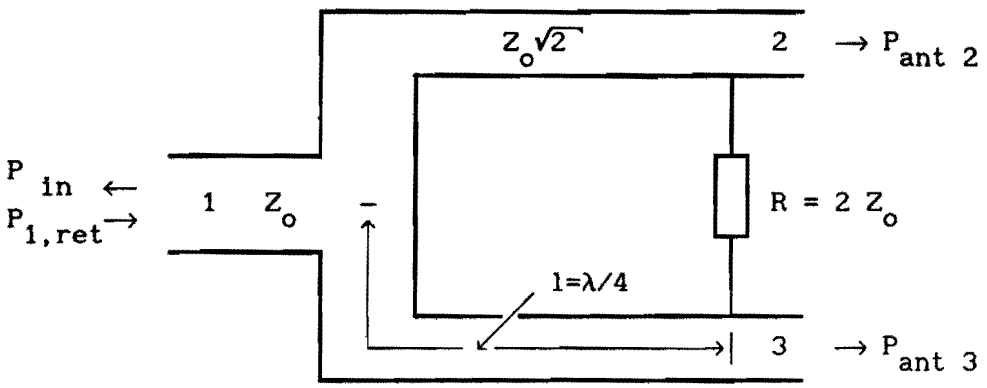

Fig. 4.10 : Layout of Wilkinson power splitter

It turns out that for equal power distribution, as required, the transmission lines and resistor must have the values indicated. Detailed information regarding this type of splitter is given in [4-6,4-7]. In the following paragraphs only a qualitative survey is given.

As shown in figure 4.10 the splitter has three ports.
The length of the transmission line between port 2 and 3 is a half wavelength. Gate 1 is connected at the middle of this transmission line. A resistor is placed between gate 2 and 3.
To obtain equal power distribution, the impedance of the quarter wave transformers, arm 2 and 3, must be equal. In other words, the power splitter must be symmetrical.

If reflected power from the antennas flows into port 2 and 3, energy will be dissipated in the resistor. This is because the half wavelength transmission line between gate 2 and 3. Reflected signals from, for example, gate 2 are at gate 3 180° out of phase with the signal at gate 2 and vice versa. Hence the reflected energy will be dissipated in the resistor.
Isolation between output ports and a good match is seen when looking in at any port and is procured by means of this resistor.

In figure 4.11 the power distribution, as function of the frequency of a Wilkinson-splitter designed for equal power splitting, is shown. The splitter is terminated by microstrip patches which are matched for their resonance frequency. All powers are normalized to the input power.

This figure shows that an equal amount of power is delivered to both output ports. Away from resonance most of the power returns at the input port and no power is dissipated in the isolation resistor.

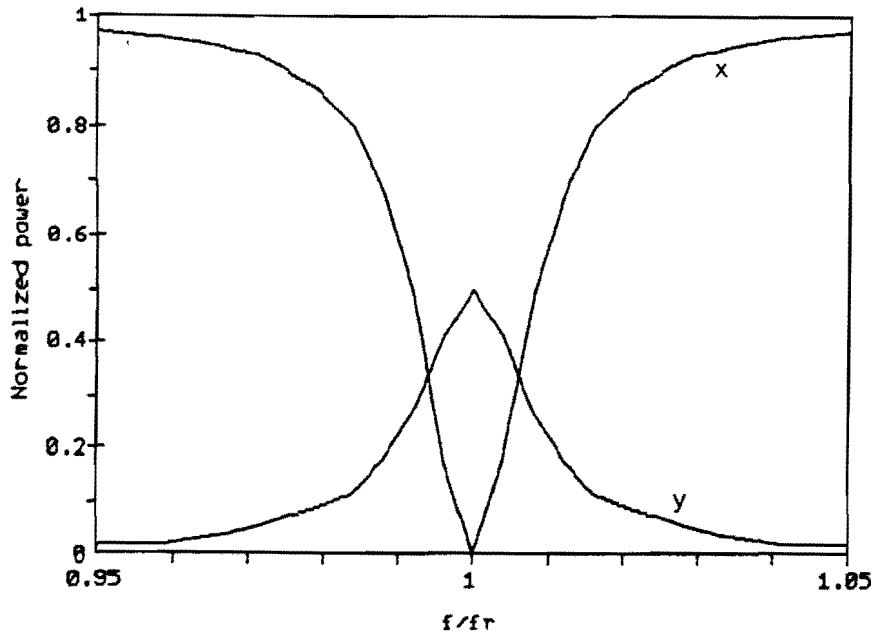

Fig. 4.11 : Power distribution Wilkinson power splitter.
TM_{11}-mode, $\beta=0$
fr=1.55 GHz , $\varepsilon_r=10.5$, $\tan(\delta)=0.0015$, h=2.54 mm
x : P_{ret} y : $P_2 = P_3$

In the next figure one of the output ports is provided with a quarter lambda transmission line to create a 90° phase shift.

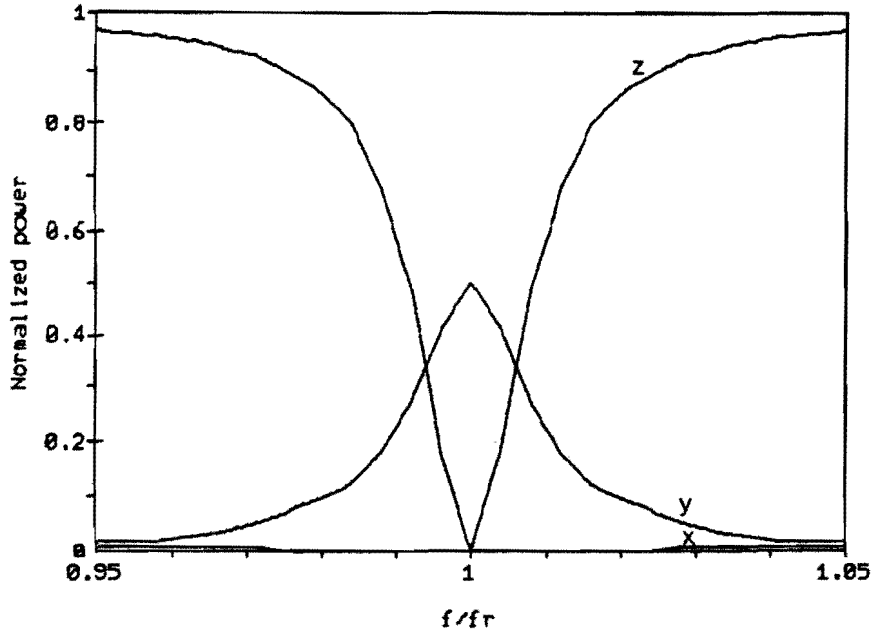

Fig. 4.12 : Power distribution Wilkinson power splitter with a quarter wavelength transmission line
TM_{11}-mode $\beta=0$
fr=1.55 GHz , $\varepsilon_r=10.5$, $\tan(\delta)=0.0015$, h=2.54 mm
x : P_{ret} y : $P_2 = P_3$ z = P_{diss}

From this figure it is clear that a small amount of power returns at the input port. The power delivered at port 2 and 3 are equal and most of the power returned is now dissipated in the isolation resistor. Accordingly the splitter is matched to the feeding network however most of the power reflected by mismatch of the microstrip antennas is dissipated in the resistor.
Measurements confirm this theory. [4-8]

To reduce the parasitic capacitance, corners of the microwave circuit are cut off. [4-9]

$W_c = 1.8\ W$

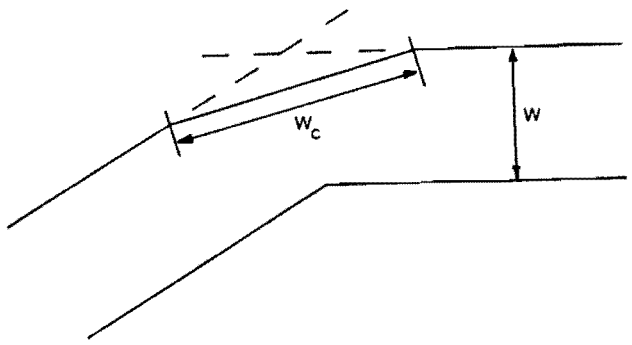

Fig. 4.13 : Reduction of parasitic capacitance of a microstrip circuit

Subsequently the total layout of the splitter and phase shifter is shown in figure 4.14.

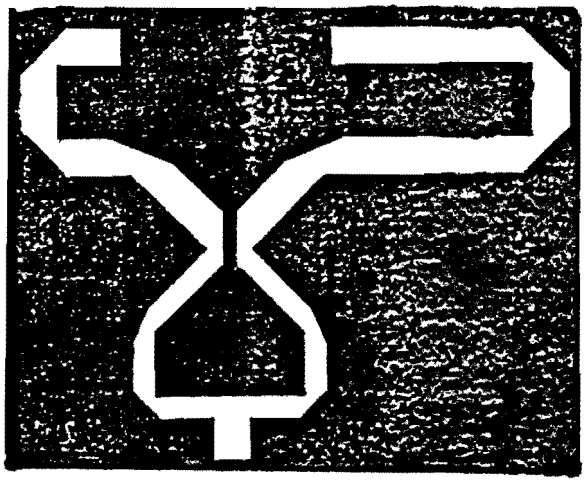

Fig. 4.14 : Wilkinson power splitter and feed network for circular polarized microstrip antenna
f_r = 1.6 GHz , ε_r = 2.2 , tan(δ) = 0.0009 , h = 1.57 mm

4.4 References.

[4-1] Jeuken M.E.J.,
'Elektromagnetische Golven en Antennes',
Lecture Notes, Eindhoven University of Technology. (in Dutch)

[4-2] Kraus J.D. and Carver K.R.,
'Electromagnetics',
Mc Graww-Hill, 1973, p. 426.

[4-3] Ma M.T.,
'Theory and Applications of Antenna Arrays',
John Wiley and Sons Inc., 1974, p. 2.

[4-4] Ramo S., Whinnery J.R. and Van Duzer T.,
'Fields and Waves in Communication Electronics',
John Wiley and Sons Inc., 1984. p. 530.

[4-5] Bahl I.J. and Bhartia P.,
'Microwave Solid State Circuit Design',
John Wiley and Sons Inc., 1988.

[4-6] Parad L.I. and Moynihan R.L.,
'Split-Tee Power Divider',
IEEE Transactions on Microwave Theory and Techniques, January 1965, p.91-95.

[4-7] Visser H.J.,
'Circularly Polarized Microstrip Phased Array Antennas for Mobile Communications', Master's Thesis, Professional Group Electromagnetism and Circuit Theory, Department of Electrical Engineering, Eindhoven University of Technology, Netherlands 1989, ET-3-89.

[4-8] Vrinten M.L.A.,
'A Wide band Circularly Polarized Microstrip Antenna Array', Master's Thesis, Professional Group Electromagnetism and Circuit Theory, Department of Electrical Engineering, Eindhoven University of Technology, Netherlands 1988, ET-4-88.

[4-9] Toom E.C. den,
'Microstripantenne voor de mobiele satelliet communicatie', Master's Thesis, Professional Group Electromagnetism and Circuit Theory ,Department of Electrical Engineering, Eindhoven University of Technology, Netherlands 1989, ET-8-89. (in Dutch)

5 Array with microstrip antennas.

In the previous chapters the radiation characteristics of single-element antennas were analyzed and discussed. The radiation pattern of a single element is relatively wide and one element provides low values of directivity (gain). From the specifications as laid down by INMARSAT for voice communication and MSATX, a gain of 10 - 12 dB must be achieved. It has been shown in chapter 4 this requirement can not be accomplished by a single element. Therefore the electrical size of the antenna has to be enlarged.
Enlarging the dimensions of the antenna is possible by forming an assembly of radiating elements. This new antenna is referred to as an array.

In the array several controls are available that can be used to shape the overall pattern of the antenna. These are: the individual elements (all the same or different), geometrical organization (linear, circular, rectangular etc.), relative displacement between the elements and the amplitude and phase excitation of the individual elements.

In the following the rectangular planar array (two dimensional planar array) configuration is discussed. To simplify this discussion, first the properties of a linear array are treated. Furthermore, the elements of which the array consists are identical; circular ring patch antennas. The elements are fed with a fixed amplitude and phase excitation, in other words: only 'fixed beam' arrays are discussed in this chapter.
By applying the appropriate phase shift to each of the elements, it will be possible to steer the beam away from broadside in any desired direction [5-1].

In the analyses performed here, the coupling between elements is neglected. The total field is determined by the vector addition of the fields radiated by the individual elements.

5.1 Array properties.

Linear array

Figure 5.1 shows a linear array consisting of M elements. The elements are considered point sources and are equally spaced along the X-axis by a distance d. The antenna is treated as receiving antenna.

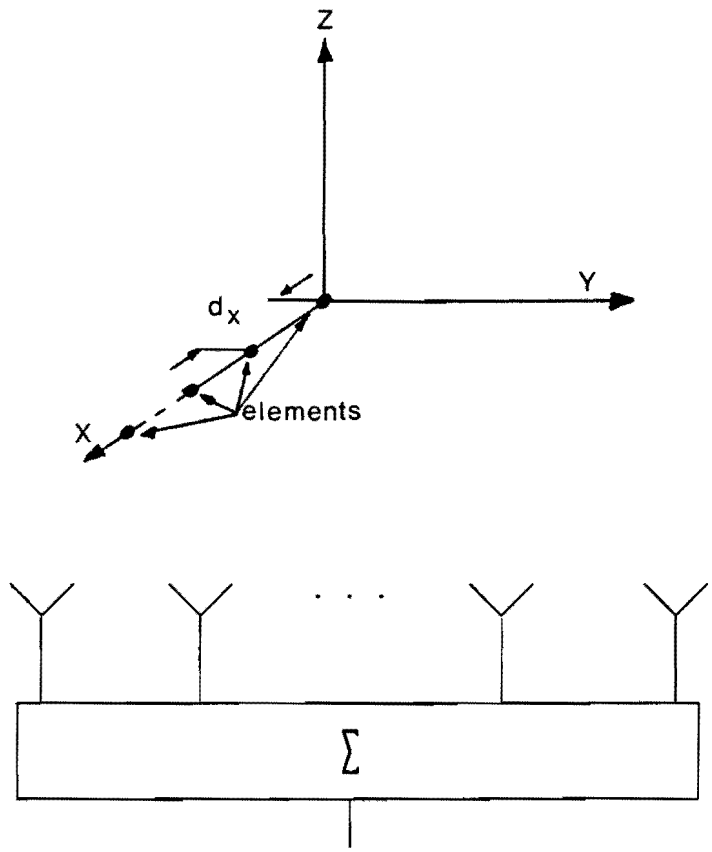

Fig. 5.1 : Linear array with elements along x-axis and summation network

Since all the points on the wave front have the same amplitude and phase, the phase difference between the signals arriving at two consecutive elements is:

$$\phi = \frac{2\pi}{\lambda_o} d \sin(\vartheta) \qquad (5.1)$$

$$= \frac{2\pi}{\lambda_o} d T \qquad (5.2)$$

with λ_o the wavelength in free space.
If the phase of the current from element 0 is zero, the current from element m can be written as:

$$I_m = S_m(\vartheta)\, e^{jm2\pi \frac{d}{\lambda} T} \qquad (5.3)$$

where $S_m(\vartheta,\phi)$ is proportional to the field of a single element at a selected reference point and is called the element factor. The other factor is called the array factor. The time variation $\exp(j\omega t)$ is omitted for the sake of convenience.

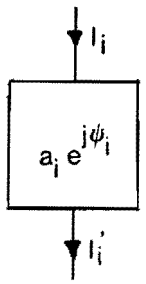

fig. 5.2 : Antenna network

If a network with a transfer function:

$$I_i' = I_i\, a_i\, e^{j\psi_i} \qquad (5.4)$$

is placed in the transmission line behind the i-th element where a_i and ψ_i are the current gain and phase shift of the network. The output signal of the summing network can be written as:

$$S(\vartheta) = \sum_{m=0}^{M-1} S_m(\vartheta)\, a_m\, e^{j\psi_m}\, e^{jm2\pi \frac{d}{\lambda} T} \qquad (5.5)$$

The same expression is valid for the radiation pattern of the array [5-1].

A grating lobe occurs when even the argument of $S_m(\vartheta)$ is a multiple of 2π . This means the array factor has multiple maxima of equal amplitude. The principal maximum is referred to as the major lobe and the remaining as the grating lobes. To avoid grating lobes in a linear array, it is necessary that:

$$\frac{d}{\lambda} \leq 1$$

Rectangular planar array

In figure 5.3 a two dimensional of the antenna array is shown. The elements along the X-axis are equally spaced at a distance d_x and along the Y-axis at a distance d_y.

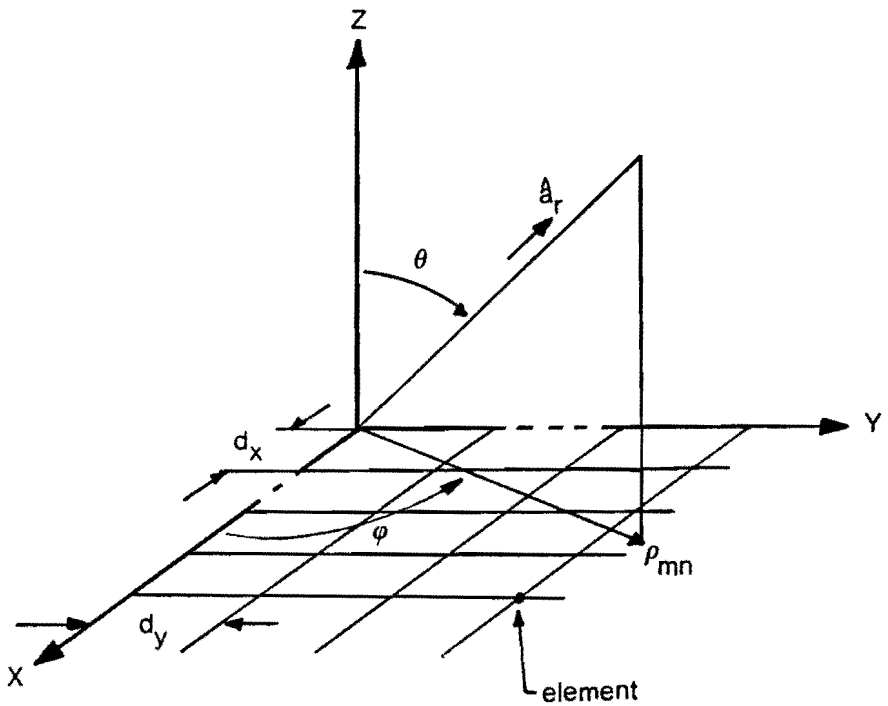

Fig. 5.3 : Planar array of radiating elements

The mn-th element of the array is located by a vector ρ_{mn} and is given by:

$$\bar{\rho}_{mn} = x_m \hat{a}_x + y_n \hat{a}_y \qquad (5.6)$$

Because of the spatial path difference between the mn-th element and the 00-th element a phase shift is introduced.
This phase delay is given by:

$$\phi_{mn} = \frac{2\pi}{\lambda} \bar{\rho}_{mn} \cdot \hat{a}_r \qquad (5.7)$$

with:

$$\hat{a}_r = \sin(\vartheta)\cos(\phi)\,\hat{a}_x + \sin(\vartheta)\sin(\phi)\,\hat{a}_y + \cos(\vartheta)\,\hat{a}_z$$

$$= T_x\,\hat{a}_x + T_y\,\hat{a}_y + T_z\,\hat{a}_z \qquad (5.8)$$

The phase difference between the mn-th element and the 00-th element is:

$$\phi_{mn} = \frac{2\pi}{\lambda}\left(x_m T_x + y_n T_y\right) \qquad (5.9)$$

For a rectangular planar array with M x N elements equally spaced along the X-axis at a distance d_x and equally spaced along the Y-axis at a distance d_y, the mn-th element is located at $x_m = m\,d_x$ and $y_n = n\,d_y$.
Analogous to eq. 5.5 the array pattern can be written as:

$$S(\vartheta,\phi) = \sum_{m=0}^{M-1}\sum_{n=0}^{N-1} S_{mn}(\vartheta,\phi)\,a_{mn}\,e^{j\psi_{mn}}\,e^{j\frac{2\pi}{\lambda}\left(md_xT_x + nd_yT_y\right)} \qquad (5.10)$$

To prevent grating lobes in this array:

$$\frac{d_x}{\lambda} \le 1 \qquad \frac{d_y}{\lambda} \le 1$$

5.2 Circularly polarized rectangular array with circularly polarized patches.

The rectangular array consists of M x N dual feed circularly polarized ring patch microstrip antennas. The patches will be considered point sources and the two orthogonal linear polarizations (horizontal and vertical) will be indicated by a horizontal and vertical arrow. To obtain circular polarization, a 90° phase shift between the two feeds of the antenna is introduced.

Consider the M x N array with equal spacing in the X-direction and Y-direction between the elements. The radiation pattern from this array can be calculated using eq. 5.10 where the term $S_{mn}(\vartheta,\phi)$ is

be replaced by $E_{mn}(\vartheta,\phi)$. All elements are fed with the same amplitude so a_{mn} is normalized at 1 and no phase difference between the elements is introduced and thus $\psi_{mn} = 0$.
In the following calculations the distance dependent part is left out of consideration.

For a circularly polarized patch and for the case $S(\vartheta,\phi) = E_\vartheta(\vartheta,\phi)$ using (eq. 4.26):

$$E_{mn}(\vartheta,\phi) = E_\vartheta(\vartheta,\phi) = - F_1(\vartheta)\, e^{j\phi} \tag{5.11}$$

and thus the ϑ-component of the total electric field becomes:

$$E_\vartheta(\vartheta,\phi) = - e^{j\phi}\, F_1(\vartheta) \sum_{m=0}^{M-1} \sum_{n=0}^{N-1} e^{j\frac{2\pi}{\lambda}\left(md_xT_x + nd_yT_y\right)} \tag{5.12}$$

Analogous $E_\phi(\vartheta,\phi)$ becomes:

$$E_\phi(\vartheta,\phi) = j\, e^{j\phi}\, F_2(\vartheta)\, \cos(\vartheta) \sum_{m=0}^{M-1} \sum_{n=0}^{N-1} e^{j\frac{2\pi}{\lambda}\left(md_xT_x + nd_yT_y\right)} \tag{5.13}$$

To determine the axial ratio of such an array the left and right hand polarized electric fields have to be calculated.

$$\begin{aligned} E_1(\vartheta,\phi) &= \frac{1}{\sqrt{2}} \left(E_\vartheta(\vartheta,\phi) - j\, E_\phi(\vartheta,\phi) \right) \\ &= - e^{j\phi}\, \frac{1}{\sqrt{2}} \left(F_1(\vartheta) - \cos(\vartheta)\, F_2(\vartheta) \right) \\ &\quad \sum_{m=0}^{M-1} \sum_{n=0}^{N-1} e^{j\frac{2\pi}{\lambda}\left(md_xT_x + nd_yT_y\right)} \end{aligned} \tag{5.14}$$

$$E_r(\vartheta,\phi) = \frac{1}{\sqrt{2}} \left(E_\vartheta(\vartheta,\phi) + j\, E_\phi(\vartheta,\phi) \right)$$

$$= - e^{j\phi} \frac{1}{\sqrt{2}} \left(F_1(\vartheta) + \cos(\vartheta)\, F_2(\vartheta) \right)$$

$$\sum_{m=0}^{M-1} \sum_{n=0}^{N-1} e^{j \frac{2\pi}{\lambda} \left(m d_x T_x + n d_y T_y \right)} \qquad (5.15)$$

The axial ratio is given by:

$$AR = \left| \frac{| F_1(\vartheta) + F_2(\vartheta) \cos(\vartheta) | + | F_1(\vartheta) - F_2(\vartheta) \cos(\vartheta) |}{| F_1(\vartheta) + F_2(\vartheta) \cos(\vartheta) | - | F_1(\vartheta) - F_2(\vartheta) \cos(\vartheta) |} \right| \qquad (5.16)$$

This formula for the axial ratio for an M x N array is exactly the same as for a single circularly polarized patch.
Note that the axial ratio is ϕ- and d- independent.

To decide what number of patches are necessary to meet the 10 - 12 dB gain requirement, the directivity as function of the element spacing is calculated.
The directivity is defined as: [5-3]

$$D = 4\pi \frac{|\bar{E}(\vartheta,\phi)|^2_{max}}{\int_0^{\pi/2} \int_0^{2\pi} |\bar{E}(\vartheta,\phi)|^2 \sin(\vartheta)\, d\vartheta\, d\phi} \qquad (5.17)$$

The series:

$$\sum_{m=0}^{M-1} \sum_{n=0}^{N-1} e^{j \frac{2\pi}{\lambda} \left(m d_x T_x + n d_y T_y \right)} =$$

$$\left[\frac{e^{j \frac{2\pi}{\lambda} d_x T_x M} - 1}{e^{j \frac{2\pi}{\lambda} d_x T_x} - 1} \right] \left[\frac{e^{j \frac{2\pi}{\lambda} d_y T_y N} - 1}{e^{j \frac{2\pi}{\lambda} d_y T_y} - 1} \right] \qquad (5.18)$$

The modulus becomes:

$$\left| \frac{\sin\left(\frac{\pi}{\lambda} M\, d_x\, T_x\right)}{\sin\left(\frac{\pi}{\lambda}\, d_x\, T_x\right)} \right| \left| \frac{\sin\left(\frac{\pi}{\lambda} N\, d_y\, T_y\right)}{\sin\left(\frac{\pi}{\lambda}\, d_y\, T_y\right)} \right| \qquad (5.19)$$

Substituting this in eq. 517 the directivity becomes:

$$D = \frac{4\,\pi \left(F_1^2(0) + F_2^2(0) \right) M^2\, N^2}{\int_0^{\pi/2}\int_0^{2\pi} \left(F_1^2(\vartheta) + F_2^2(\vartheta)\cos^2(\vartheta) \right) \frac{\sin^2\left(\frac{\pi}{\lambda} M\, d_x\, T_x\right)\sin^2\left(\frac{\pi}{\lambda} N\, d_y\, T_y\right)}{\sin^2\left(\frac{\pi}{\lambda}\, d_x\, T_x\right)\ \sin^2\left(\frac{\pi}{\lambda}\, d_y\, T_y\right)} \sin(\vartheta)\, d\vartheta\, d\phi} \qquad (5.20)$$

In fig 5.4 the results of the calculations for the directivity of a 2 x 2 and 4 x 4 array are compiled together.

A comparative survey of the individual graphs in fig. 5.4 shows that the directivity of the array increases with increasing d/λ . But at a certain spacing (d/λ) between the elements the directivity starts to decrease. This effect is reported before [5-4] and a short explanation is given here. For further details the book mentioned is advised.
In the denominator of eq. 5.20 integration of the angle ϑ is carried out. Introducing a new variable u (= k d sin(ϑ)) and substituting this in the denominator now integration over u has to be carried out. The integration limits are replaced by 0 (ϑ = 0) and k d (ϑ = $\pi/2$). This formula shows the influence of d.
Suppose the element distance increases and as a result the integration interval increases too. In other words:-integration has to be performed over a wider interval i.e. other lobes of the radiation pattern are integrated too.
The distance between the array elements does not affect value of the nominator and the directivity starts to decrease.
Since the antenna gain (G) is given by $G = \eta_r D$, the antenna gain is found from the directivity by adding the efficiency in dB.

ε_r = 2.2

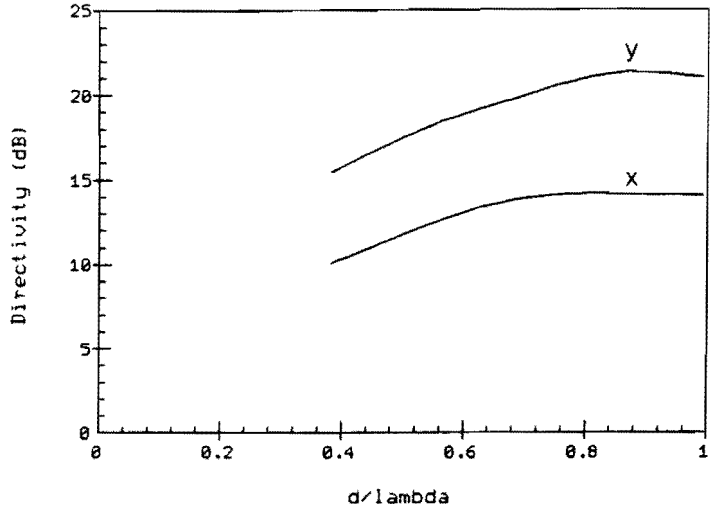

ε_r = 6.0

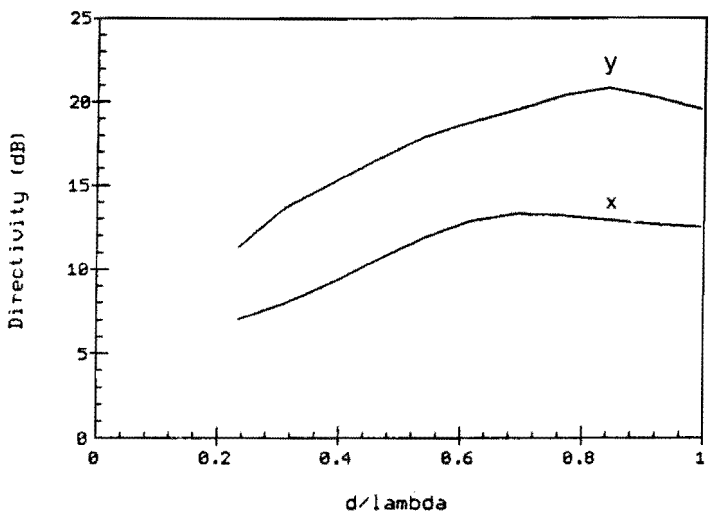

ε_r = 10.5

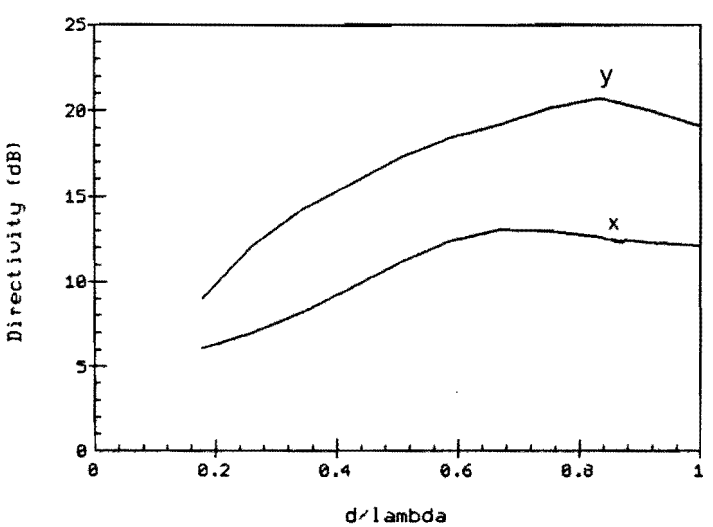

Fig. 5.4 a: Directivity (dB) vs element spacing (d/λ) for different square arrays which consist of circularly polarized patches : β=0.0

x: 2 × 2 array y: 4 × 4 array

ε_r = 2.2

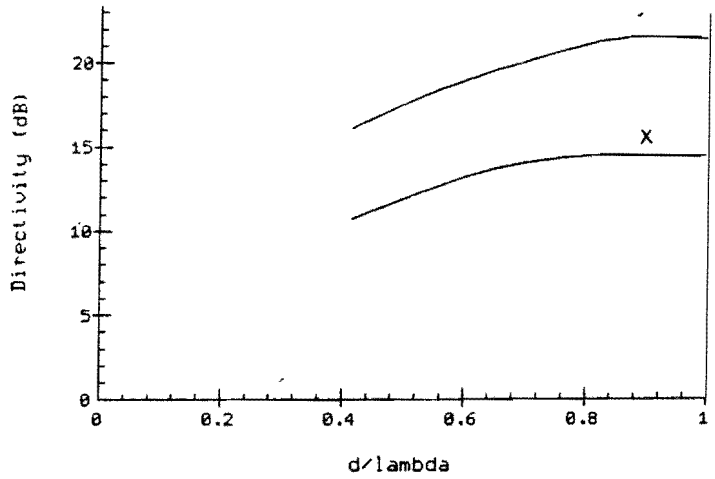

ε_r = 6.0

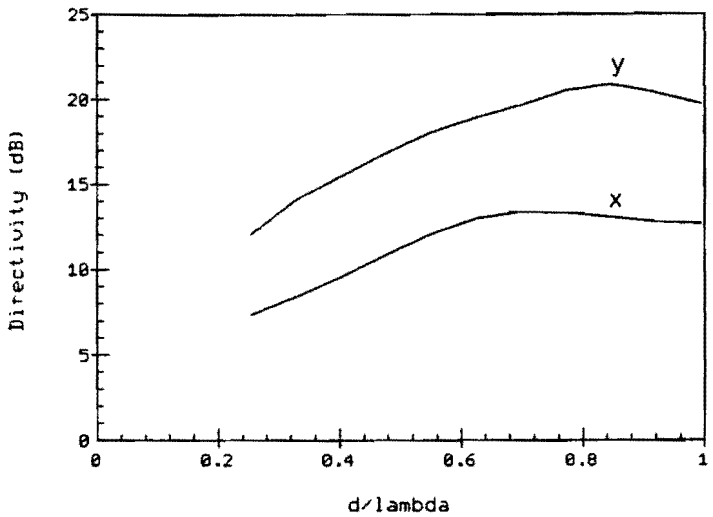

ε_r = 10.5

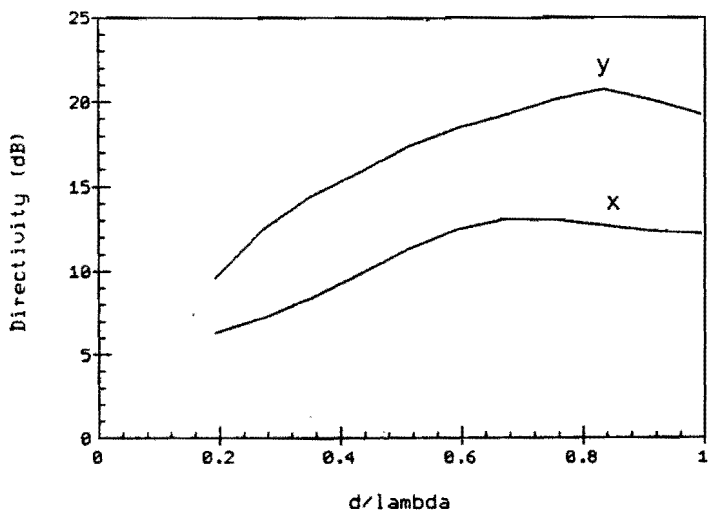

Fig. 5.4 b: Directivity (dB) vs element spacing (d/λ) for different square arrays which consist of circularly polarized patches : β=0.2

x: 2 × 2 array y: 4 × 4 array

ε_r = 2.2

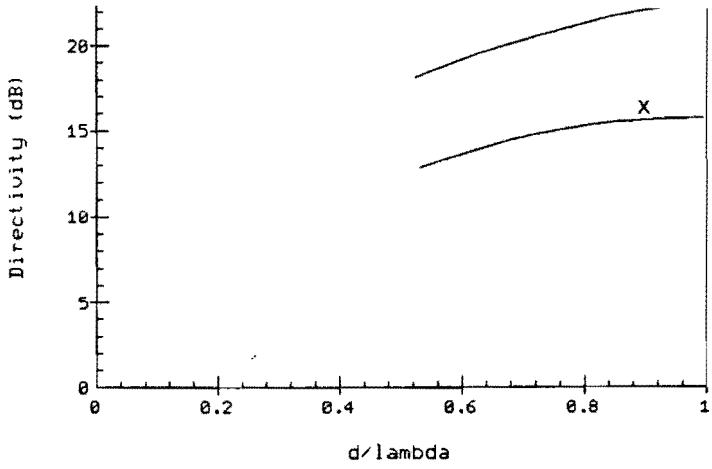

ε_r = 6.0

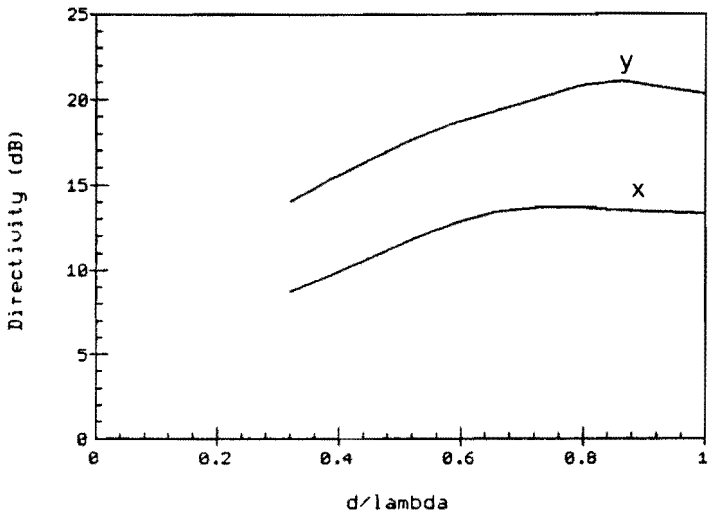

ε_r = 10.5

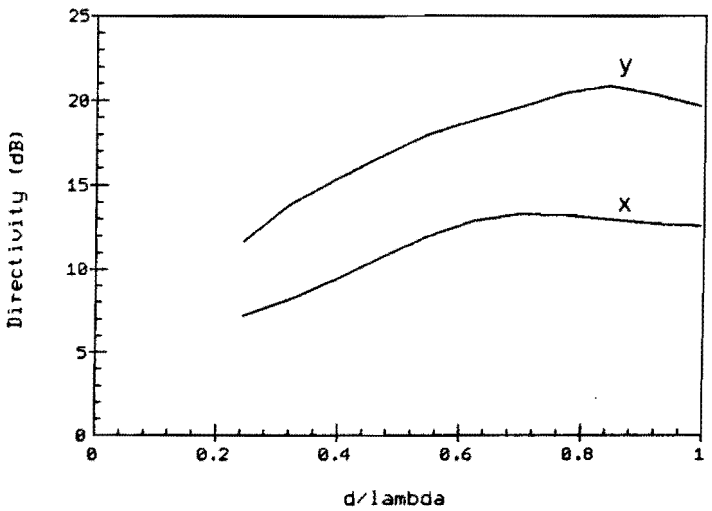

Fig. 5.4 c: Directivity (dB) vs element spacing (d/λ) for different square arrays which consist of circularly polarized patches : β=0.4

x: 2 × 2 array y: 4 × 4 array

ε_r = 2.2

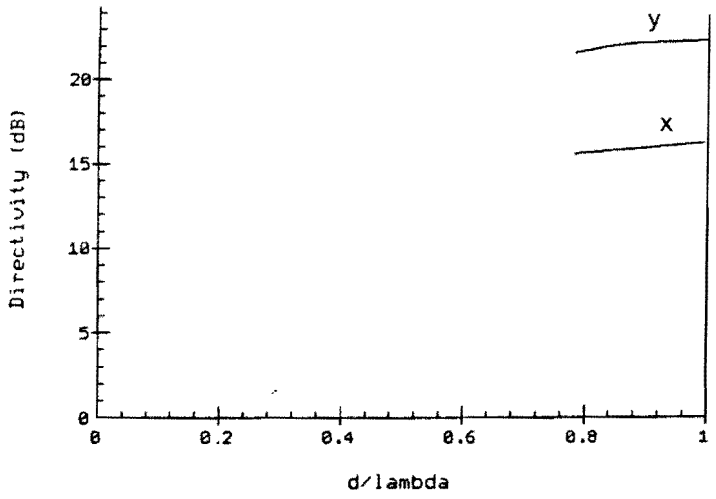

ε_r = 6.0

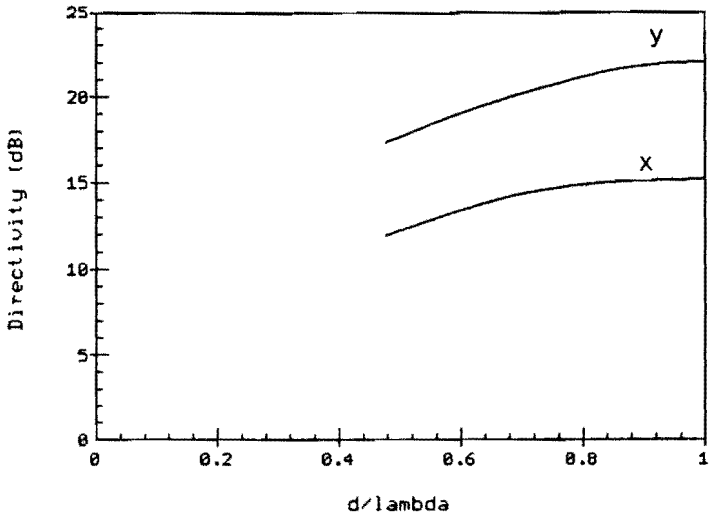

ε_r = 10.5

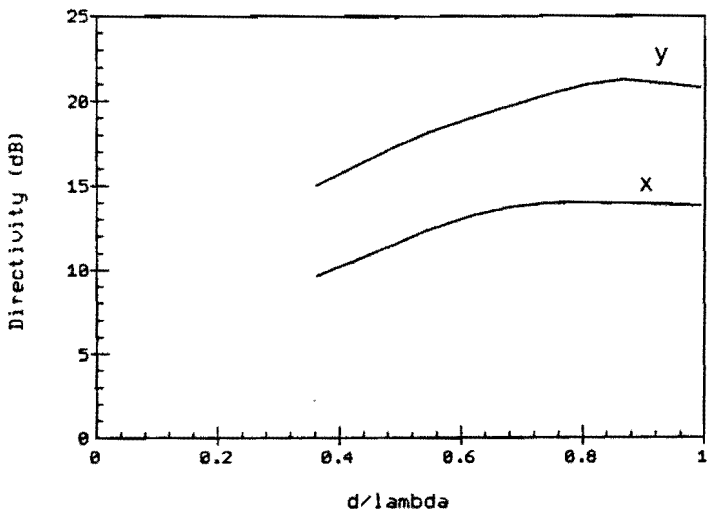

Fig. 5.4 d: Directivity (dB) vs element spacing (d/λ) for different square arrays which consist of circularly polarized patches : β=0.6

x: 2 × 2 array y: 4 × 4 array

From these figures it can also be see that the directivity follows the general trend that an increase in β for a fixed ε_r gives a corresponding increase of the directivity. Reducing ε_r for a fixed β results in an increase of the directivity.
The same behavior was observed for a single element microstrip antenna (chapter 4). and this is based on the same cause.

The ϕ-independence of an array composed of circularly polarized elements is a great advantage as will turn out when circularly polarized arrays composed of linearly polarized elements are discussed.

To meet the gain requirements and obtain good circular polarization a 2 x 2 array with an element spacing of about 0,75 λ a substrate with ε_r = 2.33 and β = 0.3 can be chosen.

The great disadvantage of an array composed of circularly polarized patches is the great number of coaxial to patch connections (2MN) and power splitter (at least MN).
By using linearly polarized elements and employing the technique of sequential rotation, a circularly polarized array can be obtained and the number of connections and power splitters can be halved.

5.3 Circularly polarized array with linearly polarized patches.

Instead of using circularly polarized antenna elements linearly polarized elements can be used to obtain a circular polarized array. This technique is called sequential rotation. In the report the 'limited' sequential rotation technique and the 'complete' sequential rotation technique are discussed. The meaning of the terms 'limited' and 'complete' becomes apparent henceforth.

Limited sequential rotation technique

Circular polarization in the broadside direction can be achieved by an array composed of two linearly polarized elements with angle and phase arranged in a 0° , 90° fashion [5-1,5-5]. Such an array is shown in fig. 5.5.

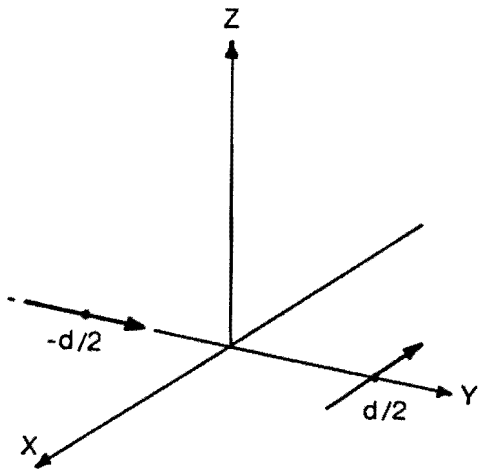

Fig. 5.5 : Array of two linearly polarized elements

For large angles ϑ however, the axial ratio already becomes poor because of the spatial phase difference ($\Delta\psi = k_o d \sin(\vartheta)$) that disturbs the 90° phase delay between the two elements (figure 5.6).

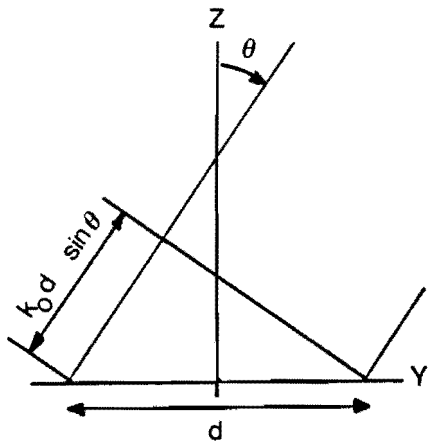

Fig. 5.6 : Spatial phase delay

The circular polarization degradation off broadside can be improved by placing four elements in the fashion shown in figure 5.7.

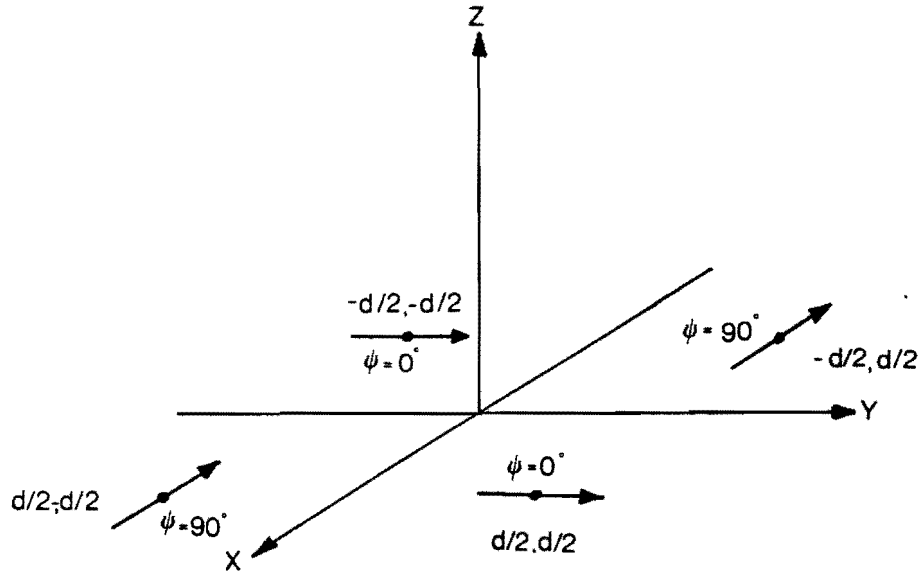

fig 5.7 : 2 × 2 array of linearly polarized elements which eliminates spatial phase delay

In the planes $\phi = 0^\circ$ and $\phi = 90^\circ$ the spatial phase difference in one row or column is opposite to that of the other row or column and, consequently, they cancel each other.

The electric field components can be calculated from:

$$E_\vartheta(\vartheta,\phi) = \sum_{p=0}^{1} \sum_{q=0}^{1} E_{\vartheta\,p,q}(\vartheta,\phi)\; e^{\,j\frac{2\pi}{\lambda}\left(p\,d_x\,T_x + q\,d_y\,T_y\right)} \tag{5.21}$$

$$E_\phi(\vartheta,\phi) = \sum_{p=0}^{1} \sum_{q=0}^{1} E_{\phi\,p,q}(\vartheta,\phi)\; e^{\,j\frac{2\pi}{\lambda}\left(p\,d_x\,T_x + q\,d_y\,T_y\right)} \tag{5.22}$$

With $E_{\vartheta\,p,q}(\vartheta,\phi)$ and $E_{\phi\,p,q}(\vartheta,\phi)$ the far field components of a linearly polarized patch (eq. 3.26 and 3.27).

For the TM_{11}-mode, these far fields are given by:

$$E_\vartheta(\vartheta,\phi) = -\,j\,\frac{E_o a h k_o}{2}\,\frac{e^{-jk_o r}}{r}\left[J_1(ka) - \alpha\,Y_1(ka)\right]$$

$$\left[J_0(X) - J_2(X)\right]\cos(\phi)$$

$$= -\,A(r)\,F_1(\vartheta)\cos(\phi) \tag{5.23}$$

$$E_\phi(\vartheta,\phi) = \;j\,\frac{E_o a h k_o}{2}\,\frac{e^{-jk_o r}}{r}\left[J_1(ka) - \alpha\,Y_1(ka)\right]$$

$$\left[J_0(X) + J_2(X)\right]\cos(\vartheta)\,\sin(\phi)$$

$$= A(r)\,F_2(\vartheta)\cos(\vartheta)\,\sin(\phi) \tag{5.24}$$

With:

$$A(r) = j\,\frac{E_o a h k_o}{2}\,\frac{e^{-jk_o r}}{r}\left[J_1(ka) - \alpha\,Y_1(ka)\right]$$

$$F_1(\vartheta) = J_0(X) - J_2(X)$$
$$F_2(\vartheta) = J_0(X) + J_2(X)$$
$$X = k_o\,a\,\sin(\vartheta)$$

$$\alpha = \frac{J_1(kb)}{Y_1(kb)}$$

Leaving the distance dependant part out of it, the following relations exist between the individual field components of the array in figure 5.7:

$$
\begin{aligned}
E_{\vartheta_{00}} &= E_{\vartheta_{11}} = -\cos(\phi)\, F_1(\vartheta) \\
E_{\phi_{00}} &= E_{\phi_{11}} = \cos(\vartheta)\sin(\phi)\, F_2(\vartheta) \\
E_{\vartheta_{01}} &= E_{\vartheta_{10}} = -j\sin(\phi)\, F_1(\vartheta) \\
E_{\phi_{01}} &= E_{\phi_{10}} = -j\cos(\vartheta)\cos(\phi)\, F_2(\vartheta)
\end{aligned}
\tag{5.25}
$$

Now the field contributions of the individual elements are known, the total electric field of the array can be calculated.

$$
\begin{aligned}
E_\vartheta(\vartheta,\phi) &= E_{\vartheta_{00}} + E_{\vartheta_{01}} e^{j\frac{2\pi}{\lambda} d_y T_y} + E_{\vartheta_{10}} e^{j\frac{2\pi}{\lambda} d_x T_x} + \\
&\quad E_{\vartheta_{11}} e^{j\frac{2\pi}{\lambda}\left(d_x T_x + d_y T_y\right)} \\
&= -\cos(\phi)\, F_1(\vartheta)\left(1 + e^{j\frac{2\pi}{\lambda}\left(d_x T_x + d_y T_y\right)}\right) + \\
&\quad -j\sin(\phi)\, F_1(\vartheta)\left(e^{j\frac{2\pi}{\lambda} d_y T_y} + e^{j\frac{2\pi}{\lambda} d_x T_x}\right)
\end{aligned}
\tag{5.26}
$$

$$
\begin{aligned}
E_\phi(\vartheta,\phi) &= E_{\phi_{00}} + E_{\phi_{01}} e^{j\frac{2\pi}{\lambda} d_y T_y} + E_{\phi_{10}} e^{j\frac{2\pi}{\lambda} d_x T_x} + \\
&\quad E_{\phi_{11}} e^{j\frac{2\pi}{\lambda}\left(d_x T_x + d_y T_y\right)}
\end{aligned}
$$

$$= \cos(\vartheta)\,\sin(\phi)\,F_2(\vartheta)\left[1 + e^{j\frac{2\pi}{\lambda}\left(d_x T_x + d_y T_y\right)}\right] +$$

$$- j\,\cos(\vartheta)\,\cos(\phi)\,F_2(\vartheta)\left[e^{j\frac{2\pi}{\lambda} d_y T_y} + e^{j\frac{2\pi}{\lambda} d_x T_x}\right] \qquad (5.27)$$

$$T_x = \sin(\vartheta)\,\cos(\phi)$$
$$T_y = \sin(\vartheta)\,\sin(\phi)$$

With these equations the left and right hand polarized electric fields can be calculated:

$$E_l(\vartheta,\phi) = \frac{1}{\sqrt{2}}\left(E_\vartheta(\vartheta,\phi) - j\,E_\phi(\vartheta,\phi)\right)$$

$$= \frac{1}{\sqrt{2}}\Bigg[-\left(\cos(\phi)\,F_1(\vartheta) + j\,\cos(\vartheta)\,\sin(\phi)\,F_2(\vartheta)\right)\left[1 + e^{j\frac{2\pi}{\lambda}\left(d_x T_x + d_y T_y\right)}\right] +$$

$$- j\left(\sin(\phi)\,F_1(\vartheta) - j\,\cos(\vartheta)\,\cos(\phi)\,F_2(\vartheta)\right)\left[e^{j\frac{2\pi}{\lambda} d_y T_y} + e^{j\frac{2\pi}{\lambda} d_x T_x}\right]\Bigg] \qquad (5.28)$$

And:

$$E_r(\vartheta,\phi) = \frac{1}{\sqrt{2}}\left(E_\vartheta(\vartheta,\phi) + j\,E_\phi(\vartheta,\phi)\right)$$

$$= \frac{1}{\sqrt{2}} \left[- \left(\cos(\phi)\, F_1(\vartheta) - j \cos(\vartheta) \sin(\phi)\, F_2(\vartheta) \right) \right.$$

$$\left(1 + e^{j \frac{2\pi}{\lambda} \left(d_x T_x + d_y T_y \right)} \right) +$$

$$- j \left(\sin(\phi)\, F_1(\vartheta) + j \cos(\vartheta) \cos(\phi)\, F_2(\vartheta) \right)$$

$$\left. \left(e^{j \frac{2\pi}{\lambda} d_y T_y} + e^{j \frac{2\pi}{\lambda} d_x T_x} \right) \right] \qquad (5.29)$$

For the principal planes ($\phi = 0^\circ$ and $\phi = 90^\circ$) and for an array with equally spaced elements ($d_x = d_y = d$) the left and right polarized fields become:

$$|E_l| = \sqrt{2}\ |\ F_1(\vartheta) + F_2(\vartheta) \cos(\vartheta)\ |\ \cos\left(\frac{1}{2}\ \frac{2\pi}{\lambda}\ d \sin(\vartheta) \right) \qquad (5.30)$$

$$|E_r| = \sqrt{2}\ |\ F_1(\vartheta) - F_2(\vartheta) \cos(\vartheta)\ |\ \cos\left(\frac{1}{2}\ \frac{2\pi}{\lambda}\ d \sin(\vartheta) \right) \qquad (5.31)$$

So the axial ratio for these planes is:

$$AR = \left| \frac{|\ F_1(\vartheta) + F_2(\vartheta) \cos(\vartheta)\ | + |\ F_1(\vartheta) - F_2(\vartheta) \cos(\vartheta)\ |}{|\ F_1(\vartheta) + F_2(\vartheta) \cos(\vartheta)\ | - |\ F_1(\vartheta) - F_2(\vartheta) \cos(\vartheta)\ |} \right| \qquad (5.32)$$

This formula is exactly the same as that one found for a single circularly polarized patch. Notice this formula is only valid for the planes $\phi = 0^\circ$ and $\phi = 90^\circ$ and is independent of the element spacing d and ϕ.

However in the plane $\phi = 45^\circ$, the axial ratio is described by another formula and the quality of the circularly polarized wave deteriorates quickly with increasing ϑ.

The fields now become($T_x = T_y = 1/\sqrt{2}\ \sin(\vartheta) = T$):

$$E_1(\vartheta,\phi) = -\frac{1}{2}\left[\left(F_1(\vartheta) + j\cos(\vartheta)\,F_2(\vartheta)\right)\left(1 + e^{j\frac{4\pi}{\lambda}dT}\right) + 2j\left(F_1(\vartheta) - j\cos(\vartheta)\,F_2(\vartheta)\right)e^{j\frac{2\pi}{\lambda}dT}\right]$$

$$= -e^{j\frac{2\pi}{\lambda}dT}\left[\left(F_1(\vartheta) + j\cos(\vartheta)\,F_2(\vartheta)\right)\cos\left(\frac{2\pi}{\lambda}dT\right) + j\left(F_1(\vartheta) - j\cos(\vartheta)\,F_2(\vartheta)\right)\right] \qquad (5.33)$$

$$|E_1(\vartheta,\phi)|^2 = \left(F_1^2(\vartheta) + F_2^2(\vartheta)\cos^2(\vartheta)\right)\left(1 + \cos^2\left(\frac{2\pi}{\lambda}dT\right)\right) + 4F_1(\vartheta)\,F_2(\vartheta)\cos(\vartheta)\cos\left(\frac{2\pi}{\lambda}dT\right) \qquad (5.34)$$

$$E_r(\vartheta,\phi) = -\frac{1}{2}\left[\left(F_1(\vartheta) - j\cos(\vartheta)\,F_2(\vartheta)\right)\left(1 + e^{j\frac{4\pi}{\lambda}dT}\right) + 2j\left(F_1(\vartheta) + j\cos(\vartheta)\,F_2(\vartheta)\right)e^{j\frac{2\pi}{\lambda}dT}\right]$$

$$= -e^{j\frac{2\pi}{\lambda}dT}\left[\left(F_1(\vartheta) - j\cos(\vartheta)\,F_2(\vartheta)\right)\cos\left(\frac{2\pi}{\lambda}dT\right) + j\left(F_1(\vartheta) + j\cos(\vartheta)\,F_2(\vartheta)\right)\right] \qquad (5.35)$$

$$|E_r(\vartheta,\phi)|^2 = \left(F_1^2(\vartheta) + F_2^2(\vartheta)\cos^2(\vartheta)\right)\left(1 + \cos^2\left(\frac{2\pi}{\lambda}dT\right)\right) - 4F_1(\vartheta)\,F_2(\vartheta)\cos(\vartheta)\cos\left(\frac{2\pi}{\lambda}dT\right) \qquad (5.36)$$

The wave is linearly polarized when:

$$\cos\left(\frac{2\pi}{\lambda}\, d\, T\right) = \cos\left(\frac{2\pi}{\lambda}\, d\, 1/\sqrt{2}\, \sin(\vartheta_{lp})\right) = 0$$

ϑ_{lp} is given by:

$$\vartheta_{lp} = \arcsin\left(\frac{\lambda}{4\,d}\sqrt{2}\right) \qquad (5.37)$$

As long as $d < \frac{1}{4}\sqrt{2}\,\lambda$, for no angle ϑ linear polarization appears.

If the array consists of several sub arrays as indicated in figure 5.7, the total electric field can be calculated by taking the just calculated electric fields of the 2 x 2 sub array and then adding all the sub array-fields taking into account the position of each sub array.

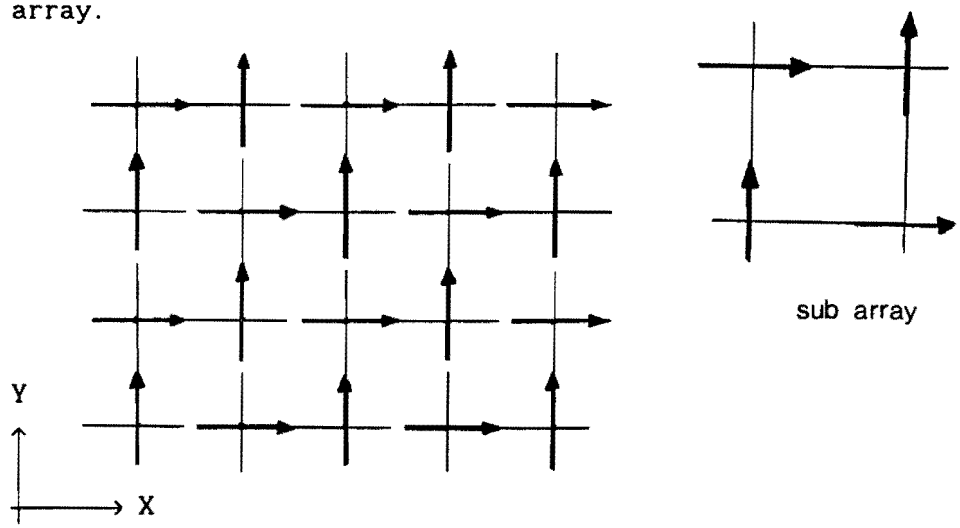

Fig. 5.8 : Four element sequentially rotated linearly polarized patches

So $E_\vartheta(\vartheta,\phi)$ and $E_\phi(\vartheta,\phi)$ of such an array can be calculated from:

$$E_\vartheta(\vartheta,\phi) = E_{\vartheta\,sub}(\vartheta,\phi) \sum_{m=0}^{\frac{M-2}{2}} \sum_{n=0}^{\frac{N-2}{2}} e^{j\frac{2\pi}{\lambda}\left(2d_x T_x + 2d_y T_y\right)} \qquad (5.38)$$

$$E_\phi(\vartheta,\phi) = E_{\phi\,sub}(\vartheta,\phi) \sum_{m=0}^{\frac{M-2}{2}} \sum_{n=0}^{\frac{N-2}{2}} e^{j\frac{2\pi}{\lambda}\left(2d_x T_x + 2d_y T_y\right)} \qquad (5.39)$$

The radiation pattern of the left and right hand polarized field for an arbitrary array are:

$$E_l(\vartheta,\phi) = \frac{1}{\sqrt{2}} \left(E_{\vartheta_{sub}}(\vartheta,\phi) - j\, E_{\phi_{sub}}(\vartheta,\phi) \right) \sum_{m=0}^{\frac{M-2}{2}} \sum_{n=0}^{\frac{N-2}{2}} e^{j\frac{2\pi}{\lambda}\left(2d_x T_x + 2d_y T_y\right)} \qquad (5.40)$$

$$E_r(\vartheta,\phi) = \frac{1}{\sqrt{2}} \left(E_{\vartheta_{sub}}(\vartheta,\phi) + j\, E_{\phi_{sub}}(\vartheta,\phi) \right) \sum_{m=0}^{\frac{M-2}{2}} \sum_{n=0}^{\frac{N-2}{2}} e^{j\frac{2\pi}{\lambda}\left(2d_x T_x + 2d_y T_y\right)} \qquad (5.41)$$

Now the axial ratio is:

$$AR = \left| \frac{\left| E_{\vartheta_{sub}}(\vartheta,\phi) - j\, E_{\phi_{sub}}(\vartheta,\phi) \right| + \left| E_{\vartheta_{sub}}(\vartheta,\phi) + j\, E_{\phi_{sub}}(\vartheta,\phi) \right|}{\left| E_{\vartheta_{sub}}(\vartheta,\phi) - j\, E_{\phi_{sub}}(\vartheta,\phi) \right| - \left| E_{\vartheta_{sub}}(\vartheta,\phi) + j\, E_{\phi_{sub}}(\vartheta,\phi) \right|} \right| \qquad (5.42)$$

For the plane $\phi = 0^\circ$ and $\phi = 90^\circ$ the axial ratio is the same as the axial ratio for a single circularly polarized patch. This was already mentioned before.

The gain of an array with linearly polarized elements can be calculated as follows:

$$D = 4\pi \frac{\left|\bar{E}(\vartheta,\phi)\right|^2_{max}}{\int_0^{\pi/2} \int_0^{2\pi} \left|\bar{E}(\vartheta,\phi)\right|^2 \sin(\vartheta)\, d\vartheta\, d\phi}$$

where the term $\left|\bar{E}(\vartheta,\phi)\right|^2$ is given by:

$$|\bar{E}(\vartheta,\phi)|^2 = |E_\vartheta(\vartheta,\phi)|^2 + |E_\phi(\vartheta,\phi)|^2$$

$$= \left(|E_{\vartheta_{sub}}(\vartheta,\phi)|^2 + |E_{\phi_{sub}}(\vartheta,\phi)|^2 \right)$$

$$\left| \sum_{m=0}^{\frac{M-2}{2}} \sum_{n=0}^{\frac{N-2}{2}} e^{j\frac{4\pi}{\lambda}\left(d_x T_x + d_y T_y\right)} \right|$$

$$= \left(|E_{\vartheta_{sub}}(\vartheta,\phi)|^2 + |E_{\phi_{sub}}(\vartheta,\phi)|^2 \right)$$

$$\frac{\sin^2\left(\frac{\pi}{\lambda} M\, d_x\, T_x\right) \sin^2\left(\frac{\pi}{\lambda} N\, d_y\, T_y\right)}{\sin^2\left(\frac{\pi}{\lambda}\, d_x\, T_x\right)\ \sin^2\left(\frac{\pi}{\lambda}\, d_y\, T_y\right)} \qquad (5.43)$$

Using formulas 5.26 and 5.27 working this out gives:

$$E_{\vartheta_{sub}}(\vartheta,\phi) = -F_1(\vartheta) \left[\cos(\phi) \left(1 + e^{j\frac{2\pi}{\lambda}\left(d_x T_x + d_y T_y\right)} \right) + \right.$$

$$\left. j \sin(\phi)\, F_1(\vartheta) \left(e^{j\frac{2\pi}{\lambda} d_y T_y} + e^{j\frac{2\pi}{\lambda}\, d_x T_x} \right) \right]$$

$$= -F_1(\vartheta) \left(\cos(\phi)\, P + j \sin(\phi)\, Q \right) \qquad (5.44)$$

And:

$$E_{\phi_{sub}}(\vartheta,\phi) = \cos(\vartheta)\, F_2(\vartheta) \left[\sin(\phi) \left(1 + e^{j\frac{2\pi}{\lambda}\left(d_x T_x + d_y T_y\right)} \right) + \right.$$

$$\left. - j \cos(\phi) \left(e^{j\frac{2\pi}{\lambda} d_y T_y} + e^{j\frac{2\pi}{\lambda}\, d_x T_x} \right) \right]$$

$$= \cos(\vartheta)\, F_2(\vartheta) \left(\sin(\phi)\, P - j \cos(\phi)\, Q \right) \qquad (5.45)$$

From this it is clear that:

$$|E_{\vartheta_{sub}}(\vartheta,\phi)|^2 = F_1^2(\vartheta)$$

$$\left(\cos(\phi)\ P + j\ \sin(\phi)\ Q\right)\left(\cos(\phi)\ P^* - j\ \sin(\phi)\ Q^*\right)$$

$$= 2\ F_1^2(\vartheta)\ \left(\cos^2(\phi)\ \left[1 + \cos\left(\frac{2\pi}{\lambda}\ (d_xT_x + d_yT_y\right)\right] + \right.$$

$$\left.\sin^2(\phi)\ \left[1 + \cos\left(\frac{2\pi}{\lambda}\ (d_xT_x - d_yT_y\right)\right]\right) \qquad (5.46)$$

$$|E_{\vartheta_{sub}}(\vartheta,\phi)|^2 = \cos(\vartheta)\ F_2^2(\vartheta)$$

$$\left(\sin(\phi)\ P - j\ \sin(\phi)\ Q\right)\left(\sin(\phi)\ P^* + j\ \cos(\phi)\ Q^*\right)$$

$$= 2\ \cos^2(\vartheta)\ F_2^2(\vartheta)$$

$$\left(\sin^2(\phi)\ \left[1 + \cos\left(\frac{2\pi}{\lambda}\ (d_xT_x + d_yT_y\right)\right] + \right.$$

$$\left.\cos^2(\phi)\ \left[1 + \cos\left(\frac{2\pi}{\lambda}\ (d_xT_x - d_yT_y\right)\right]\right) \qquad (5.47)$$

Because:

$$P\ P^* = 2\ \left[\ 1 + \cos\left(\frac{2\pi}{\lambda}\ (d_xT_x + d_yT_y\right)\ \right]$$

$$Q\ Q^* = 2\ \left[\ 1 + \cos\left(\frac{2\pi}{\lambda}\ (d_xT_x - d_yT_y\right)\ \right]$$

$$P\ Q^* - P^*\ Q = 2\ \mathrm{Im}(P\ Q^*) = 0$$

the directivity becomes:

$$D = \frac{4\pi \cdot \left(F_1^2(0) + F_2^2(0) \right) \cdot \frac{1}{8} \cdot M^2 \cdot N^2}{\int_0^{\frac{\pi}{2}} \int_0^{2\pi} \left[\left\{ \cos^2(\varphi) F_1^2(\theta) + \cos^2(\theta) \sin^2(\varphi) F_2^2(\theta) \right\} \cdot \left\{ 1 + \cos\left[\frac{2\pi}{\lambda} \cdot (d_x T_x + d_y T_y) \right] \right\} + \left\{ \sin^2(\varphi) F_1^2(\theta) + \cos^2(\theta) \cos^2(\varphi) F_2^2(\theta) \right\} \cdot \left\{ 1 + \cos\left[\frac{2\pi}{\lambda} \cdot (d_x T_x - d_y T_y) \right] \right\} \right] \cdot \frac{\sin^2\left(\frac{\pi}{\lambda} \cdot M \cdot d_x T_x \right)}{\sin^2\left(2 \cdot \frac{\pi}{\lambda} \cdot d_x T_x \right)} \cdot \frac{\sin^2\left(\frac{\pi}{\lambda} \cdot N \cdot d_y T_y \right)}{\sin^2\left(2 \cdot \frac{\pi}{\lambda} \cdot d_y T_y \right)} \cdot \sin(\theta) d\theta d\varphi}$$

(5.48)

ε_r = 2.2

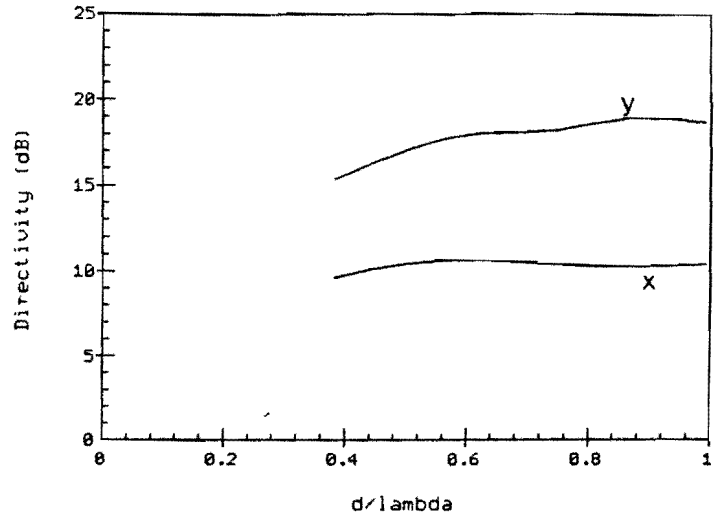

ε_r = 6.0

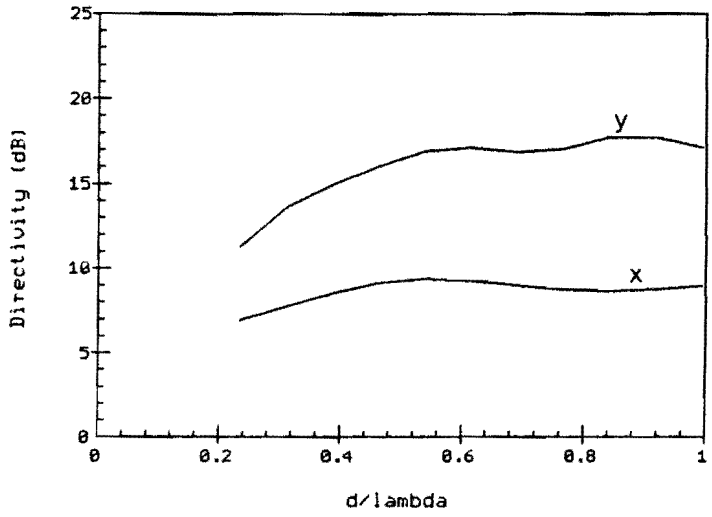

ε_r = 10.5

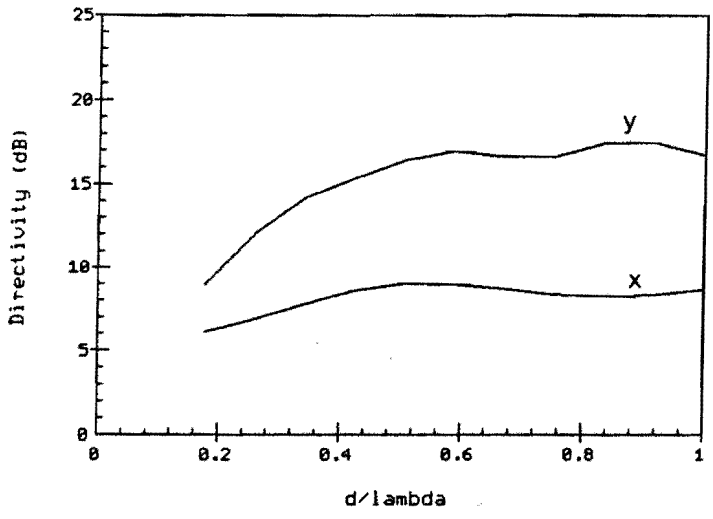

Fig. 5.9 a: Directivity (dB) vs element spacing (d/λ) for different square arrays which consist of linearly polarized patches : β=0.0

x: 2 × 2 array y: 4 × 4 array

ε_r = 2.2

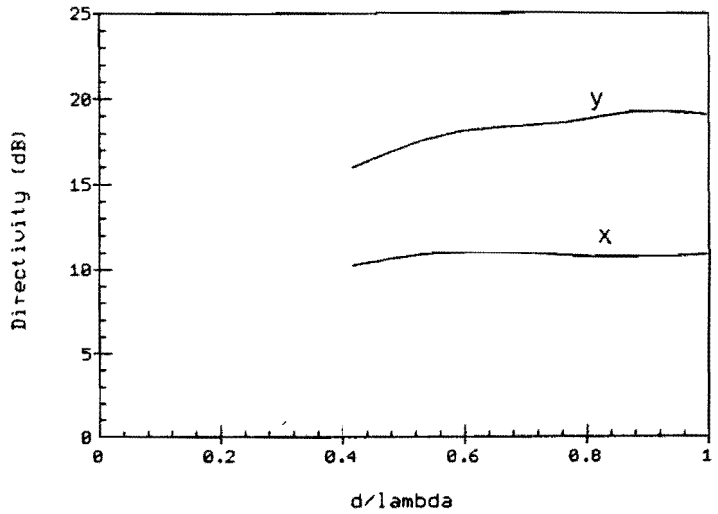

ε_r = 6.0

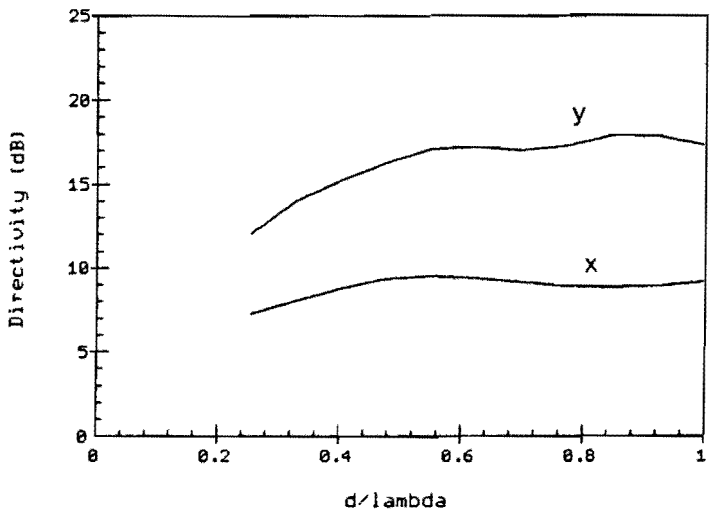

ε_r = 10.5

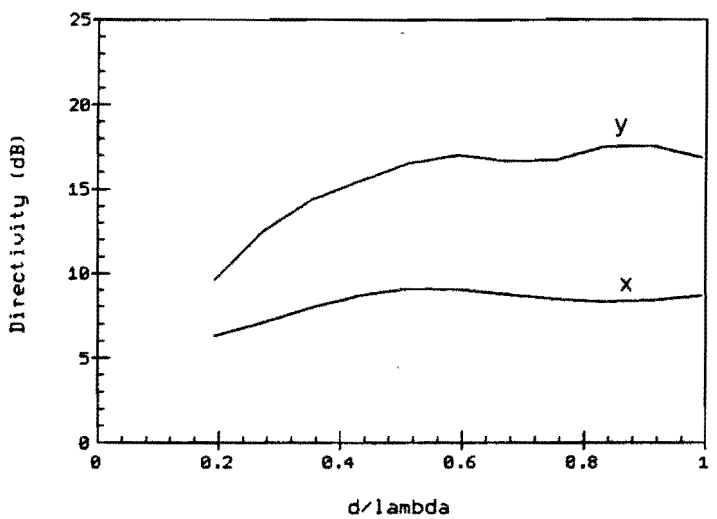

Fig. 5.9 b: Directivity (dB) vs element spacing (d/λ) for different square arrays which consist of linearly polarized patches : β=0.2

x: 2 × 2 array y: 4 × 4 array

ε_r = 2.2

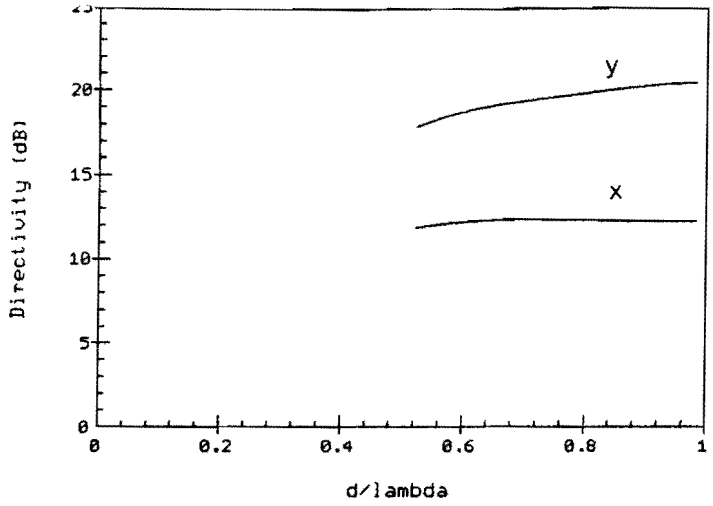

ε_r = 6.0

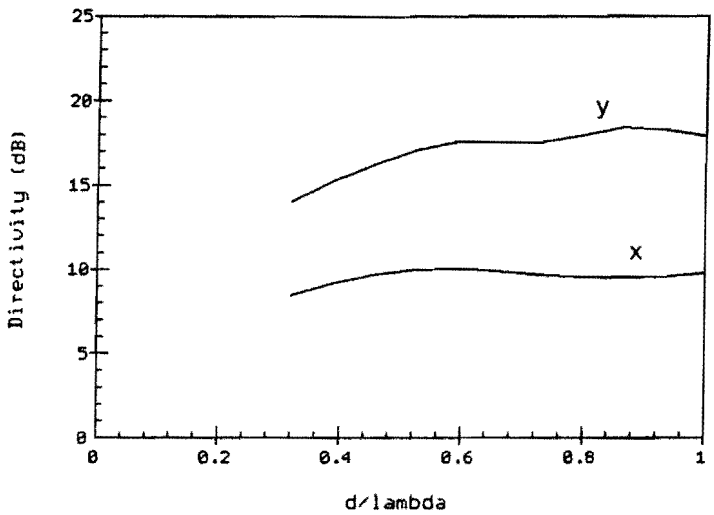

ε_r = 10.5

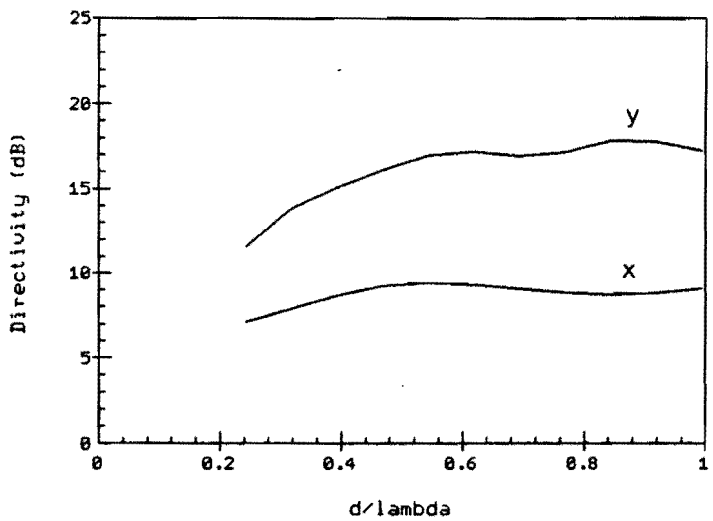

Fig. 5.9 c: Directivity (dB) vs element spacing (d/λ) for different square arrays which consist of linearly polarized patches : β=0.4

x: 2 × 2 array y: 4 × 4 array

ε_r = 2.2

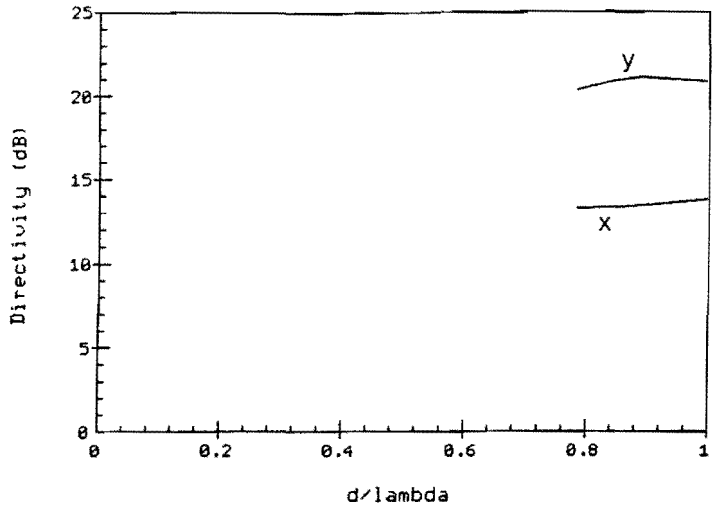

ε_r = 6.0

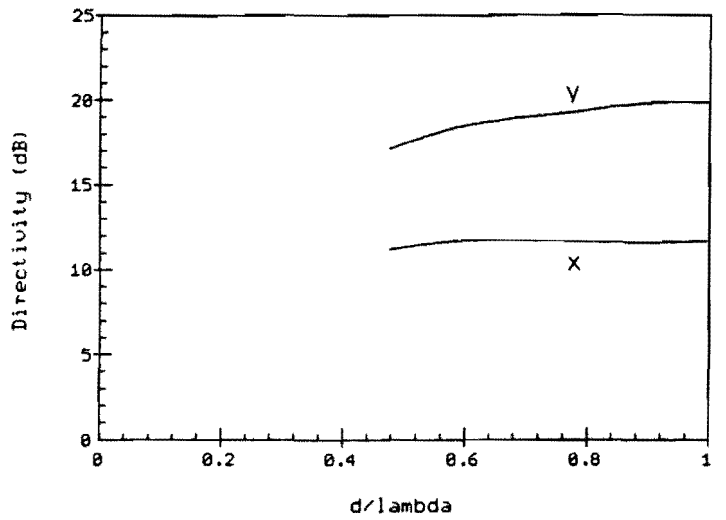

ε_r = 10.5

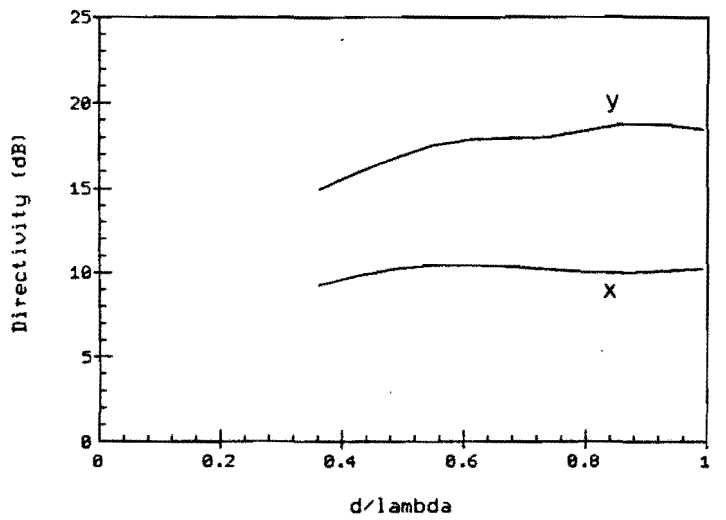

Fig. 5.9 d: Directivity (dB) vs element spacing (d/λ) for different square arrays which consist of linearly polarized patches : β=0.6

x: 2 × 2 array y: 4 × 4 array

The directivity for twelve different square ($d_x = d_y$) arrays is calculated and the results are given in figure 5.9.

From these graphs displaying the directivity as function of d/λ it can be concluded that the same characteristics appear as for an array composed of circularly polarized patches:- D increases for a fixed β and decreasing ε_r and for a fixed ε_r and increasing β. A comparison of the curves for the directivity of an array composed of circularly polarized patches and one composed of linearly polarized patches, the directivity of this last type of array can be much less for relatively large element distances. This phenomenon was reported in [5-6] too.

Because η_r decreases with increasing ε_r and thus a low ε_r is preferred. To reach the 10 - 12 dB gain with linearly polarized patches, a 4 x 4 array with $\varepsilon_r = 2.2$ can be chosen. As can be seen from fig. 5.9 it is better to chose β as large as possible.

Because the axial ratio is ϕ-dependent it is calculated in the plane $\phi = 45^\circ$ for various situations.

From these graphs it is clear that the axial ratio in the range of ϑ before the wave becomes linearly polarized hardly is affected by a β-variation. Interesting is the improvement of the axial ratio outside this range when β increases. (fig. 5.10 c)) This indicates the same correlation between β and ε_r as seen in chapter 4. (see fig. 4.6)

If the relative element spacing in the array is varied the axial ratio will be affected too. Fig. 5.11 shows the results of these calculations.

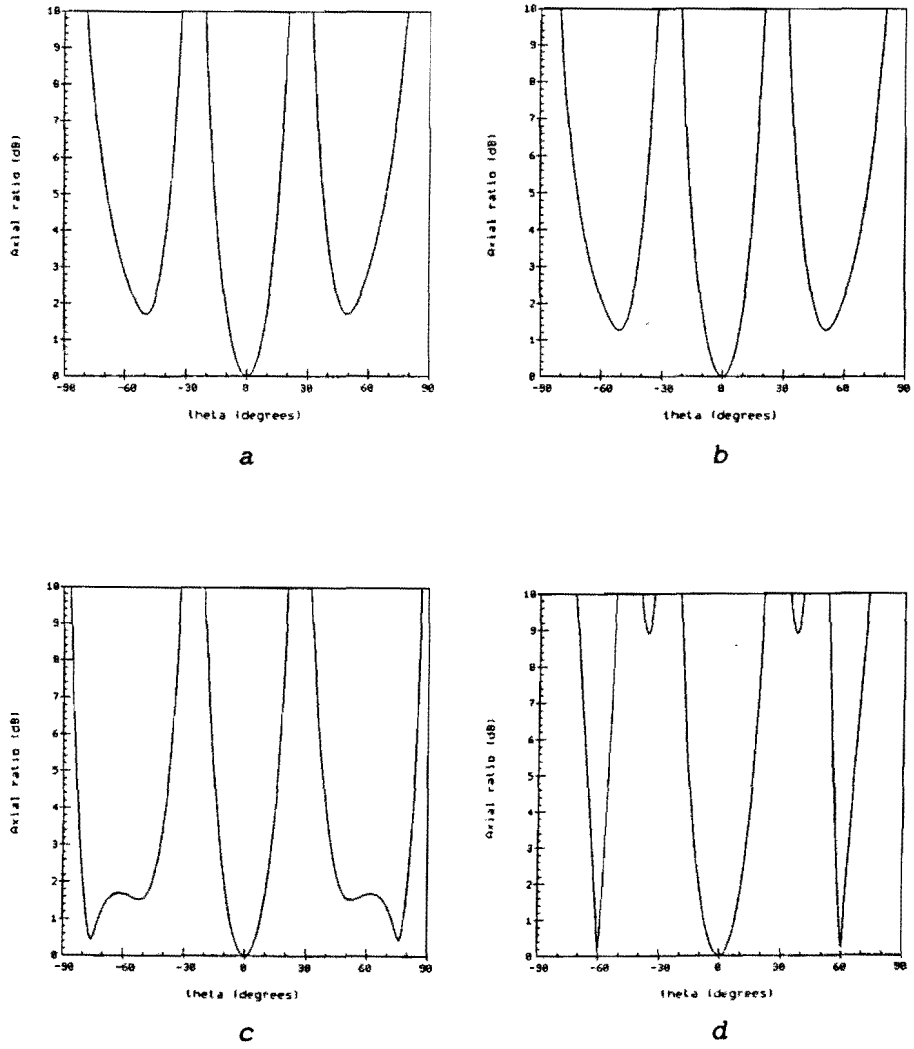

Fig. 5.10 : Axial ratio (dB) vs ϑ (degrees) of a circularly polarized 2 × 2 array composed of linearly polarized patches as function of β ($\phi = 45^{\circ}$)
f_r=1.6 GHz , d/λ=0.8 , ε_r=2.2
a) β=0.0 b) β=0.2 c) β=0.4 d) β=0.6

a

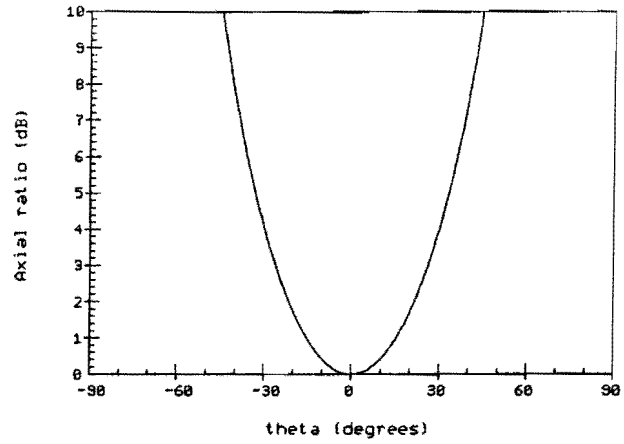

b

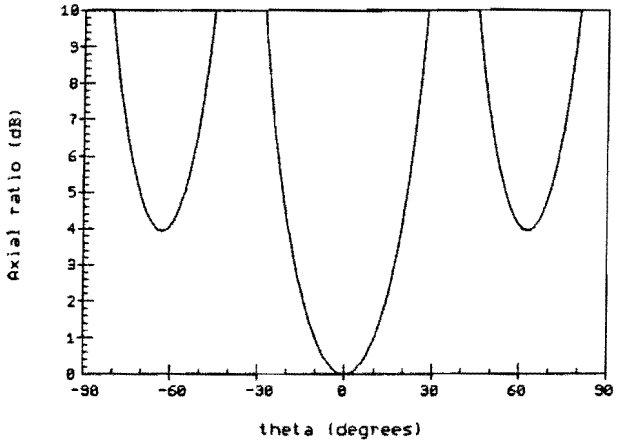

c

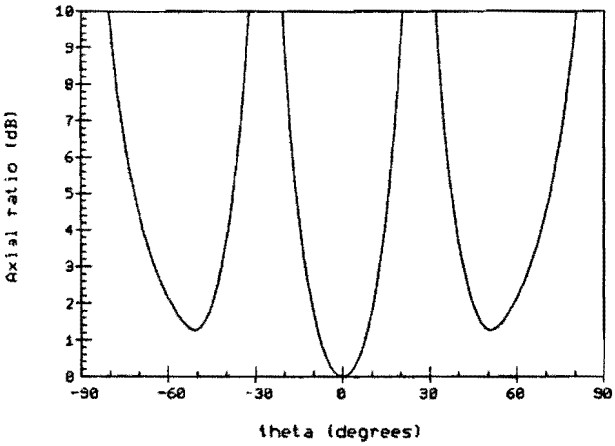

Fig. 5.11 : Axial ratio (dB) vs θ (degrees) of a circularly polarized 2 × 2 array composed of linearly polarized patches as function of d/λ (ϕ = 45°)

f_r=1.6 GHz , β=0.2 , ε_r=2.2

a) d/λ=0.4 b) d/λ=0.6 c) d/λ=0.8

The minimum element spacing can be calculated from eq. 3.19 and $r_{min} = 2\,a$ and is given by:

$$\left(\frac{d}{\lambda}\right)_{min} = \frac{\chi_{nm}}{\pi\sqrt{\varepsilon_r}}$$

The graphs show a small element spacing improves the axial ratio of the 'main lobe' and it becomes wider. This is in conformity with eq. 5.37. Note this equation is independent of ε_r. But when β increases the axial ratio in the 'side lobes' improves.

Fig. 5.12 shows that the axial ratio in the 'main lobe' is not affected by a variation of ε_r. Although to obtain a better axial ratio in the 'side lobes' ε_r should be small.

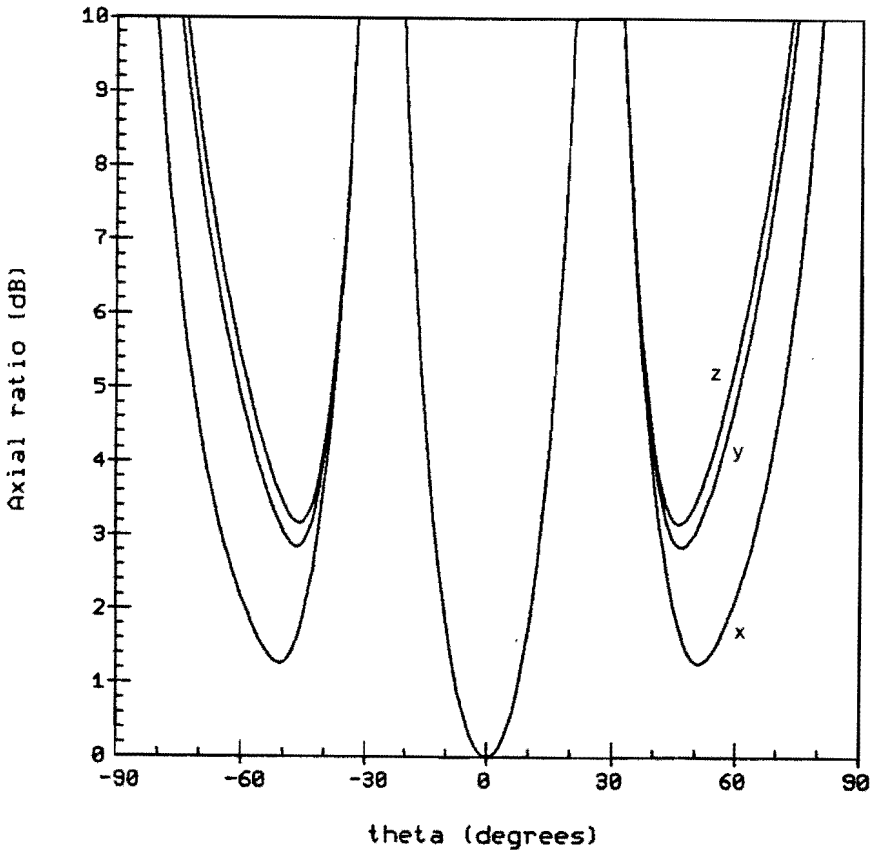

Fig. 5.12 : Axial ratio of a circularly polarized 2 × 2 array composed of linearly polarized patches as function of ε_r (ϕ = 45°)
f_r=1.6 GHz , β=0.2 , ε_r=2.2 , d/λ=0.8
x: ε_r=2.2 y: ε_r=6.0 z: ε_r=10.5

Based on the graphs it can be conclude that it is impossible to meet the INMARSAT requirements. To meet the MSATX requirements two ways to approach this requirement are possible.
Method 1:-try to make the 'main lobe' of the axial ratio as wide as possible (fig. 5.11 a)). Therefore d/λ should be chosen as small as possible.
Method 2:-try to shape the 'main lobe' in such a manner that the axial ratio in the 'side lobes' meets the requirement. This is especially suitable the MSATX requirements because the axial ratio must be met for elevation angles between 20° and 60°. Using this approach ε_r should be taken small (see fig. 5.12), β small too and d/λ should be large (see eq. 5.37 and fig. 5.11).
The combination β and ε_r small provides also a good axial ratio in the planes $\phi = 0^{\circ}$ and 90°.
Table 5.1 presents a summary of the results just discussed.

Table 5.1 : Optimum choice for gain and axial ratio related to the design parameters.

	Gain	Axial ratio	
		Method 1	Method 2
ε_r	small	~	small
β	large	~	small
d/λ	large	small	large

(~ : no direct relation to establish)

Concluding from this table method 2 harmonizes best with the design parameters for the directivity. Although a trade off for β must be made.

Complete sequential rotation technique

The foregoing calculations were based on the sub array as given in figure 5.7. These calculations also hold true for the sub array as depicted in figure 5.13. [5-1]

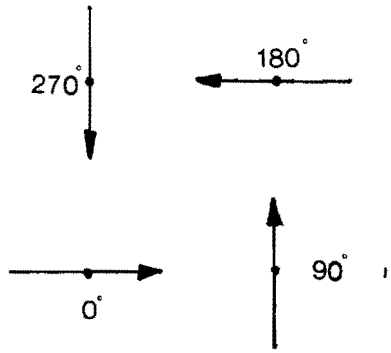

Fig. 5.13 : Complete sequential rotated array composed of linearly polarized patches

Actually this array can be called completely sequentially rotated. The idea behind this 0°, 90°, 180°, 270° rotation configuration is that radiation impurity (due to asymmetrical feed point location and higher order modes [5-7]) from the 0° element cancels that from the 180° element and vice versa and likewise for the 90° and 270° elements.

In the complete sequential rotation technique each radiating element has a unique orientation angle and phase shift [5-1]. For the n-th element of an array, located at an arbitrary position:

$$\psi_n = \Psi_n = \frac{n\ 2\ \pi}{N} \qquad 0 \leq n \leq N-1 \qquad (5.49)$$

with Ψ_n the element rotation angle and ψ_n the element phase shift. Note that for N = 4 the situation is the same as for a 2 x 2 sub array in the limited sequential rotation technique.

5.4 References.

[5-1] Visser H.J.,
'Circularly Polarized Microstrip Phased Array Antennas for Mobile Communications', Master's Thesis, Professional Group Electromagnetism and Circuit Theory, Department of Electrical Engineering, Eindhoven University of Technology, Netherlands, 1989, ET-3-89.

[5-2] Jeuken M.E.J.,
'Elektromagnetische Golven en Antennes',
Lecture Notes, Eindhoven University of Technology. (in Dutch), chapter 8.

[5-3] Balanis C.A.,
'Antenna Theory',
John Wiley And Sons, 1982.

[5-4] Ma M.T.,
'Theory and Applications of Antenna Arrays',
John Wiley and Sons Inc., 1974.

[5-5] Vrinten M.L.A.,
'A Wide band Circularly Polarized Microstrip Antenna Array', Master's Thesis, Professional Group Electromagnetism and Circuit Theory, Department of Electrical Engineering, Eindhoven University of Technology, Netherlands, 1988, ET-4-88.

[5-6] Huang J. and Y. Rahmat-Samii,
'Recent Array Developments at JPL',
Proceedings ofthe COST213/KUL Phased Array Workshop, Leuven Belgium, October 1988, p. 53-61.

[5-7] Huang J.,
'A Technique for am Array to Generate Circular Polarization with Linearly Polarized Elements',
IEEE Transactions on Antennas and Propagation, Vol. 34, september 1986.

6 Experimental results.

In this chapter the practical results of the investigation are discussed. The objective of this research was to develop a dual frequency feed stacked microstrip antenna, suitable for the frequency band 1.5 - 1.6 GHz. (see fig. 6.1)
Therefore the following characteristics of the circular patch microstrip antenna and the circular ring patch antenna must be verified:

- resonance frequency
- radiation pattern of the linearly polarized antenna
- gain of the antenna
- radiation pattern of the circularly polarized antenna
- co- and cross-polarization pattern and the corresponding axial ratio pattern.

The power splitting properties (3 dB) and phase shift (90°) properties between the two output ports of each microstrip network, which were designed for obtaining circular polarization, should also be verified.

The material used for the microstrip network and the microstrip antennas was Duroid 5880. This material has a dielectric substrate with a dielectric constant $\varepsilon_r = 2.2$, the loss tangent is 0.0009 and the thickness is h = 1.57 mm. Further information about this material can be found in appendix G.

The frequency bands that have to be covered are:

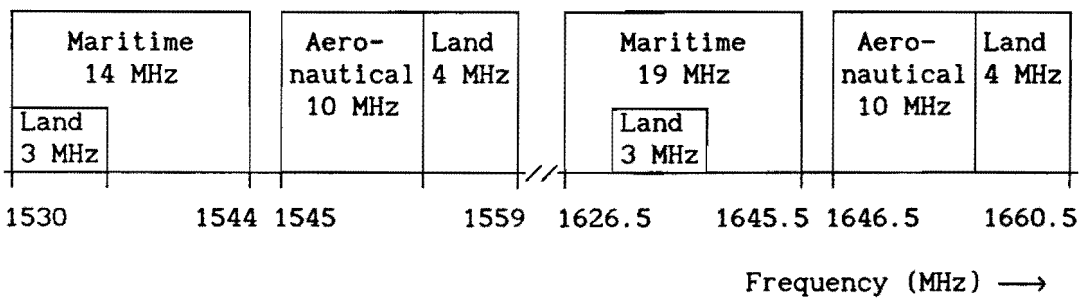

Fig. 6.1 : Mobile satellite communications frequency allocations

Because the bandwidth of a circular ring patch microstrip antenna is less than that of a circular patch microstrip antenna the circular antenna is dedicated for the frequency band at 1.6 GHz and the ring patch antenna is dedicated for the frequency band at 1.5 GHz.
When stacking the two antennas the upper antenna must be smaller than the lower one.
In order to maintain the specific advantage of microstrip antennas namely the small thickness, the feeding network for both antennas should be made on one substrate.

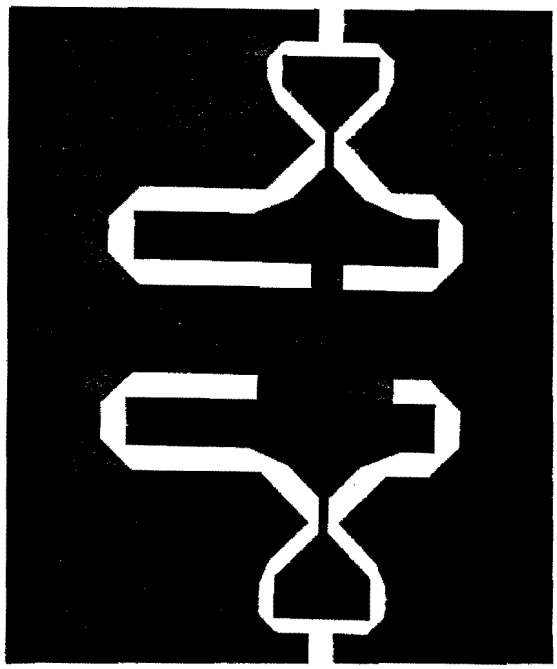

Fig. 6.2 : Layout of the microstrip network for both antennas

Another design consideration is feed point location of the circular antenna. This position determines the radius b of the ring patch antenna.

6.1 Experiments with the circular microstrip antenna.

Resonance should occur for a center frequency 1.64 GHz, this results in a radius a of 34.88 mm and to obtain an impedance match with a 50 Ω transmission line the feed point location ρ_o is 8.4 mm.

In appendix H, fig. H.1 the reflection coefficient as function of the frequency is plotted. This diagram shows that the resonance frequency is exactly 1.64 GHz. From this figure it can also be seen that the reflection coefficient at resonance is -18.9 dB or 0.11. This corresponds with a VSWR of 1.25.
If the maximum tolerable VSWR is 1.4, the maximum tolerable reflection coefficient is 0.17 or -15.4 dB. Now the bandwidth can be determined from this diagram and is 8.7 MHz or 0.50 %. This value closely resembles the calculated bandwidth of 0.52 %.
Furthermore the radiation patterns of the linearly polarized antenna in the planes $\phi = 0^\circ$ and $\phi = 90^\circ$ were measured.
Antenna measurements were done at the antenna test range at the Eindhoven University of Technology. First a short overview of the measurement technique applied is given here. At the range the antenna under test is used as in the receiving mode while a corner reflector dipole is used to generate plane waves.

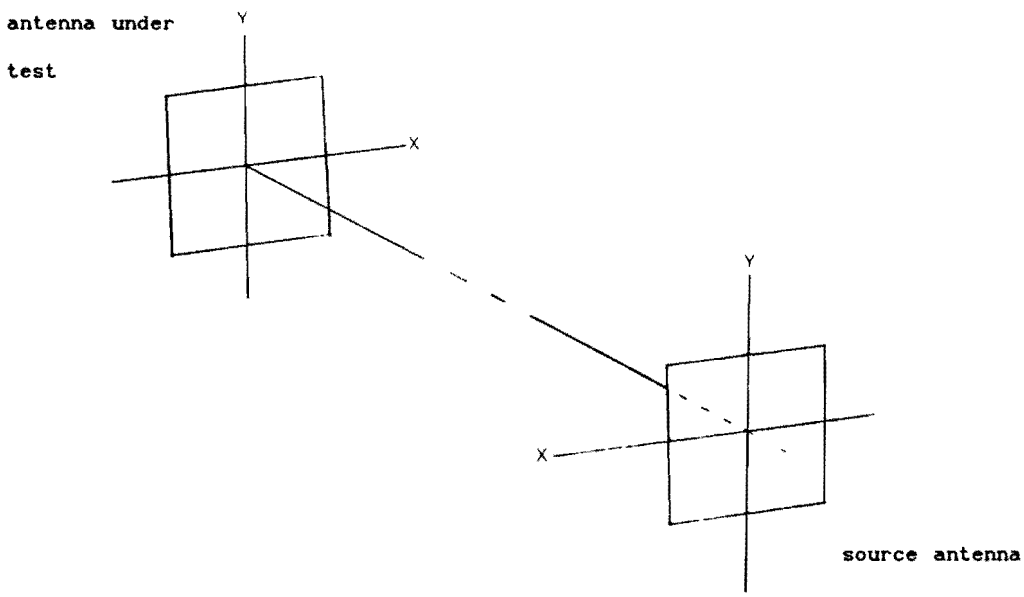

Fig. 6.3 : Antenna test range

The far field relations may be used if the distance R between source and test antenna satisfies the condition:

$$R > \frac{2\,D^2}{\lambda} \qquad (6.1)$$

with λ the smallest wavelength used (= 0.12 m) and D the largest dimension of the antenna (= 0.25 m). Thus the far field condition is satisfied if R > 1.05 m.

Reflections will still occur although the walls of the antenna test range are provided with absorbers. A gating technique was used to distinguish the direct radiation from the indirect radiation caused by reflections. This gating technique, which requires the usage of a computer system, is described briefly.
The amplitude and phase of the received signal are measured over a wide frequency band. An inverse Fourier transform of these data delivers the time domain response. The direct received radiation component can be extracted by placing a suitable time gate. Transformation of this time gate to the frequency domain provides a calibration set. This calibration set is needed to adjust the data obtained during the measurement of the antenna radiation pattern.

Results of these measurements of a linearly polarized circular patch are presented in appendix H, fig. H.2.
The graphs illustrate that the calculated and measured diagrams agree very well. For large values of ϑ ($\vartheta > 70^\circ$) a discrepancy exists between calculated and measured values. This is due to the, in contrast with the assumption made for the theoretical analysis, finiteness of the ground plane.
It is also clear that the diagrams are not perfectly symmetrical around $\vartheta = 0^\circ$. Due to the asymmetrical feed point location and a phase difference of the currents on the patch the diagram becomes asymmetrical. In the analysis it was assumed that the currents on the patch are in phase.
This asymmetry phenomenon has been reported in other articles.

Last property of the linearly polarized antenna that has to be checked is the gain. Theoretically a gain of 3.6 dB was predicted

which agrees very well with the measured gain of 3.5 dB.

In order to generate circularly polarized waves the feeding network must be attached to the antenna. First it necessary to check if the power divider and phase shifter are designed properly. This means the two output signals must have equal amplitude with a relative phase difference of 90°.
The phase difference measured was 89° and corresponds very well with the desired phase shift of 90°. The measured power distribution of the output ports was: 0 dB and 0.7 dB or 0.48 and 0.52. Despite this small deviation from the desired power distribution 0.5 and 0.5, this deflection should be kept in mind.

Before the results of the circular polarization measurements are discussed a brief introduction about the measurements is given. In the literature several possibilities to measure the characteristics of circular polarization are known. An excellent survey of microwave antenna measurements is given in [6-1].
The purpose is to determine the co- and cross-polarization and axial ratio as function of the polar angle ϑ. The method applied for measurements at the Eindhoven University of Technology test facility is described here.
This method requires that a linearly polarized antenna, usually a dipole, is used to probe the polarization in the plane that contains the direction of the desired polarization. With the measurement system installed it is possible to do both amplitude and phase measurements at once. Using the linearly polarized antenna in the transmitting mode and the antenna under test in the receiving mode, two measurements have to be done as indicated in fig. 6.4.

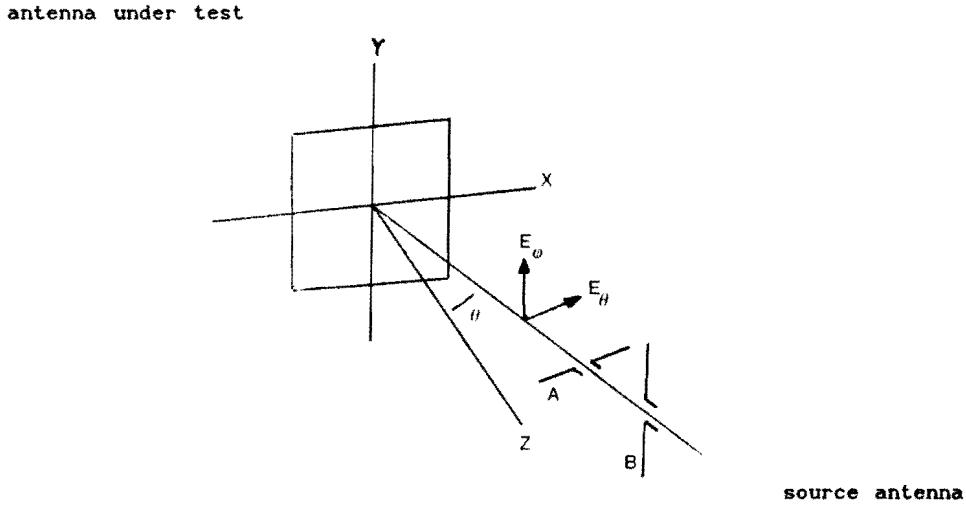

Fig. 6.4 : Measurement set-up for measuring circular polarized antennas

In the first measurement the transmitting antenna stands in position A and the E_ϑ-component of the electric field of the antenna under test as function of ϑ is obtained. The second measurement in which the transmitting antenna is rotated over 90° (position B) and now the E_ϕ-component of the electric field as function of ϑ is measured. Applying eq. 4.32 and 4.33 at this data, co- and cross-polarization fields and the axial ratio, using eq. 4.34, can be calculated. These calculations are carried out by a computer program.

In appendix H, fig. H-3 and H-4 the radiation patterns measured in the planes $\phi = 0°$ and $\phi = 45°$ with two orthogonal polarizations are shown. Deviations between the calculated and measured results can be explained from the finiteness of the ground plane. Because of the narrow bandwidth of this type of antenna, the influence of other modes that disturb the radiation characteristics is not likely.

From these graphs the co- and cross-polarization fields were calculated and the results are shown in appendix H, fig. H-5 and H-6. The measured co-polarization agrees very well with the

calculated values for $\vartheta > 0$. However for $\vartheta < 0$ the calculations and measurements differ considerably. Asymmetric feed point of the antenna is probably the cause of this effect.
The cross-polarization is completely different compared with the calculated values and so is the axial ratio pattern. A possible cause is that the cross-polarization is very sensitive to deviations in its parameters. This is illustrated by a discussion of eq. 4.12 and 4.13.

$$E_l = \frac{1}{\sqrt{2}} \left(E_\vartheta - j\, E_\phi \right) \tag{6.2}$$

$$E_r = \frac{1}{\sqrt{2}} \left(E_\vartheta - j\, E_\phi \right) \tag{6.3}$$

with:

$$E_\vartheta = |E_\vartheta|\, e^{j\phi_\vartheta} \tag{6.4}$$

$$E_\phi = |E_\phi|\, e^{j\phi_\phi} \tag{6.5}$$

Now the modulus becomes:

$$|E_l| = \frac{1}{\sqrt{2}} \left(|E_\vartheta|^2 + |E_\phi|^2 + 2\, |E_\vartheta|\, |E_\phi|\, \sin(\phi_\vartheta - \phi_\phi) \right)^{1/2} \tag{6.6}$$

$$|E_r| = \frac{1}{\sqrt{2}} \left(|E_\vartheta|^2 + |E_\phi|^2 - 2\, |E_\vartheta|\, |E_\phi|\, \sin(\phi_\vartheta - \phi_\phi) \right)^{1/2} \tag{6.7}$$

The cross-polarization originates from the subtraction of two nearly equal values resulting in large relative errors if its parameters slightly alter. Consequently the axial ratio is also sensitive for parameter variations.

6.2 Experiments with the circular ring patch microstrip antenna.

According to fig. 6.1 this antenna must be resonant for f=1.54 GHz. To feed the upper antenna through the lower one an inner radius of at least 12 mm must be chosen. To obtain a good axial ratio over a wide range ϑ, β was chosen to be 0.35. Resulting in the following dimensions of the ring patch: a = 47.33 mm, b = 16.6 mm and ρ_o = 23.3 mm.

For this antenna the same measurements were done as for the circular patch microstrip antenna.
First the reflection coefficient was measured and the resonance frequency appeared to be 1.5 GHz instead of 1.54 GHz (appendix H, fig. H-9). After repositioning the ring of this antenna the resonance frequency was 1.52 GHz. This discrepancy between calculated and measured resonance frequency was caused by too much tolerance (± 1 mm) between the ring and substrate. Previous experiments with a 2.04 GHz ring patch antenna shows that the model predicts the resonance frequency correct.
In this graph also shows the occurrence of the TM_{01} mode (first 'dip' in Fig. H-9). The occurrence of this mode was already mentioned in chapter 3.

The bandwidth measured is 5.7 MHz or 0.41 % which corresponds very well with the calculated bandwidth of 0.43 % and the measured gain of 4.8 dB closely resembles the calculated gain of 4.9 dB.

Radiation characteristics of this antenna were also measured and are shown in fig. H-10.
A good correlation between theory and practice was found. Although in the plane $\phi = 0^\circ$ the radiation pattern is slightly asymmetric. This is caused by the asymmetrical position of the feed point in this plane. In the plane $\phi = 90^\circ$ the antenna is symmetrical and this phenomenon does not occur.
A method that would reduce this effect is by adding an extra feed point. This extra feed point is spatially rotated 180° with respect to the first feed point and is fed 180° out of phase.

With this antenna also circular polarization measurements were done. But first the response of the microstrip network was verified. The phase shifter provided a relative phase between the two output signals of 92°. The power difference between the two output signals was 0.6 dB. Consequently the power distribution of the two output signals was 0.47 and 0.53.

The radiation characteristics in the planes ϕ = 0° and ϕ = 45° with two orthogonal polarizations were measured. Theoretical results are given in the next figures to compare these with the measured results.

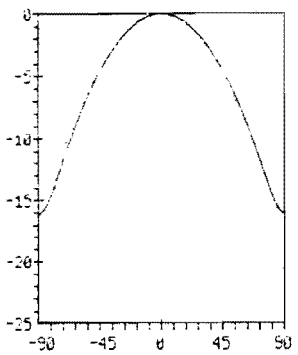

a

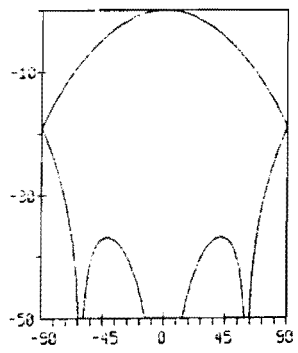

b

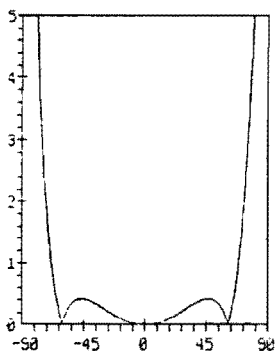

c

Fig. 6.5 : Calculated results for a ring patch antenna with fr=1.54 GHz , β=0.35 , ε_r=2.2 and tan(δ)=0.0009

a) radiation pattern

b) co- and cross-polarization pattern

c) axial ratio pattern

The discrepancy between the measured co- and cross-polarization (appendix H, fig. H-13 and H-14) from the theoretical curves originates from the same causes as described for the circular patch. As it can be seen from fig. H-15 and H-16 the axial ratio is improved over a wider range ϑ and closely resembles the calculated curve. Deflections are due to fabrication and material tolerances and measurement faults. Extensive research into possible measurement faults did not result in one or more unique causes for this deviation.

6.3 Experiments with the dual frequency feed stacked microstrip antenna.

Finally the antenna was built together with the individual elements. Because the antennas are fed by a feeding network it was impossible to check the resonance frequencies. Thus only the radiation patterns were verified.

First the radiation pattern of the circularly polarized circular microstrip antenna were measured. While measuring the characteristics of one antenna, the feeding network of the other antenna was terminated with its characteristic impedance. The result are given in fig. H-17. Radiation intensity for two orthogonal directions broadside to antenna seemed to be different. This was not expected. Several experiments were done to verify this measurement but no specific causes could be pointed out. Due to this discrepancy the co- and cross-polarization patterns and the axial ratio pattern (appendix H, fig. H-19) don not coincide with the theoretical results.

In fig. H-20 and H-21 the radiation patterns of the circular ring patch antenna are shown. Both patterns in the planes $\phi = 0^\circ$ and $\phi = 45^\circ$ became more identical and symmetrical in comparison with the measurements of the separate ring patch antenna. However the axial ratio (appendix H, fig. H-24 and H-25) now deteriorates in comparison with the separate antenna. This is probably caused by a

phase shift of the currents due to mutual coupling between the two antennas. This effect was not considered in the theoretical analysis. To understand this discrepancy this effect should be taken into account.

6.4 References.

6-1 Hollis J.S., Lyon T.J. and Clayton Jr. L., 'Microwave Antenna Measurements', Scientific Atlanta Inc., Atlanta, 1970.

7 Conclusions and recommendations.

The general conclusion which may be drawn after the analysis given, is that the narrow bandwidth is the greatest drawback of the ring patch microstrip antenna.
Unless exceptional thick substrates or substrates with extremely low relative dielectric constant are used, the bandwidth of a ring patch antenna for a resonance frequency of 1.6 GHz is less than 10 MHz which is insufficient for meeting the specifications.
To illustrate this the frequency allocations are stated below.

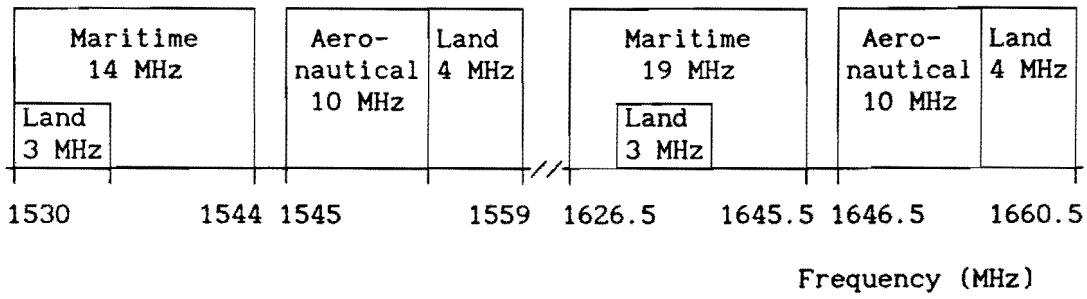

Fig. 7.1 : Mobile satellite communications frequency allocations

Instead of covering the whole receiving or transmitting frequency band it is possible to dedicate each antenna element in order to cover the frequency bands for land mobile communication.
Material and manufacturing tolerances should be minimized because uncertainty in the resonance frequency is in the same order of magnitude as the bandwidth.
The bandwidth of the element being less than 2.5 % at 1.6 GHz the method of impedance matching described by [7-1] is not applicable.
It is therefore recommended that research be done into inherent wide band microstrip antennas.

The advantage of a ring patch antenna is the possibility for improving the axial ratio by choosing an optimum combination of β and ε_r. It has been shown that it is possible to limit the axial ratio for a wide range of angle ϑ. The general trend is that β and ε_r are proportional i.e. when β is small ε_r should be small and when β is large ε_r should be large.

A single element cannot meet the stipulated gain requirement and consequently array techniques are applied. To obtain circular polarization the array can be composed either of circularly polarized elements or sequentially rotated linearly polarized elements. In the former case the axial ratio of the array is ϕ-independent and exactly the same as for one circularly polarized antenna element.

When the first method is used a 4 × 4 array on a dielectric substrate with $\varepsilon_r = 2.2$ is recommended.

For the array composed of sequentially rotated linearly polarized elements a new technique is introduced in order to optimize the axial ratio for the elevation angles desired. This is possible by choosing a suitable combination of β, ε_r and the element spacing d/λ. In order to meet the gain requirements a 4 × 4 array is recommended.

When choosing the sequential rotation technique the element spacing should be chosen most carefully. Exceeding an element spacing of approximately $0.7 * \lambda$, corresponding to a diagonal element spacing of approximately λ, which results in the occurrence of grating lobes. [7-2]

For the antenna feeding network, Wilkinson power splitters are recommended, because they provide not only good isolation between the output ports but also a low reflection coefficient at the input of the feeding network.

Not considered in either the analysis of the stacked microstrip antenna and of the arrays, is the effect of mutual coupling. It has been shown this effect causes a discrepancy between calculations and measurements.

7.1 References.

[7-1] Toom E.C. den,
'Microstripantenne voor de mobiele satelliet communicatie', Master's Thesis, Professional Group Electromagnetism and Circuit Theory, Department of Electrical Engineering, Eindhoven University of Technology, Netherlands, 1989, ET-8-89. (in Dutch)

[7-2] Hall P.S., Huang J., Rammos E. and Roederer A.,
'Gain of Circularly Polarized Arrays Composed of Linearly Polarized Elements', Electronic Letters, January 1989, Vol. 25, No. 2, p. 124.

Acknowledgements.

I want to acknowledge Ing. M. Knoben for his support in antenna design and measurements, and Mr. I. Ongers for his help in the development of software.

L.J. Cleven.

APPENDIX A Wave equation and its solution.

Consider fields in a region that is source-free ($\bar{J} = \bar{0}$, $\bar{M} = \bar{0}$), linear, homogeneous and isotropic. The complex field equations are then:

$$\nabla \times \bar{E} = -j\omega\mu \bar{H} \tag{A.1}$$

$$\nabla \times \bar{H} = j\omega\varepsilon \bar{E} \tag{A.2}$$

The curl of the first equation is:

$$\nabla \times \nabla \times \bar{E} = -j\omega\mu \nabla \times \bar{H} \tag{A.3}$$

Substituting for $\nabla \times \bar{H}$ eq. A.2 gives:

$$\nabla \times \nabla \times \bar{E} = \omega^2\mu\varepsilon \bar{E} \tag{A.4}$$

Or:

$$\nabla \times \nabla \times \bar{E} - k^2 \bar{E} = \bar{0} \tag{A.5}$$

With: $k^2 = \omega^2\mu\varepsilon$

Which is called the complex vector wave equation. With a well known vector relations equation A.5 can be written as:

$$\nabla (\nabla \cdot \bar{E}) - \nabla^2 \bar{E} - k^2 \bar{E} = \bar{0} \tag{A.6}$$

From equation A.2 it follows that:

$$\nabla \cdot \bar{E} = 0 \tag{A.7}$$

So the complex vector wave equation becomes:

$$\nabla^2 \bar{E} + k^2 \bar{E} = \bar{0} \tag{A.8}$$

For $E_z \neq 0$, the vector wave equation can be written in cylindrical coordinates as:

$$\frac{1}{\rho}\frac{\partial}{\partial\rho}\left(\frac{\partial E_z}{\partial\rho}\right) + \frac{1}{\rho^2}\frac{\partial^2 E_z}{\partial\phi^2} + \frac{\partial^2 E_z}{\partial z^2} + k^2 E_z = 0 \tag{A.9}$$

Using the method of separation of variables, we seek to find solutions of the form:

$$E_z = P(\rho)\,\Phi(\phi)\,Z(z) \tag{A.10}$$

Substituting this solution into equation A.9 gives:

$$\frac{1}{\rho P}\frac{d}{d\rho}\left(\rho\frac{dP}{d\rho}\right) + \frac{1}{\rho^2\Phi}\frac{d^2\Phi}{d\phi^2} + \frac{1}{Z}\frac{d^2Z}{dz^2} + k^2 = 0 \tag{A.11}$$

Because $d \ll \lambda_0$, $\frac{dZ}{dz} = 0$ and thus:

$$\frac{1}{\rho P}\frac{d}{d\rho}\left(\rho\frac{dP}{d\rho}\right)+\frac{1}{\rho^2\Phi}\frac{d^2\Phi}{d\phi^2}+k^2=0 \qquad (A.12)$$

Multiplying this by ρ^2 gives:

$$\frac{\rho}{P}\frac{d}{d\rho}\left(\rho\frac{dP}{d\rho}\right)+\frac{1}{\Phi}\frac{d^2\Phi}{d\phi^2}+\rho^2k^2=0 \qquad (A.13)$$

The second term is explicitly independent of ρ, hence:

$$\frac{1}{\Phi}\frac{d^2\Phi}{d\phi^2}=-\nu^2 \qquad (A.14)$$

And has the solution:

$$\Phi(\phi)=A\cos(\nu\phi)+B\sin(\nu\phi) \qquad (A.15)$$

With A and B constants.

The preceding equation then becomes:

$$\frac{\rho^2}{P}\frac{d^2P}{d\rho^2}+\frac{\rho}{P}\frac{dP}{d\rho}+\rho^2k^2=\nu^2 \qquad (A.16)$$

This differential equation is called Bessel's equation of order ν and has the solution [A-1]:

$$P(\rho)=C\,J_\nu(k\rho)+D\,Y_\nu(k\rho) \qquad (A.17)$$

With J_ν and Y_ν Besselfunctions of the first and second kind and order ν.

Substituting eq..14 and A.16 in A.10 gives:

$$E_z(\rho,\phi)=\left(A\cos(\nu\phi)+B\sin(\nu\phi)\right)\cdot \left(C\,J_\nu(k\rho)+D\,Y_\nu(k\rho)\right) \qquad (A.18)$$

The only difference between $\cos(\nu\phi)$ and $\sin(\nu\phi)$ is the origin, so for convenience A is chosen 1 and B is chosen 0.

The ϕ coordinate is an angle coordinate and places restriction to the choice of ν. In a cylindrical region containing all ϕ from 0 to 2π, it is necessary that $E_z(\rho,\phi)=E_z(\rho,\phi+2\pi)$. This means ν must be an integer: n.

Now, consider the solution of Bessel's equation. Graphs of the lower order Bessel functions are given in [A-1] and show that only $J_n(k\rho)$ functions are nonsingular at $\rho=0$. Because the fields must be finite for $b\leq\rho\leq a$ ($b\neq0$), both Besselfunctions must to be taken

into account.

So the solution of the wave equation that must meet the boundary conditions is:

$$E_z = \cos(n\phi) \left(C\, J_n(k\rho) + D\, Y_n(k\rho) \right) \qquad (A.19)$$

In addition this solution must meet the following boundary condition:

$$E_z(\rho=b) = 0 \qquad 0 \le \phi \le 2\pi \qquad (A.20)$$

This gives the following solution:

$$E_z = E_0 \cos(n\phi) \left(J_n(k\rho) - \frac{J_n(k\rho)}{Y_n(kb)}\, Y_n(k\rho) \right)$$

References:

[A-1] Abramowitz M. and Stengun I.A.,
'Handbook of Mathematical Functions'
Dover Publications Inc., New York, 1965

Appendix B Far field calculations.

From the preceding it is known that:

$$E_z(\rho,\phi) = E_0 \left(J_n(k\rho) - \frac{J_n(kb)}{Y_n(kb)} Y_n(k\rho) \right) \cos(n\phi) \qquad (B.1)$$

Or:

$$E_z(\rho,\phi) = E_0 \left(J_n(k\rho) - \alpha\, Y_n(k\rho) \right) \cos(n\phi) \qquad (B.2)$$

$$\text{Where : } \alpha = \frac{J_n(kb)}{Y_n(kb)} \qquad (B.3)$$

Now the field distribution in the cavity is known, Huygen's principle may be applied to the magnetic wall of the cavity. For that a magnetic current on the perimeter of the cavity is defined:

$$\bar{M} = 2\, \hat{n} \times \bar{E} \,|_{\rho=a} \qquad (B.4)$$

$$= 2\, \hat{e}_\rho \times E_z \bar{e}_\phi \,|_{\rho=a} \qquad (B.5)$$

$$= 2\, E_z\, \hat{e}_\phi \,|_{\rho=a} \qquad (B.6)$$

$$= 2\, E_0 \left(J_n(ka) - \alpha\, Y_n(ka) \right) \cos(n\phi)\, \delta(r-a)\, \hat{e}_\phi \qquad (B.7)$$

Defining:

$$A_0 = 2\, E_0 \left(J_n(ka) - \alpha\, Y_n(ka) \right) \qquad (B.8)$$

$\bar{M}$ becomes:

$$\bar{M} = A_0 \cos(n\phi)\, \delta(r-a) \qquad (B.9)$$

To determine the far fields, the integral:

$$\int_{V'} \bar{M}(\bar{r}')\, e^{jk_0(\hat{r}\cdot\bar{r}')}\, dV' \qquad (B.10)$$

must be calculated.

Therefore the current $\bar{M}$ is written as:

$$\bar{M} = M_x\, \hat{e}_x + M_y\, \hat{e}_y \qquad (B.11)$$

With:

$$M_x = - \sin(\phi) \; | \; \bar{M} \; | \tag{B.12}$$

$$M_y = \cos(\phi) \; | \; \bar{M} \; | \tag{B.13}$$

The integrals then become:

$$\int_{V'} M_x \, e^{jk_o(\hat{r}\cdot\bar{r}')} \, dV' = \int_0^{2\pi} \int_0^{h} \int_{-\infty}^{\infty} - A_o \sin(\phi') \cos(n\phi') \; \delta(r'-a) \; e^{jk_o a \sin(\vartheta) \cos(\phi-\phi')} \; a \, d\phi' \, dr' \, dz' \tag{B.14}$$

Henceforth this integral will be named I_x.

$$I_x = - A_o \, a \, h \int_0^{2\pi} \sin(\phi') \cos(n\phi') \, e^{jk_o a \sin(\vartheta) \cos(\phi-\phi')} \, d\phi' \tag{B.15}$$

Abbreviating $k_0 a \sin(\vartheta)$ by X and using the relation [B-1]:

$$e^{jX \cos(\phi-\phi')} = J_o(X) + 2 \sum_{k=1}^{\infty} j^k \, J_k(X) \cos(k(\phi-\phi')) \tag{B.16}$$

Working out the brackets and using some basic trigonometric relations I_x becomes:

$$I_x = - \frac{1}{2} \, A_o \, a \, h \int_0^{2\pi} \Big(\sin((n+1)\phi') - \sin((n-1)\phi') \Big) \cdot \Big(J_o(X) + 2 \sum_{k=1}^{\infty} j^k \, J_k(X) \cos(k(\phi-\phi')) \Big) \, d\phi'$$

$$= - \frac{1}{2} \, A_o \, a \, h \Bigg[\int_0^{2\pi} \Big(\sin((n+1)\phi') - \sin((n-1)\phi') \Big) \, J_o(X) \, d\phi' + \int_0^{2\pi} \sum_{k=1}^{\infty} j^k \, J_k(X)$$

$$\Big[\sin((n+k+1)\phi' - k\phi) + \sin((n-k+1)\phi' + k\phi)) + \sin((n-k-1)\phi' + k\phi) + \sin((n+k-1)\phi' - k\phi) \Big] \, d\phi' \qquad (B.17)$$

Because integration in eq. (B.17) is carried out over one or more complete periods, these integrals only contribute to I_x when the argument of the sinus is zero.
In the summation k is ≥ 1 and in appendix A it is shown that n ≥ 0. Both variables are integers.

Now the following situations occur:

$n + 1 = 0$	→	$n = -1$	not permitted
$n - 1 = 0$	→	$n = 1$	permitted, but sin(0) = 0 and thus it does not contribute.
$n - k + 1 = 0$	→	$k = n + 1$	all n and k are permitted
$n + k + 1 = 0$	→	$k = - n - 1$	not permitted
$n - k - 1 = 0$	→	$k = n - 1$	only $n \geq 2$ permitted
$n + k - 1 = 0$	→	$k = - n + 1$	only the combination: n = 0 k = 1 is permitted

The terms that do contribute give the following result:

$$I_x = - A_o \, a \, h \, \pi \left(j^{n+1} J_{n+1}(X) \sin((n+1)\phi) - j^{n-1} J_{n-1}(X) \sin((n-1)\phi) \right) \qquad (B.18)$$

With:

$$A_o = 2 E_0 \left(J_n(ka) - \alpha Y_n(ka) \right) \qquad (B.19)$$

$$\alpha = \frac{J_n(kb)}{Y_n(kb)} \qquad (B.20)$$

$$X = k_0 a \sin(\vartheta) \qquad (B.21)$$

$$\text{For } I_y = \int_{V'} M_y \, e^{jk_o(\hat{r}\cdot\bar{r}')} \, dV'$$

$$= \int_0^{2\pi} \int_0^{h} \int_{-\infty}^{\infty} A_o \cos(\phi') \cos(n\phi')$$

$$\delta(r'-a) \, e^{jk_o a \sin(\vartheta) \cos(\phi-\phi')} \, a \, d\phi' \, dr' \, dz' \qquad \text{(B.22)}$$

The same calculations can be made and these give the following result:

$$I_y = A_o \, a \, h \, \pi \left(j^{n+1} J_{n+1}(X) \cos((n+1)\phi) + j^{n-1} J_{n-1}(X) \cos((n-1)\phi) \right) \qquad \text{(B.23)}$$

With:

$$A_o = 2 E_0 \left(J_n(ka) - \alpha Y_n(ka) \right) \qquad \text{(B.24)}$$

$$\alpha = \frac{J_n(kb)}{Y_n(kb)} \qquad \text{(B.25)}$$

$$X = k_0 a \sin(\vartheta) \qquad \text{(B.26)}$$

To obtain expressions for the far field in spherical coordinates, the transformation to spherical coordinates must be used.

$$\hat{e}_r = \sin(\vartheta) \cos(\phi) \, \hat{e}_x + \sin(\vartheta) \sin(\phi) \, \hat{e}_y + \cos(\vartheta) \, \hat{e}_z \qquad \text{(B.27)}$$

$$\hat{e}_\vartheta = \cos(\vartheta) \cos(\phi) \, \hat{e}_x + \cos(\vartheta) \sin(\phi) \, \hat{e}_y - \sin(\vartheta) \, \hat{e}_z \qquad \text{(B.28)}$$

$$\hat{e}_\phi = - \sin(\phi) \, \hat{e}_x + \cos(\phi) \, \hat{e}_y \qquad \text{(B.29)}$$

Using the abbreviations I_r, I_ϑ and I_ϕ for the integrals:

$$I_r = \int_{V'} \bar{M}_r \, e^{jk_o(\hat{r}\cdot\bar{r}')} \, dV' \qquad \text{(B.30)}$$

$$I_\vartheta = \int_{V'} \bar{M}_\vartheta \, e^{jk_o(\hat{r}\cdot\bar{r}')} \, dV' \tag{B.31}$$

$$I_\phi = \int_{V'} \bar{M}_\phi \, e^{jk_o(\hat{r}\cdot\bar{r}')} \, dV' \tag{B.32}$$

The result of the transformation is:

$$I_r = A_o \; a \; h \; \pi \; \sin(\vartheta) \; \sin(n\phi) \left(j^{n-1} \, J_{n-1}(X) - j^{n+1} \, J_{n+1}(X) \right) \tag{B.33}$$

$$I_\vartheta = A_o \; a \; h \; \pi \; \cos(\vartheta) \; \sin(n\phi) \left(j^{n-1} \, J_{n-1}(X) - j^{n+1} \, J_{n+1}(X) \right) \tag{B.34}$$

$$I_\phi = A_o \; a \; h \; \pi \; \cos(n\phi) \left(j^{n-1} \, J_{n-1}(X) + j^{n+1} \, J_{n+1}(X) \right) \tag{B.35}$$

With:

$$A_o = 2 \, E_0 \left(J_n(ka) - \alpha \, Y_n(ka) \right) \tag{B.36}$$

$$\alpha = \frac{J_n(kb)}{Y_n(kb)} \tag{B.37}$$

$$X = k_0 a \sin(\vartheta) \tag{B.38}$$

The far field is now determined by:

$$\bar{E} = jk_o \, \frac{e^{-jk_o r}}{4 \, \pi \, r} \, \hat{r} \times \int_{V'} \bar{M}(\bar{r}') \, e^{jk_o(\hat{r}\cdot\bar{r}')} \, dV' \tag{B.39}$$

Working out the vector product:

$$\hat{r} \times \int_{V'} \bar{M}(\bar{r}') \, e^{-jk_o(\hat{r}\cdot\bar{r}')} \, dV' = \hat{r} \times \left(\int_{V'} \bar{M}_r(\bar{r}') \, e^{-jk_o(\hat{r}\cdot\bar{r}')} \, dV' + \int_{V'} \bar{M}_\vartheta(\bar{r}') \, e^{-jk_o(\hat{r}\cdot\bar{r}')} \, dV' + \int_{V'} \bar{M}_\phi(\bar{r}') \, e^{-jk_o(\hat{r}\cdot\bar{r}')} \, dV' \right) \tag{B.40}$$

$$\hat{r} \times \int_{V'} \bar{M}(\bar{r}') \, e^{-jk_o(\hat{r}\cdot\bar{r}')} \, dV' = \hat{r} \times \left(I_r \hat{e}_r + I_\vartheta \hat{e}_\vartheta + I_\phi \hat{e}_\phi \right) \tag{B.41}$$

$$\hat{r} \times \int_{V'} \bar{M}(\bar{r}') \, e^{-jk_o(\hat{r}\cdot\bar{r}')} \, dV' = I_\vartheta \, \hat{e}_\phi - I_\phi \, \hat{e}_\vartheta \tag{B.42}$$

So the E_ϕ-component of the far field is:

$$E_\phi = jk_o \frac{e^{-jk_o r}}{4 \pi r} I_\vartheta \tag{B.43}$$

$$= jk_o \frac{e^{-jk_o r}}{4 \pi r} A_o \, a \, h \, \pi \cos(\vartheta) \sin(n\phi)$$

$$\left(j^{n-1} J_{n-1}(X) - j^{n+1} J_{n+1}(X) \right) \tag{B.44}$$

$$= j^n \frac{e^{-jk_o r}}{2 \; r} E_o \, a \, h \, k_o \cos(\vartheta) \sin(n\phi)$$

$$\left(J_n(ka) - \alpha \, Y_n(ka) \right) \cdot \left(J_{n+1}(X) + J_{n-1}(X) \right) \tag{B.45}$$

$$E_\vartheta = -jk_o \frac{e^{-jk_o r}}{4 \pi r} I_\phi \tag{B.46}$$

$$= -jk_o \frac{e^{-jk_o r}}{4 \pi r} A_o \, a \, h \, \pi \cos(n\phi)$$

$$\left(j^{n-1} J_{n-1}(X) + j^{n+1} J_{n+1}(X) \right) \tag{B.47}$$

$$= j^n \frac{e^{-jk_o r}}{2\,r} E_0\, a\, h\, k_o \cos(n\phi)$$

$$\left(J_n(ka) - \alpha\, Y_n(ka) \right) \cdot \left(J_{n+1}(X) - J_{n-1}(X) \right) \qquad \text{(B.48)}$$

And:

$$\alpha = \frac{J_n(kb)}{Y_n(kb)} \qquad \text{(B.49)}$$

References:

[B-1] Jeuken M.E.J.,
'Corrugated Horn Antennas',
Lecture Notes, Eindhoven University of technology, 1986

Appendix C Power radiated.

The radiated power may be calculated by integrating the Poynting vector over a sphere at infinity.

$$P_r = \frac{1}{2}\, Re \int\int_S (\bar{E} \times \bar{H}^*) \cdot d\bar{S} \qquad (C.1)$$

Because of the conducting ground plane, no radiation is assumed to be radiated in the lower half space, so an extra factor $\frac{1}{2}$ is introduced.

$$P_r = \frac{1}{2}\ \frac{1}{2}\, Re \int\int_S (\bar{E} \times \bar{H}^*) \cdot d\bar{S} \qquad (C.2)$$

$$= \frac{1}{4}\, Re \int\int_S ((E_\vartheta H_\phi^* - E_\phi H_\vartheta^*)\, \hat{e}_r) \cdot d\bar{S} \qquad (C.3)$$

Using $d\bar{S} = dS\, \hat{e}_r$ and the relation:

$$\bar{H} = \frac{1}{Z_o}\ \hat{e}_r \times \bar{E} \qquad (C.4)$$

the power radiated becomes:

$$P_r = \frac{1}{4\, Z_o} \int_0^{2\pi}\int_0^{\pi} \left(|E_\vartheta|^2 + |E_\phi|^2 \right) r^2 \sin(\vartheta)\, d\vartheta\, d\phi \qquad (C.5)$$

$$= \frac{1}{4\, Z_o} \int_0^{2\pi}\int_0^{\pi} \frac{\left(E_o a h k_o\right)^2 \cos^2(n\phi)}{4\, r^2} \left(J_n(ka) - \alpha\, Y_n(ka) \right)^2$$

$$\left(J_{n+1}(X) - J_{n-1}(X) \right)^2 r^2 \sin(\vartheta)\, d\vartheta\, d\phi \quad +$$

$$\frac{1}{4\, Z_o} \int_0^{2\pi}\int_0^{\pi} \frac{\left(E_o a h k_o\right)^2 \sin^2(n\phi) \cos^2(\vartheta)}{4\, r^2}$$

$$\left(J_n(ka) - \alpha\, Y_n(ka) \right)^2 \cdot \left(J_{n+1}(X) + J_{n-1}(X) \right)^2$$

$$r^2 \sin(\vartheta)\, d\vartheta\, d\phi \qquad (C.6)$$

With:

$$X = k_o a \sin(\vartheta) \tag{C.7}$$

$$\alpha = \frac{J_n(kb)}{Y_n(kb)} \tag{C.8}$$

After some basic mathematical operations, this can be written as:

$$P_r = \frac{\pi}{16 Z_o} \left(ahk_o E_o \left[J_n(ka) - \alpha Y_n(ka) \right] \right)^2$$

$$\int_0^{\pi} \sin(\vartheta) \left(\left[J_{n+1}(k_o a \sin(\vartheta)) - J_{n-1}(k_o a \sin(\vartheta)) \right]^2 + \right.$$

$$\left. \cos^2(\vartheta) \left[J_{n+1}(k_o a \sin(\vartheta)) + J_{n-1}(k_o a \sin(\vartheta)) \right]^2 \right) d\vartheta \tag{C.9}$$

For this last integral no analytical solution is known and this integral must be calculated numerically.

Appendix D Power loss in conductors.

The power dissipated in the conductors can be evaluated from the I^2R relationship by integrating over the patch and ground plane areas.

$$P_c = \frac{R_s}{2} \int\int_{\text{patch}} |\bar{I}|^2 \, dS + \frac{R_s}{2} \int\int_{\substack{\text{ground} \\ \text{plane}}} |\bar{I}|^2 \, dS \tag{D.1}$$

$$= 2 \, \frac{R_s}{2} \int\int_{\text{patch}} |\bar{I}|^2 \, dS \tag{D.2}$$

With R_s the real part of the surface impedance and is given by [C-1]:

$$R_s = \sqrt{\frac{\pi \, f \, \mu}{\sigma}} \tag{D.3}$$

The surface current $\bar{I}$ is given by:

$$\bar{I} = \bar{n} \times \bar{H} \tag{D.4}$$

$$= -\hat{e}_z \times \bar{H} \tag{D.5}$$

$$= H_\rho \hat{e}_\phi - H_\phi \hat{e}_\rho \tag{D.6}$$

So P_c becomes:

$$P_c = R_s \int_b^a \int_0^{2\pi} \left(|K_\rho|^2 + |K_\phi|^2 \right) \rho \, d\rho \, d\phi \tag{D.7}$$

Using the expressions for H_ρ and H_ϕ as calculated in § 3.2 gives the following result:

$$P_c = R_s \, E_o^2 \left(\int_b^a \int_0^{2\pi} \left[\frac{\rho k^2}{\omega^2 \mu^2} \left(J_n'(k\rho) - \alpha \, Y_n'(k\rho) \right)^2 \cos^2(n\phi) + \frac{n^2}{\rho \, \omega^2 \mu^2} \left(J_n(k\rho) - \alpha \, Y_n(k\rho) \right)^2 \sin^2(n\phi) \right] d\rho \, d\phi \right) \tag{D.8}$$

$$P_c = \pi \, R_s \, E_o^2 \left(\int_b^a \left[\frac{\rho k^2}{\omega^2 \mu^2} \left(J_n'(k\rho) - \alpha \, Y_n'(k\rho) \right)^2 + \frac{n^2}{\rho \, \omega^2 \mu^2} \left(J_n(k\rho) - \alpha \, Y_n(k\rho) \right)^2 \right] d\rho \right) \tag{D.9}$$

With the relation:

$$\frac{1}{\omega^2\mu^2} = \frac{\varepsilon}{k^2\mu} \tag{D.10}$$

The expression for P_c can be written as:

$$P_c = \pi R_s E_o^2 \frac{\varepsilon}{\mu} \left(\int_b^a \left[\rho \left(J_n'(k\rho) - \alpha Y_n'(k\rho) \right)^2 + \frac{n^2}{\rho k^2} \left(J_n(k\rho) - \alpha Y_n(k\rho) \right)^2 \right] d\rho \right) \tag{D.11}$$

Taking only the integral itself into account and eliminating the brackets:

$$I = \int_b^a \left[\rho \left(J_n'(k\rho) - \alpha Y_n'(k\rho) \right)^2 + \frac{n^2}{\rho k^2} \left(J_n(k\rho) - \alpha Y_n(k\rho) \right)^2 \right] d\rho \tag{D.12}$$

$$I = \int_b^a \left[\left(\frac{n^2}{k^2\rho} J_n^2(k\rho) + \rho J_n'^2(k\rho) \right) + \alpha^2 \left(\frac{n^2}{k^2\rho^2} Y_n^2(k\rho) + Y_n'^2(k\rho) \right) + - 2\alpha \left(\frac{n^2}{k^2\rho^2} J_n(k\rho) Y_n(k\rho) + J_n'(k\rho) Y_n'(k\rho) \right) \rho \, d\rho \right] \tag{D.13}$$

Taking only the first part of eq. D.13:

$$I = \int_b^a \left(\frac{n^2}{k^2\rho} J_n^2(k\rho) + \rho J_n'^2(k\rho) \right) \rho \, d\rho \tag{D.14}$$

Define:

$$t = k\rho \tag{D.15}$$

The integral then becomes:

$$I = \frac{1}{k^2} \int_{kb}^{ka} \left(J_n'^2(t) + \frac{n^2}{t^2} J_n^2(t) \right) t \, dt \tag{D.16}$$

Splitting this integral in two partial integrals:

$$I = I_1 + I_2 \tag{D.17}$$

With:

$$I_1 = \frac{1}{k^2} \int_{kb}^{ka} J_n'^2(t)\ t\ dt \tag{D.18}$$

$$I_2 = \frac{1}{k^2} \int_{kb}^{ka} \frac{n^2}{t^2} J_n^2(t)\ t\ dt \tag{D.19}$$

Partial integrating of the first integral results in:

$$I_1 = \frac{1}{k^2} \left(t\ J_n'(t)\ J_n(t) \Big|_{kb}^{ka} - \int_{kb}^{ka} J_n(t) \left(t\ J_n'(t) \right)' dt \right) \tag{D.20}$$

Now use Bessel's differential equation:

$$J_n''(t) + \frac{1}{t}\ J_n'(t) + \left(1 - \frac{n^2}{t^2} \right) J_n(t) = 0 \tag{D.21}$$

$$\left(t\ J_n'(t) \right)' + t \left(1 - \frac{n^2}{t^2} \right) J_n(t) = 0 \tag{D.22}$$

And I_1 can be written:

$$I_1 = \frac{1}{k^2} \left(t\ J_n'(t)\ J_n(t) \Big|_{kb}^{ka} + \int_{kb}^{ka} t \left(1 - \frac{n^2}{t^2} \right) J_n^2(t)\ dt \right) \tag{D.23}$$

The same steps can be followed for I_2 and that leads to:

$$I_2 = \frac{1}{k^2} \left(t\ J_n'(t)\ J_n(t) \Big|_{kb}^{ka} + \int_{kb}^{ka} t\ \frac{n^2}{t^2} \right) J_n^2(t)\ dt \tag{D.24}$$

So I becomes:

$$I = \frac{1}{k^2} \left(t\ J_n'(t)\ J_n(t) \Big|_{kb}^{ka} + \int_{kb}^{ka} t\ J_n^2(t)\ dt \right) \tag{D.25}$$

The solution of the integral:

$$\int z\ A_\nu(kz)\ B_\nu(kz)\ dz$$

is known from complex analysis and is:

$$\frac{(k^2z^2 - \nu^2)\, A_\nu(kz)\, B_\nu(kz) + k^2z^2\, A_\nu'(kz)\, B_\nu'(kz)}{2\, k^2} + C \qquad (D.26)$$

Applying this to eq. D.25 gives:

$$I = \frac{1}{k^2} \left(t\, J_n'(t)\, J_n(t) + \frac{(t^2-n^2)\, J_n^2(t) + t^2 J_n'^2(t)}{2} \right) \Bigg|_{kb}^{ka} \qquad (D.27)$$

Now taking only the second part of eq. D.13 and applying the same techniques to the second integral:

$$I = \alpha^2 \int_b^a \left(\frac{n^2}{k^2\rho^2}\, Y_n^2(k\rho) + Y_n'^2(k\rho) \right) \rho\, d\rho \qquad (D.28)$$

gives:

$$I = \frac{\alpha^2}{k^2} \left(t\, Y_n'(t)\, Y_n(t) + \frac{(t^2-n^2)\, Y_n^2(t) + t^2 Y_n'^2(t)}{2} \right) \Bigg|_{kb}^{ka} \qquad (D.29)$$

The last integral that has to be determined is:

$$I = -2\,\alpha \int_b^a \left(\frac{n^2}{k^2\rho^2}\, J_n(k\rho)\, Y_n(k\rho) + J_n'(k\rho)\, Y_n'(k\rho) \right) \rho\, d\rho \qquad (D.30)$$

Again use the definition D.15 and the integral can be written as:

$$I = -\frac{2\,\alpha}{k^2} \int_{kb}^{ka} \left(J_n'(t)\, Y_n'(t) + \frac{n^2}{t^2}\, J_n(t)\, Y_n(t) \right) t\, dt \qquad (D.31)$$

Splitting this integral in two parts:

$$I = -\frac{2\,\alpha}{k^2} \left(I_1 + I_2 \right) \qquad (D.32)$$

With:

$$I_1 = \int_{kb}^{ka} J_n'(t)\, Y_n'(t)\, t\, dt \qquad (D.33)$$

$$I_2 = \int_{kb}^{ka} \frac{n^2}{t^2} J_n(t)\, Y_n(t)\, t\, dt \qquad (D.34)$$

Partial integration of the first integral results in:

$$I_1 = t\, J_n(t)\, Y_n'(t) \Big|_{kb}^{ka} - \int_{kb}^{ka} J_n(t) \left(t\, Y_n'(t) \right)' dt \qquad (D.35)$$

Now use Bessel's differential equation again:

$$Y_n''(t) + \frac{1}{t}\, Y_n'(t) + \left(1 - \frac{n^2}{t^2} \right) Y_n(t) = 0 \qquad (D.36)$$

$$\left(t\, Y_n'(t) \right)' + t \left(1 - \frac{n^2}{t^2} \right) Y_n(t) = 0 \qquad (D.37)$$

And I_1 can be written:

$$I_1 = t\, J_n(t)\, Y_n'(t) \Big|_{kb}^{ka} + \int_{kb}^{ka} t \left(1 - \frac{n^2}{t^2} \right) J_n(t)\, Y_n(t)\, dt \Bigg) \qquad (D.38)$$

The same steps can be followed for I_2 and that leads to:

$$I_2 = t\, J_n(t)\, Y_n'(t) \Big|_{kb}^{ka} + \int_{kb}^{ka} t\, \frac{n^2}{t^2} J_n(t)\, Y_n(t)\, dt \qquad (D.39)$$

So I becomes:

$$I = -\frac{2\,\alpha}{k^2} \left(t\, J_n(t)\, Y_n'(t) \Big|_{kb}^{ka} + \int_{kb}^{ka} t\, J_n(t)\, Y_n(t)\, dt \right) \qquad (D.40)$$

Using eq. D.26 again we find as solution of the integral:

$$I = -\frac{2\,\alpha}{k^2} \left(t\, J_n(t)\, Y_n'(t) + \frac{(t^2 - n^2)\, J_n(t)\, Y_n(t) + t^2\, J_n'(t)\, Y_n'(t)}{2} \right) \Bigg|_{kb}^{ka} \qquad (D.41)$$

And finally the total dissipated power in the conductors becomes:

$$P_c = E_o^2 \frac{\varepsilon}{\mu} \frac{\pi}{k^2} \sqrt{\frac{\pi f \mu}{\sigma}} \left[t J_n'(t) J_n(t) + \frac{(t^2-n^2) J_n^2(t) + t^2 J_n'^2(t)}{2} + \right.$$

$$- 2\alpha \left[t J_n(t) Y_n'(t) + \frac{(t^2-n^2) J_n(t) Y_n(t) + t^2 J_n'(t) Y_n'(t)}{2} \right]$$

$$\left. + \alpha^2 \left[t Y_n'(t) Y_n(t) + \frac{(t^2-n^2) Y_n^2(t) + t^2 Y_n'^2(t)}{2} \right] \right] \Bigg|_{kb}^{ka} \quad \text{(D.42)}$$

The factor:

$$E_o^2 \frac{\varepsilon}{\mu} \frac{\pi}{k^2} \sqrt{\frac{\pi f \mu}{\sigma}} \quad \text{(D.43)}$$

can be written as:

$$E_o^2 \frac{1}{4} \sqrt{\frac{1}{\sigma \pi f^3 \mu^3}} \quad \text{(D.44)}$$

Using the resonance condition:

$$J_n'(ka) - \frac{J_n(kb)}{Y_n(kb)} Y_n'(kb) = 0 \quad \text{(D.45)}$$

All terms $Y_n'(kb)$ can be eliminated and using a large amount of algebra the following expression for the conductor loss can be derived:

$$Pc = \frac{1}{8\sqrt{\pi \sigma \mu_o^3 f^3}} \cdot \left[\left(2 k a J_n'(ka) \left(-J_n(ka) + \alpha Y_n(ka) \right) + \right. \right.$$

$$\left. \left((k a)^2 - n^2 \right) \left(J_n(ka) - \alpha Y_n(ka) \right)^2 \right) -$$

$$\left[2\,k\,b\,J_n(kb)\left(J_n'(kb) - \alpha\, Y_n'(kb) \right) + (k\,b)^2 \left(J_n'(kb) - \alpha\, Y_n'(kb) \right)^2 \right] \right] \qquad (D.46)$$

And:

$$\alpha = \frac{J_n(kb)}{Y_n(kb)} \qquad (D.47)$$

References:

[D-1] Ramo S., Whinnery J.R. and Van Duzer T., 'Fields and Waves in Communication Electronics', p. 152, John Wiley and Sons Inc., 1984.

Appendix E Losses in the dielectric substrate.

The losses in the dielectric substrate can be calculated from:

$$P_d = \frac{\omega \varepsilon \tan(\delta)}{2} \iiint_V \bar{E} \cdot \bar{E}^* \, dV \qquad (E.1)$$

Using the expression for E_z as derived in § 3.2:

$$P_d = \frac{\omega \varepsilon \tan(\delta)}{2} \int_0^h \int_b^a \int_0^{2\pi} E_o^2 \cos^2(n\phi) \left(J_n(k\rho) - \alpha Y_n(k\rho) \right)^2 \rho \, d\rho \, d\phi \, dz \qquad (E.2)$$

With:

$$\alpha = \frac{J_n(kb)}{Y_n(kb)} \qquad (E.3)$$

Working out the integrals:

$$P_d = \frac{\omega \varepsilon \tan(\delta)}{2} E_o^2 \, h \, \pi \int_b^a \left(J_n(k\rho) - \alpha Y_n(k\rho) \right)^2 \rho \, d\rho \qquad (E.4)$$

Eliminating the brackets:

$$P_d = \frac{\omega \varepsilon \tan(\delta)}{2} E_o^2 \, h \, \pi \int_b^a \left(J_n^2(k\rho) - 2 \alpha J_n(k\rho) Y_n(k\rho) + \alpha^2 Y_n^2(k\rho) \right) \rho \, d\rho \qquad (E.5)$$

The solution of the integral:

$$\int z A_\nu(kz) B_\nu(kz) \, dz$$

is known from complex analysis and is:

$$\frac{(k^2z^2 - \nu^2) A_\nu(kz) B_\nu(kz) + k^2 z^2 A_\nu'(kz) B_\nu'(kz)}{2k^2} + C \qquad (E.6)$$

And by using the abbreviation:

$$t = k\rho$$

the result of the integral is:

$$P_d = \frac{\omega\,\varepsilon\,\tan(\delta)}{2} E_o^{\,2}\, h\,\pi \left[\frac{(t^2-n^2)\, J_n^{\,2}(t) + t^2\, J_n^{\,\prime 2}(t)}{2\,k^2} + \right.$$

$$- 2\,\alpha \left(\frac{(t^2-n^2)\, J_n(t)\, Y_n(t) + t^2\, J_n'(t)\, Y_n'(t)}{2\,k^2} \right) +$$

$$\left. \alpha^2 \left(\frac{(t^2-n^2)\, Y_n^{\,2}(t) + t^2\, Y_n^{\,\prime 2}(t)}{2\,k^2} \right) \right] \Bigg|_{kb}^{ka} \qquad \text{(E.7)}$$

Bringing the factor $\frac{1}{k^2}$ outside the brackets:

$$P_d = \frac{h\,\tan(\delta)}{8\,f\,\mu_o} E_o^{\,2} \left[(t^2-n^2)\, J_n^{\,2}(t) + t^2\, J_n^{\,\prime 2}(t) \right.$$

$$- 2\,\alpha \left((t^2-n^2)\, J_n(t)\, Y_n(t) + t^2\, J_n'(t)\, Y_n'(t) \right)$$

$$\left. \alpha^2 \left((t^2-n^2)\, Y_n^{\,2}(t) + t^2\, Y_n^{\,\prime 2}(t) \right) \right] \Bigg|_{t=kb}^{t=ka} \qquad \text{(E.8)}$$

By using the resonance condition, and carrying out a large amount of algebra, this expression can be simplified to:

$$P_d = \frac{h\,\tan(\delta)}{8\,f\,\mu_o}$$

$$\left[\left(\left[(ka)^2 - n^2 \right] \left(J_n(ka) - \alpha\, Y_n(ka) \right)^2 \right) - \right.$$

$$\left. \left((kb)^2 \left(J_n'(kb) - \alpha\, Y_n'(kb) \right)^2 \right) \right] \qquad \text{(E.9)}$$

Appendix F Calculation of the stored energy in the cavity.

To calculate the quality factor of the resonator, the energy stored in the cavity must be calculated. Namely:

$$Q_T = \frac{\omega W_T}{P_T} \tag{F.1}$$

With ω the angular frequency, W_T the energy stored in the cavity and P_T the power supplied to the cavity. Since the power P_T can be calculated from the preceding theory, the only quantity that must be calculated is the energy stored in the cavity W_T.
As it is well-known from fundamental electromagnetic theory, the energy stored in a cavity with volume V can be calculated from:

$$W_T = \frac{\varepsilon}{2} \iiint_V |\bar{E}|^2 \, dV \tag{F.2}$$

Using the expressions for E_z as derived in § 3.2 , this can be written as:

$$W_T = \frac{\varepsilon}{2} \int_b^a \int_0^h \int_0^{2\pi} E_o^2 \cos^2(n\phi) \left[J_n(k\rho) - \alpha Y_n(k\rho) \right]^2 \rho \, d\rho \, d\phi \, dz \tag{F.3}$$

$$\frac{\varepsilon E_o^2 \pi h}{2} \int_b^a \left[J_n(k\rho) - \alpha Y_n(k\rho) \right]^2 \rho \, d\rho \tag{F.4}$$

This exactly the same integral as already has been explained in Appendix E, so only the final result of these calculations is mentioned here.

$$W_T = \frac{\varepsilon E_o^2 \pi h}{2} \left(\frac{(t^2-n^2) J_n^2(t) + t^2 J_n'^2(t)}{2 k^2} + \right.$$

$$- 2\alpha \left(\frac{(t^2-n^2) J_n(t) Y_n(t) + t^2 J_n'(t) Y_n'(t)}{2 k^2} \right) +$$

$$\left. \alpha^2 \left(\frac{(t^2-n^2) Y_n^2(t) + t^2 Y_n'^2(t)}{2 k^2} \right) \right) \Bigg|_{kb}^{ka} \tag{F.5}$$

Where the abbreviation:

$$t = k\rho \tag{F.6}$$

has been introduced.

Bringing the factor $\frac{1}{k^2}$ outside the brackets:

$$W_T = \frac{h\,E_o}{16\,\pi\,\mu\,f^2} \left[(t^2-n^2)\,J_n^{\,2}(t) + t^2\,J_n^{\,'2}(t) \right.$$

$$- 2\,\alpha \left((t^2-n^2)\,J_n(t)\,Y_n(t) + t^2\,J_n^{'}(t)\,Y_n^{'}(t) \right)$$

$$\left. \alpha^2 \left((t^2-n^2)\,Y_n^{\,2}(t) + t^2\,Y_n^{\,'2}(t) \right) \right] \Bigg|_{kb}^{ka} \tag{F.7}$$

By using the resonance condition, this expression can be simplified to:

$$W_T = \frac{1}{16\,\pi\,\mu_o\,f^2}$$

$$\left[\left(\left((ka)^2 - n^2 \right) \left(J_n(ka) - \alpha\,Y_n(ka) \right)^2 \right) - \right.$$

$$\left. \left((kb)^2 \left(J_n^{'}(kb) - \alpha\,Y_n^{'}(kb) \right)^2 \right) \right] \tag{F.8}$$

With:

$$\alpha = \frac{J_n(kb)}{Y_n(kb)} \tag{F.9}$$

Appendix G Material specifications.

RT/duroid® A BETTER CLASS OF HIGH PRECISION MICROWAVE LAMINATES

RT/duroid® 5870 and 5880 substrates are composed of uniformly dispersed glass microfibres in a PTFE matrix, thus providing the microwave engineer with a microscopically controlled uniform dielectric constant (dk).
The 6000 series are composed of uniformly dispersed ceramic filler in PTFE matrix.

	Material Dielectric constant* (at 10 GHz nominal)	Dissipation factor (at 10 GHz nominal)
RT/duroid 5870	2.33 +/-0.02	0.0012 typical
RT/duroid 5880	2.20 +/-0.02	0.0009 typical
RT/duroid 6006	6.00 +/-0.20	0.0020 typical
RT/duroid 6010.2	10.2 +/-0.25	0.0020 typical
RT/duroid 6010.5	10.5 +/-0.25	0.0020 typical
RT/duroid 5500	2.5 +/-0.04	0.0025 typical

*Stripline test method

RT/duroid® substrates may be supplied:

— copper clad on one or both sides with either electrodeposited (EDC) copper or rolled (RC) copper for lower loss.
— clad with thick copper, brass or aluminium planes.

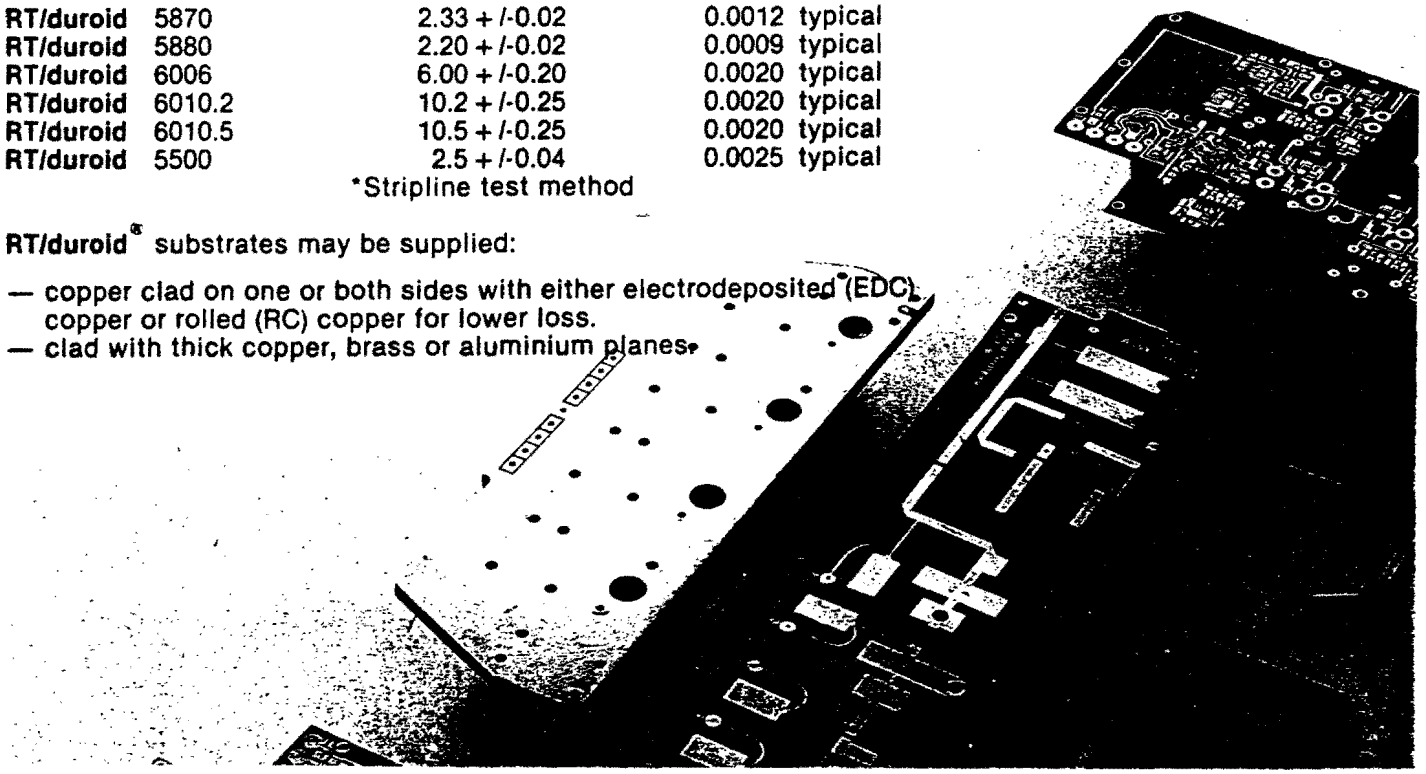

AVAILABILITY

RT/duroid® 5870 AND 5880

DIELECTRIC CONSTANT

RT/D 5870: $\epsilon_r = 2.33 \pm 0.02$
RT/D 5880: $\epsilon_r = 2.20 \pm 0.02$ ←
Specification MIL-P-13949F type GRN

CLADDING

COPPER 1/8 oz ED Copper
1/4 oz ED Copper
1/2 oz Rolled or ED Copper
1 oz Rolled or ED Copper
2 oz Rolled or ED Copper

THICK METAL BACKING
On special request we can supply Aluminium, Brass or Copper backed material

SHEET SIZE AND THICKNESS

Size:	inches	mm
	18 x 12	457 x 305
	18 x 24	457 x 610
	18 x 36	457 x 915
	18 x 48	457 x 1219

Thickness and tolerance:

0,005 ± 10%	0,13 ± 10%
0,010 ± 7%	0,25 ± 7%
0,015 ± 7%	0,38 ± 7%
0,020 ± 0,001	0,51 ± 0,03
0,031 ± 0,001	0,79 ± 0,03
0,062 ± 0,002	1,57 ± 0,05
0,125 ± 0,004	3,18 ± 0,10

Other sheetsizes and thicknesses available on request

RT/duroid® 6010

DIELECTRIC CONSTANT

RT/D 6010.2: $\epsilon_r = 10.2 \pm 0.25$
RT/D 6010.5: $\epsilon_r = 10.5 \pm 0.25$
RT/D 6006 : $\epsilon_r = 6 \pm 0.20$

CLADDING

COPPER 1/8 oz ED Copper
1/4 oz ED Copper
1/2 oz Rolled Copper or ED Copper
1 oz Rolled Copper or ED Copper
2 oz Rolled Copper or ED Copper

THICK METAL BACKING
On special request we can supply Aluminium, Brass of Copper backed material.

SHEET SIZE AND THICKNESS

Size:	inches	mm
	20 x 20	508 x 508
	10 x 20	254 x 508
	10 x 10	254 x 254

Thickness and tolerance:

0,010 ± 0,001*	0,25 ± 0,03
0,025 ± 0,001	0,64 ± 0,03
0,050 ± 0,002	1,27 ± 0,05
0,075 ± 0,004	1,91 ± 0,10
0,100 ± 0,005	2,54 ± 0,13

* not available in RT/duroid 6010.2

RT/duroid® 5500

DIELECTRIC CONSTANT

RT/D 5500: $\epsilon_r = 2.5 \pm 0.04$

CLADDING

COPPER: 1 oz ED Copper
other copper claddings available on request.

THICK METAL BACKING
On special request we can supply Aluminium, Brass or Copper backed material.

SHEET SIZE AND THICKNESS

Size:	inches	mm
	18 x 12	457 x 305
	18 x 24	457 x 610
	18 x 36	457 x 915
	18 x 48	457 x 1219

Thickness and tolerance:

0,015 ± 0,001	0,38 ± 7%
0,031 ± 0,001	0,79 ± 0,03
0,062 ± 0,002	1,57 ± 0,05
0,093 ± 0,003	2,36 ± 0,07
0,125 ± 0,004	3,18 ± 0,10

Other sheetsizes and thicknesses available on request.

Appendix H Measurements.

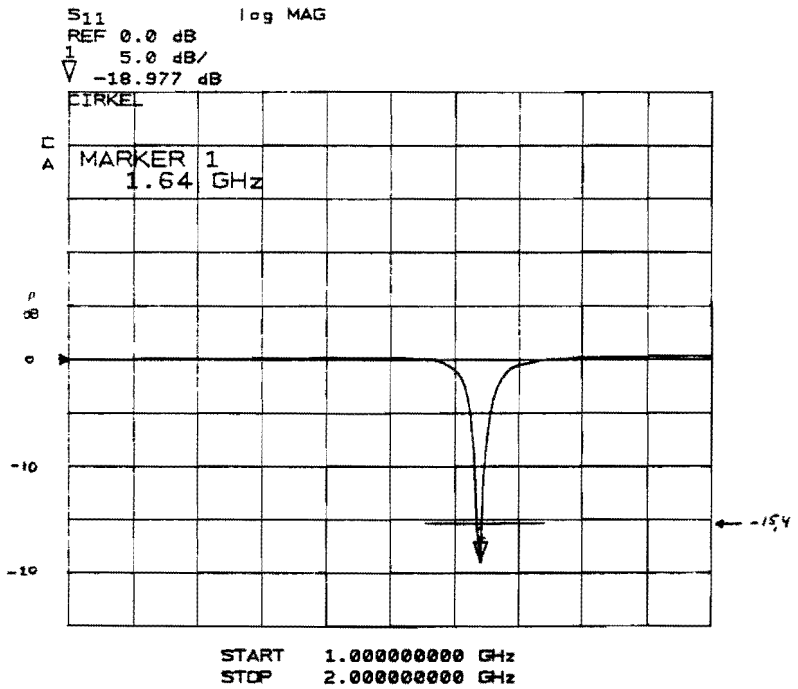

Fig. H.1 : Reflection coefficient of the circular microstrip antenna as function of the frequency

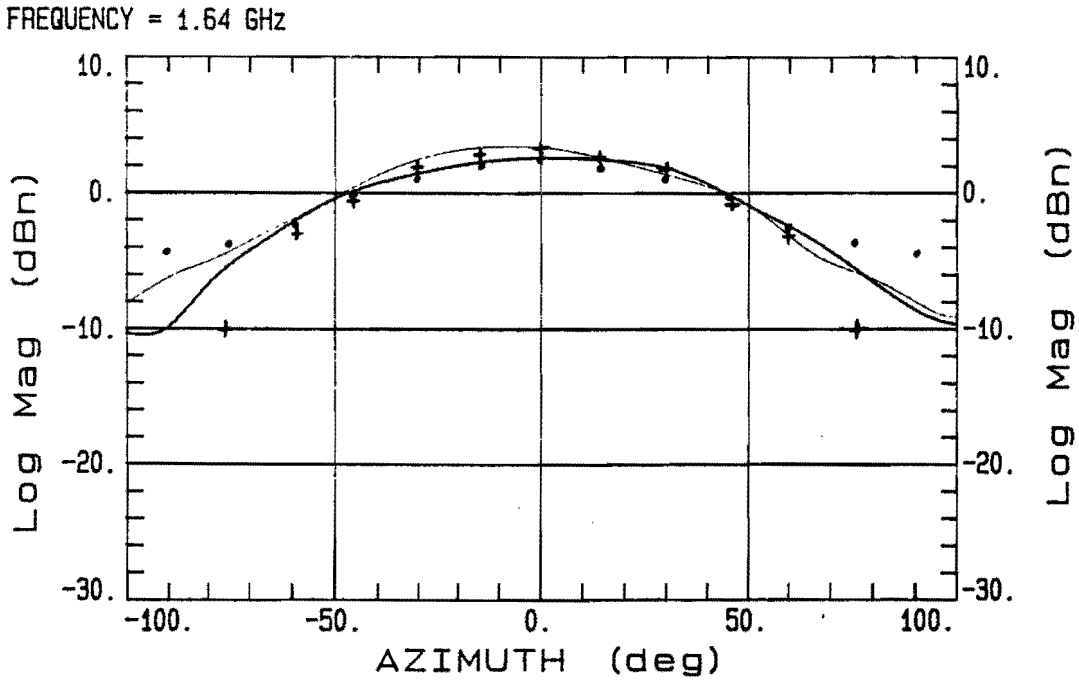

Fig. H.2 : Radiation patterns of the linearly polarized circular microstrip antenna in planes $\phi=0^\circ$ and $\phi=90^\circ$
plane $\phi=0^\circ$: calculated : + ; measured : -
plane $\phi=90^\circ$: calculated : • ; measured : —

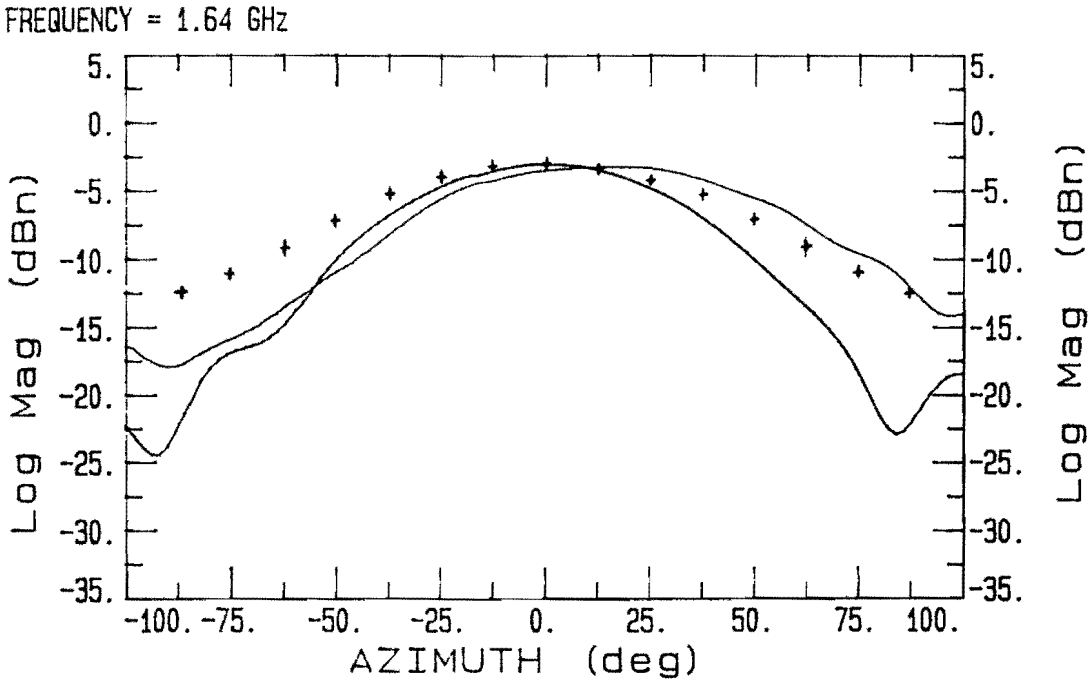

Fig. H.3 : Radiation patterns of the circularly polarized circular microstrip antenna in plane $\phi=0^{\circ}$
calculated : + ; measured : –

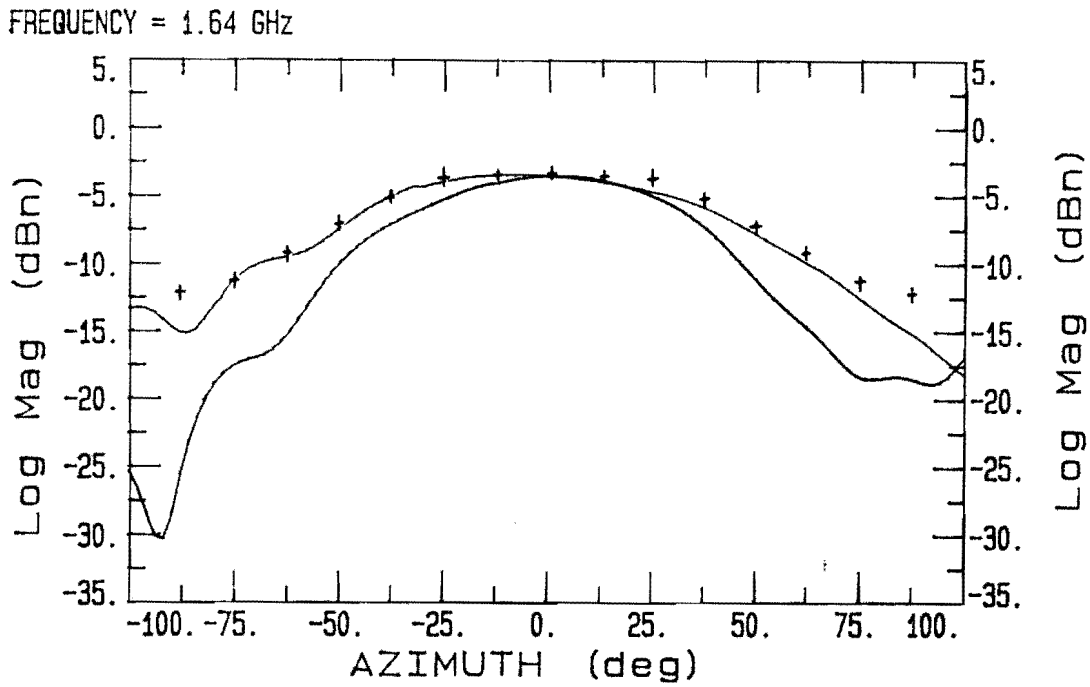

Fig. H.4 : Radiation patterns of the circularly polarized circular microstrip antenna in plane $\phi=45^{\circ}$
calculated : + ; measured : –

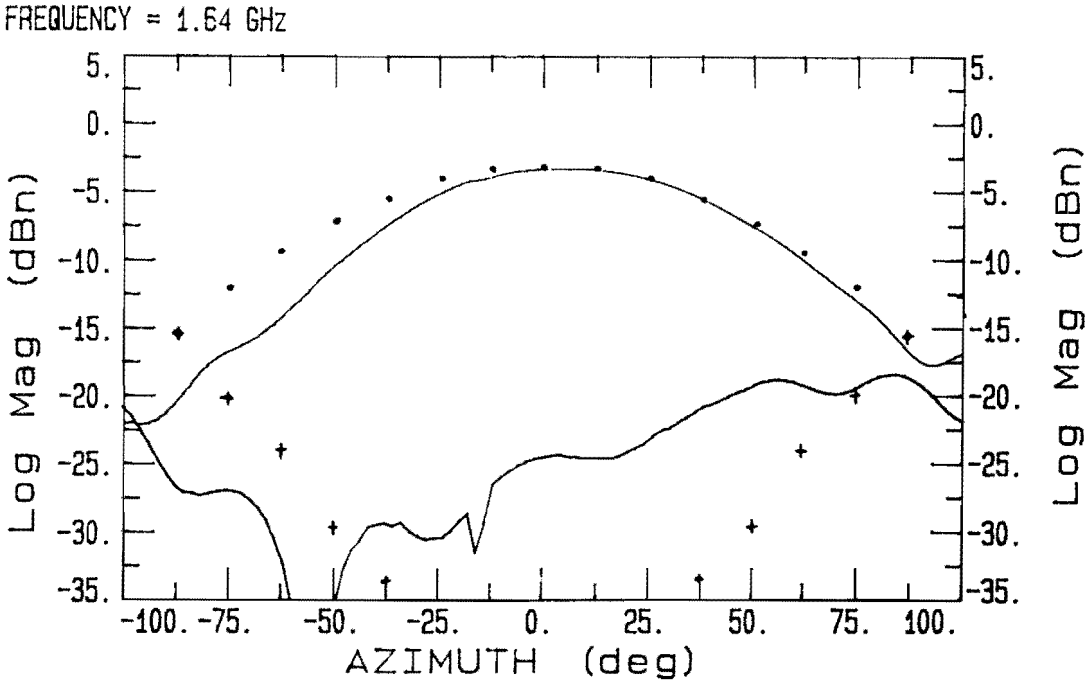

Fig. H.5 : Co- and cross-polarization patterns of the circularly polarized circular microstrip antenna in plane $\phi=0^{\circ}$
co polarization : calculated : • ; measured : -
cross polarization : calculated : + ; measured : –

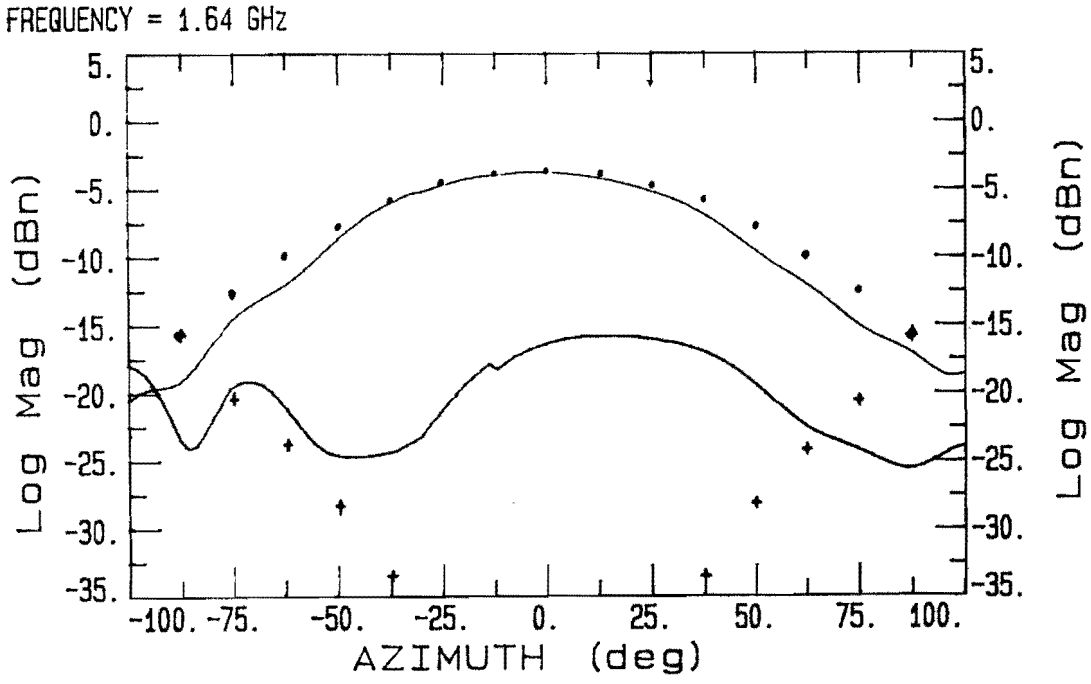

Fig. H.6 : Co- and cross-polarization patterns of the circularly polarized circular microstrip antenna in plane $\phi=45^{\circ}$
co polarization : calculated : • ; measured : -
cross polarization : calculated : + ; measured : –

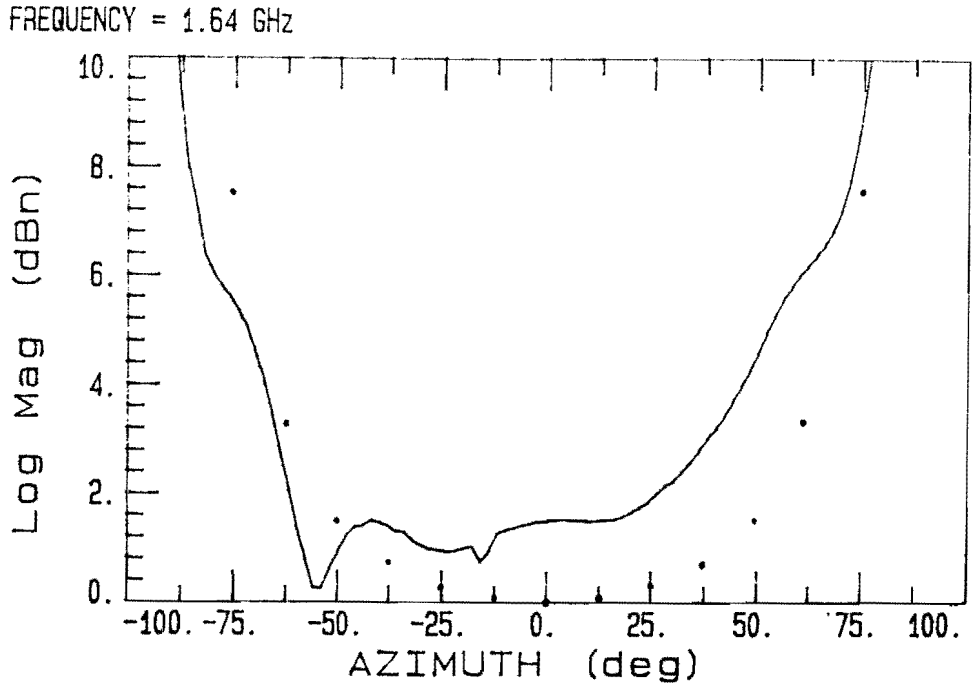

Fig. H.7 : Axial ratio pattern of the circularly polarized circular microstrip antenna in plane $\phi=0^{\circ}$
calculated : • ; measured : -

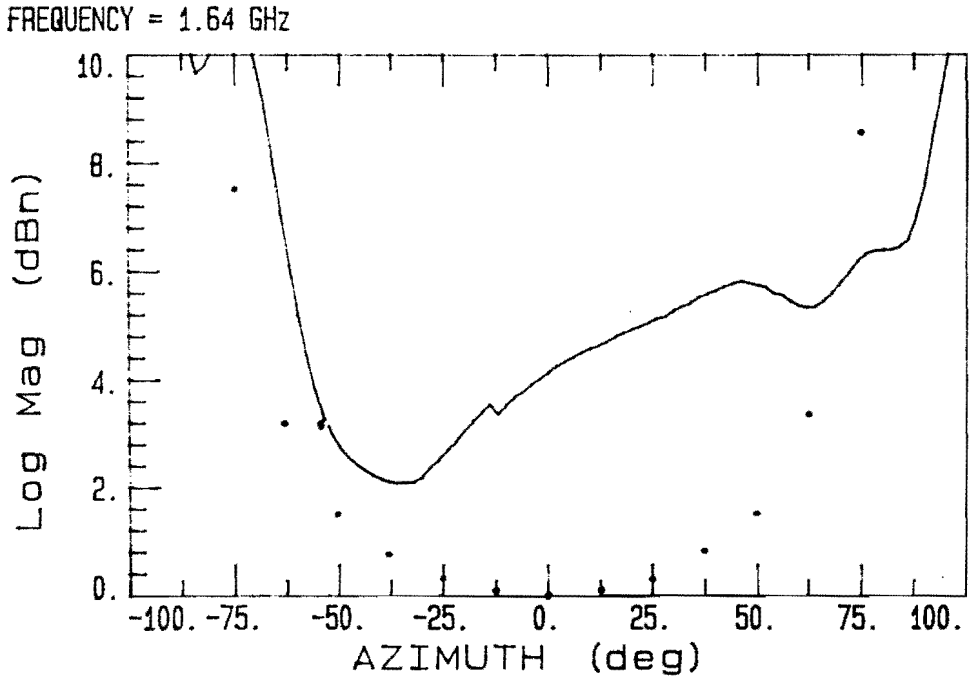

Fig. H.8 : Axial ratio pattern of the circularly polarized circular microstrip antenna in plane $\phi=45^{\circ}$
calculated : • ; measured : -

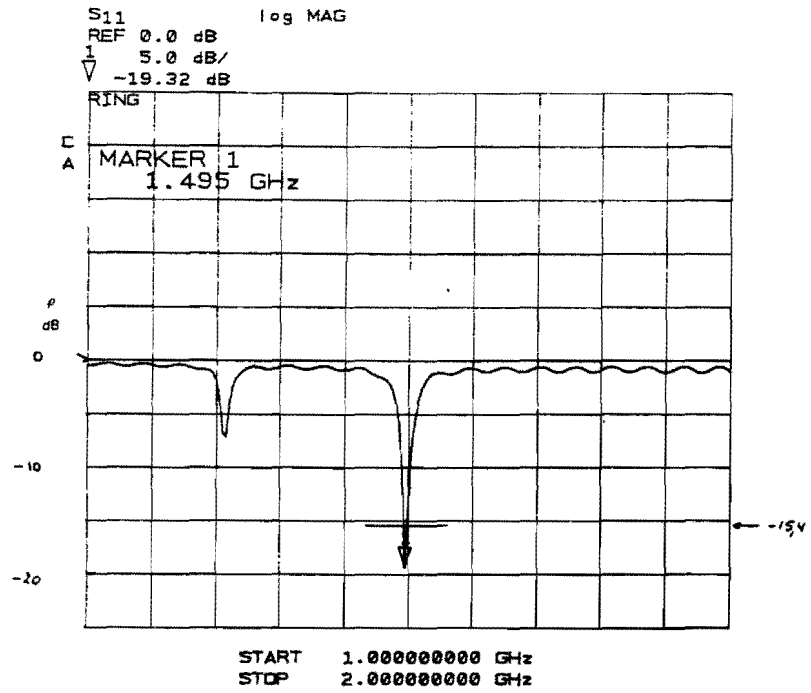

Fig. H.9 : Reflection coefficient of the circular ring microstrip antenna as function of the frequency

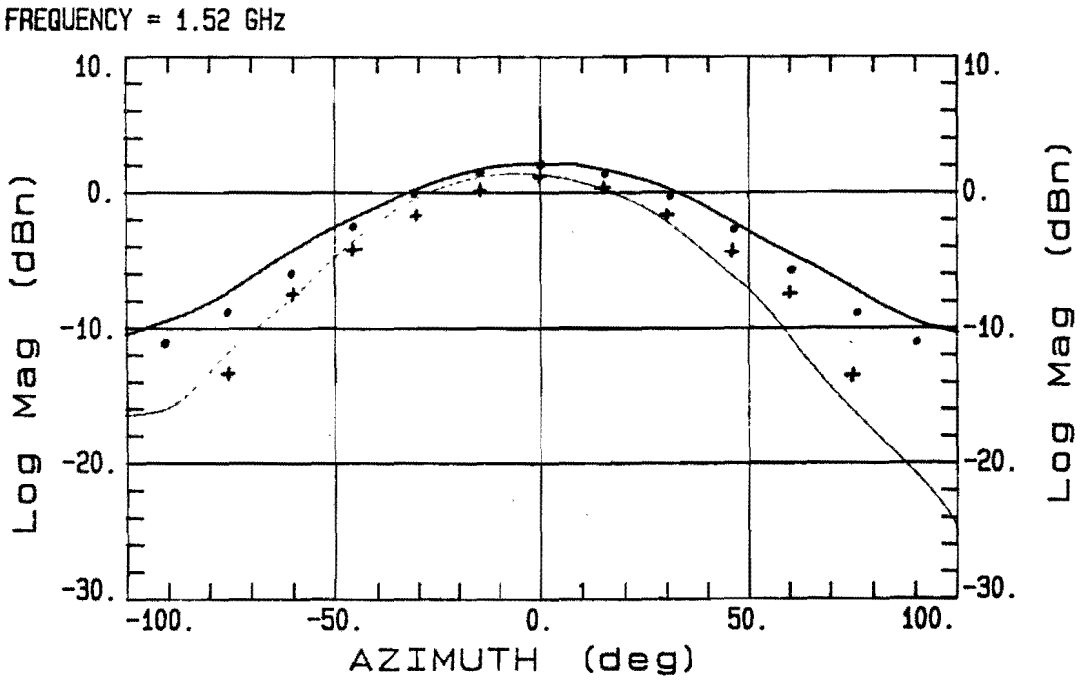

Fig. H.10 : Radiation patterns of the linearly polarized circular ring microstrip antenna in planes $\phi=0^\circ$ and $\phi=90^\circ$
plane $\phi=0^\circ$: calculated : + ; measured : -
plane $\phi=90^\circ$: calculated : • ; measured : –

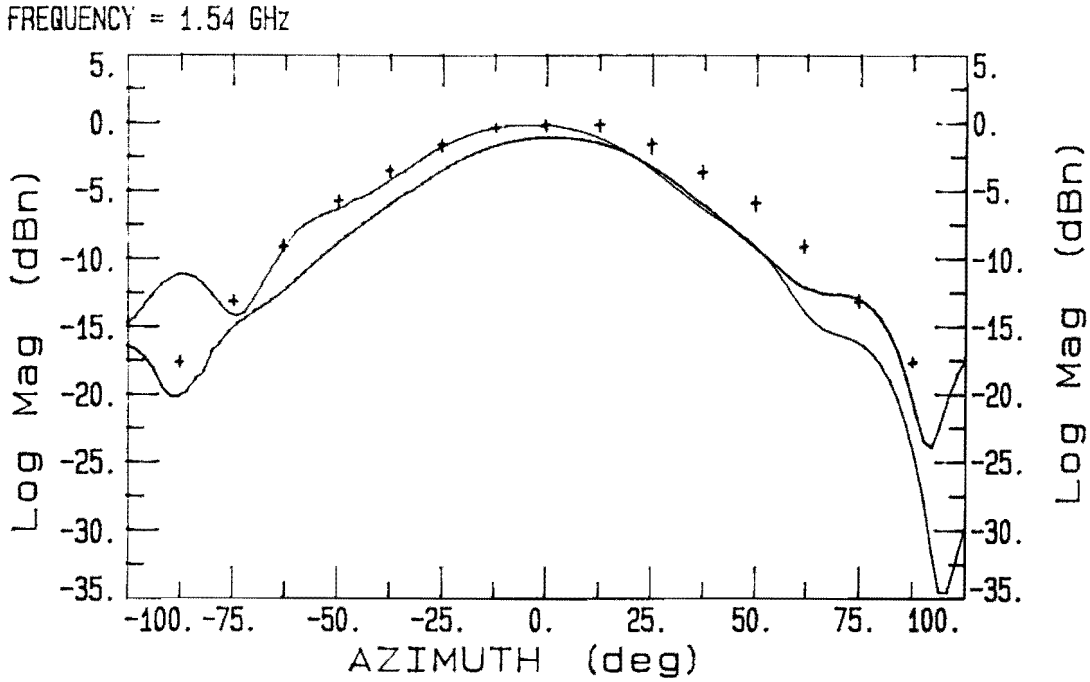

Fig. H.11 : Radiation patterns of the circularly polarized circular ring microstrip antenna in plane $\phi=0^{\circ}$
calculated : + ; measured : –

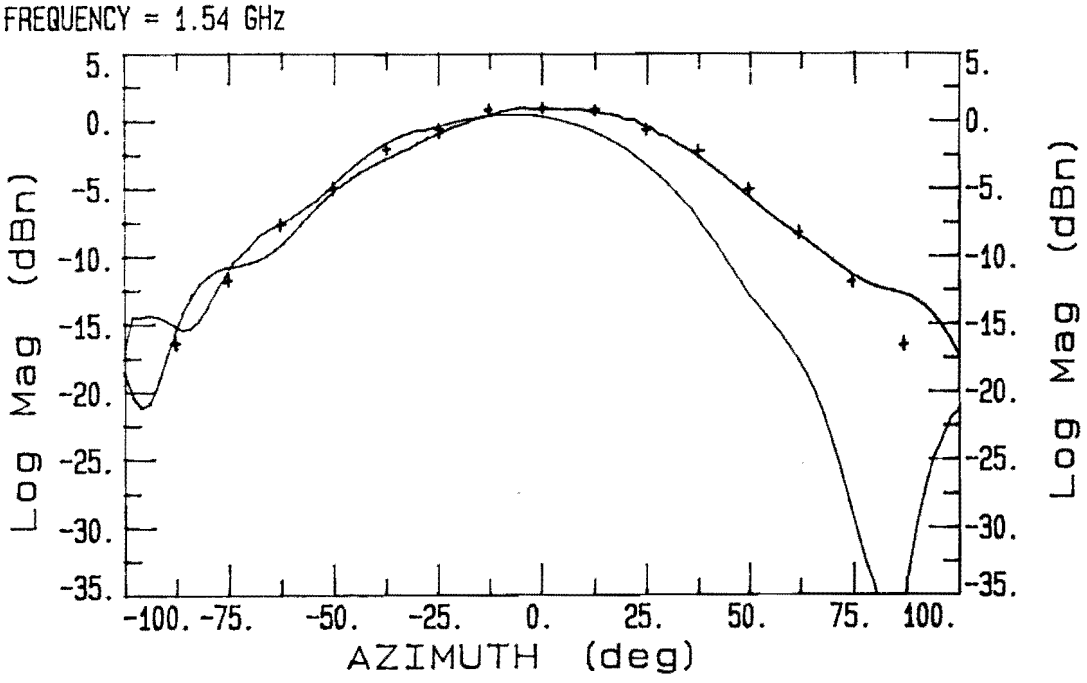

Fig. H.12 : Radiation patterns of the circularly polarized circular ring microstrip antenna in plane $\phi=45^{\circ}$
calculated : + ; measured : –

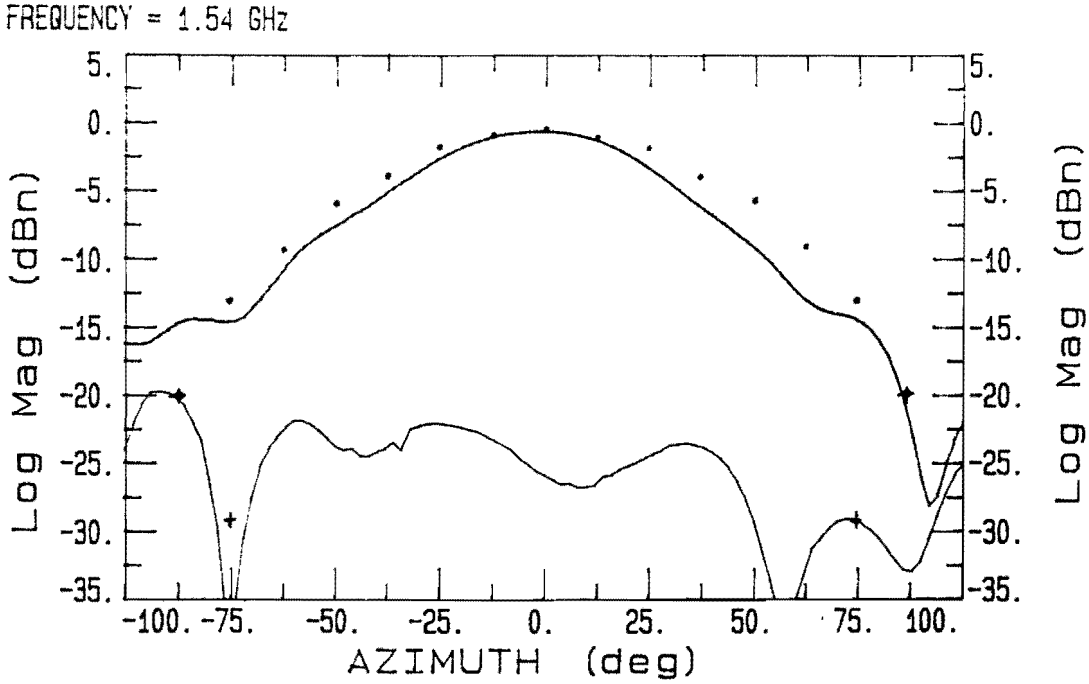

Fig. H.13 : Co- and cross-polarization patterns of the circularly polarized circular ring microstrip antenna in plane $\phi=0^{\circ}$
co polarization : calculated : • ; measured : -
cross polarization : calculated : + ; measured : –

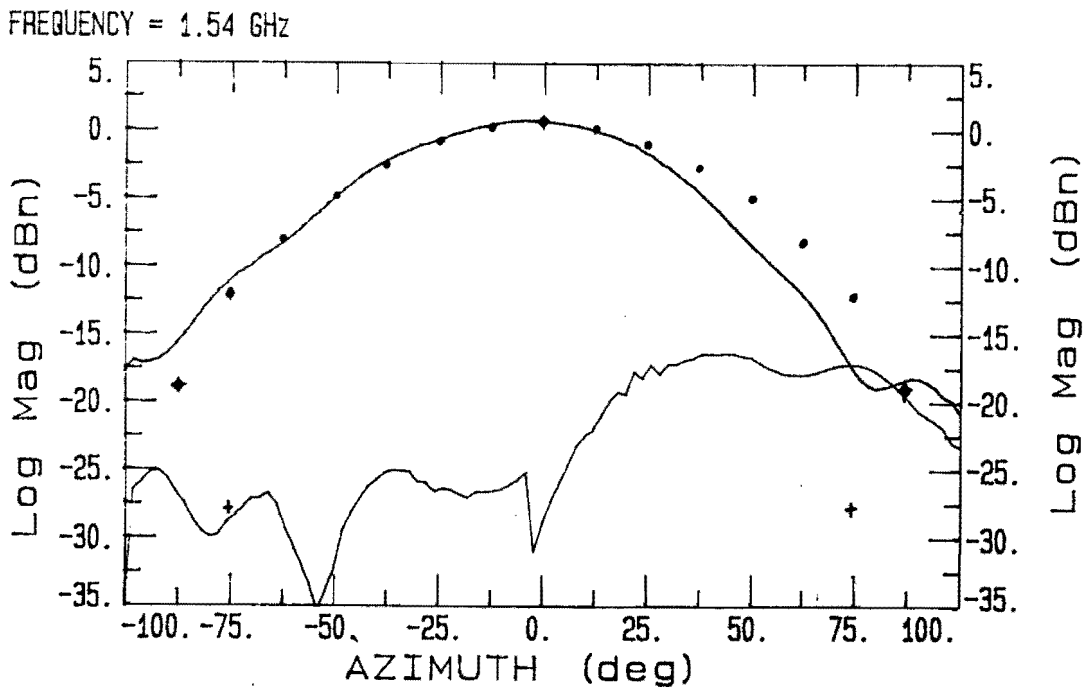

Fig. H.14 : Co- and cross-polarization patterns of the circularly polarized circular ring microstrip antenna in plane $\phi=45^{\circ}$
co polarization : calculated : • ; measured : -
cross polarization : calculated : + ; measured : –

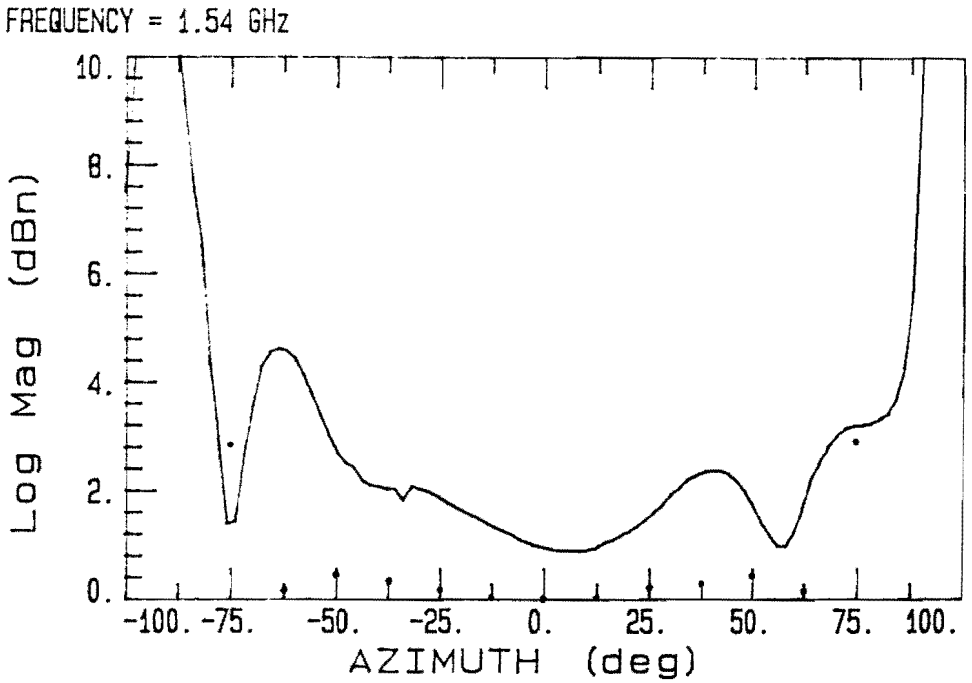

Fig. H.15 : Axial ratio pattern of the circularly polarized circular ring microstrip antenna in plane $\phi=0^{\circ}$ calculated : • ; measured : -

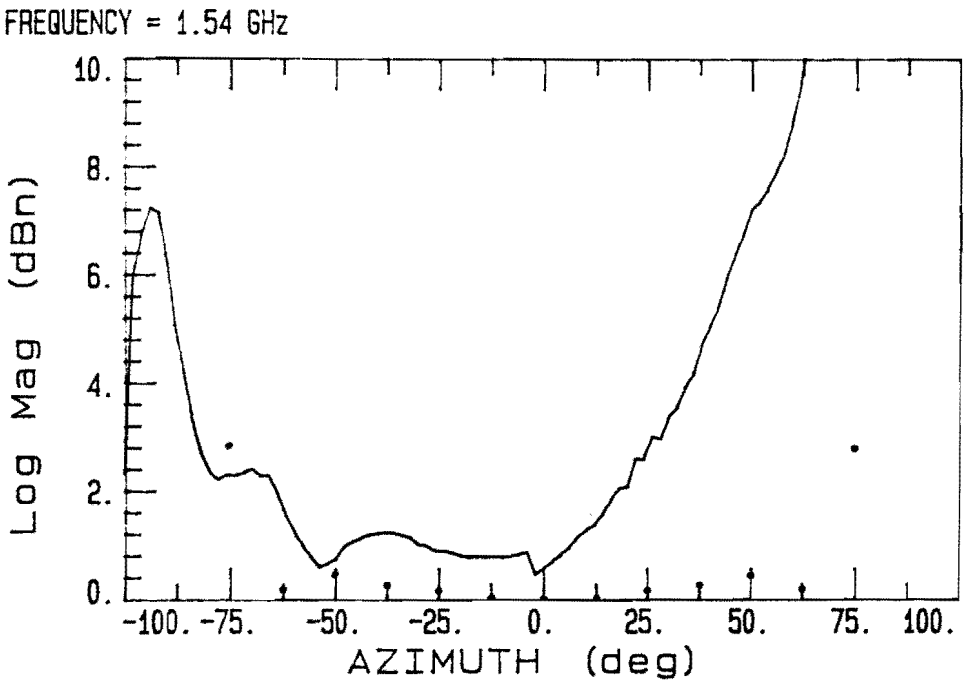

Fig. H.16 : Axial ratio pattern of the circularly polarized circular ring microstrip antenna in plane $\phi=45^{\circ}$ calculated : • ; measured : -

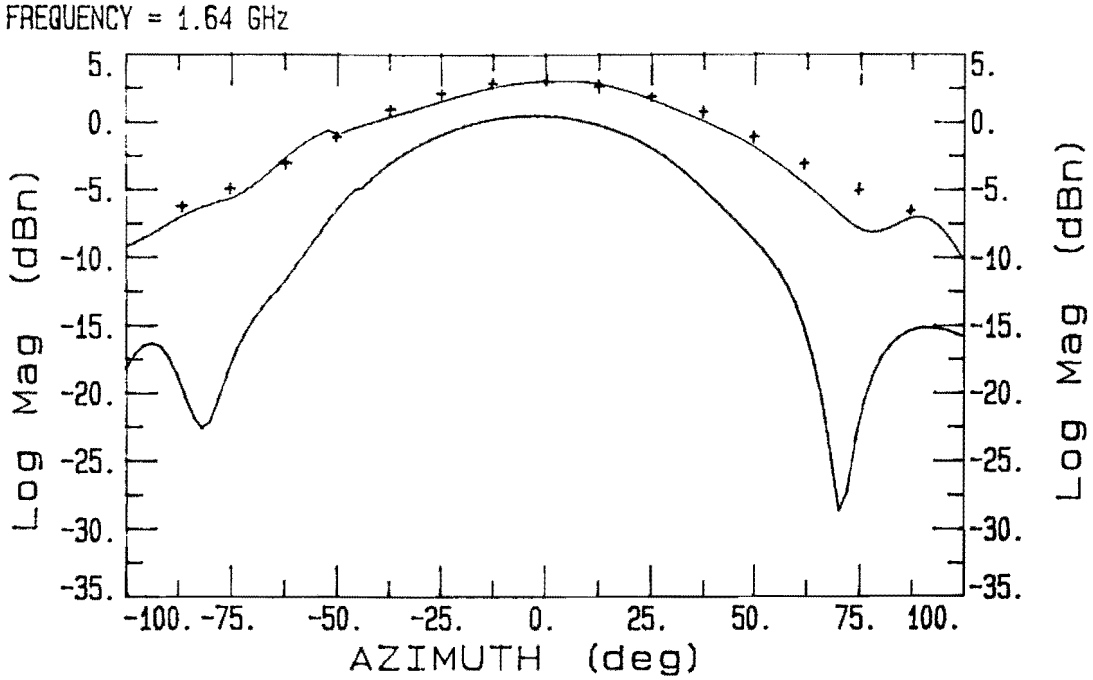

Fig. H.17 : Radiation patterns of the circularly polarized circular stacked microstrip antenna in plane $\phi=0^{\circ}$
calculated : + ; measured : –

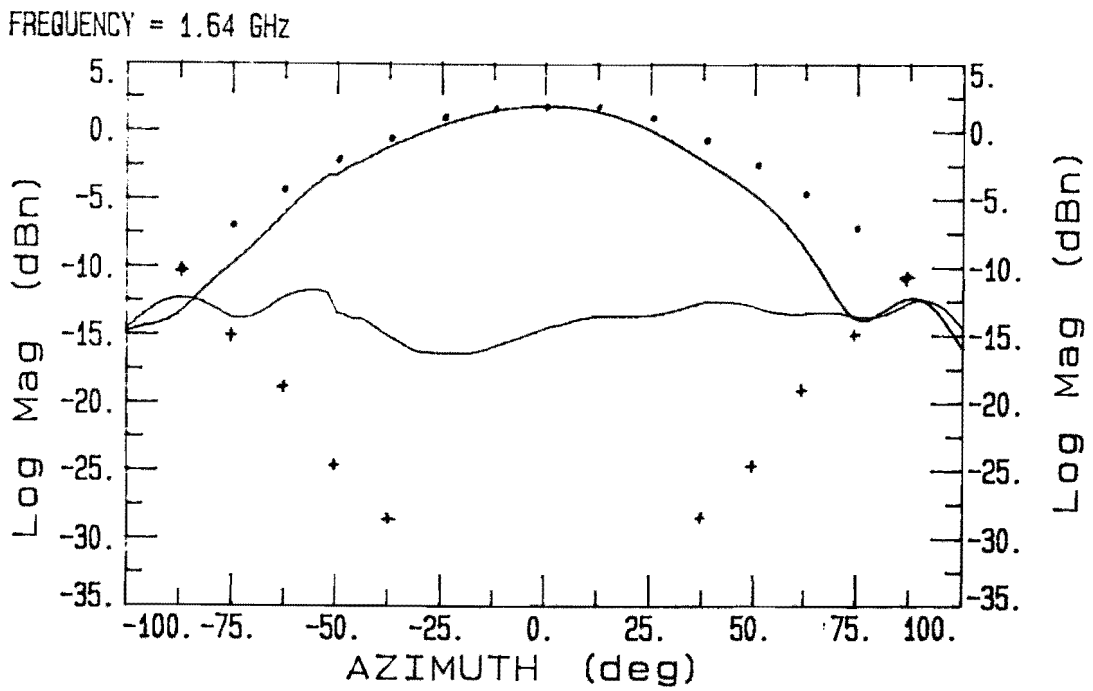

Fig. H.18 : Co- and cross-polarization patterns of the circularly polarized circular stacked microstrip antenna in plane $\phi=0^{\circ}$
co polarization : calculated : • ; measured : -
cross polarization : calculated : + ; measured : –

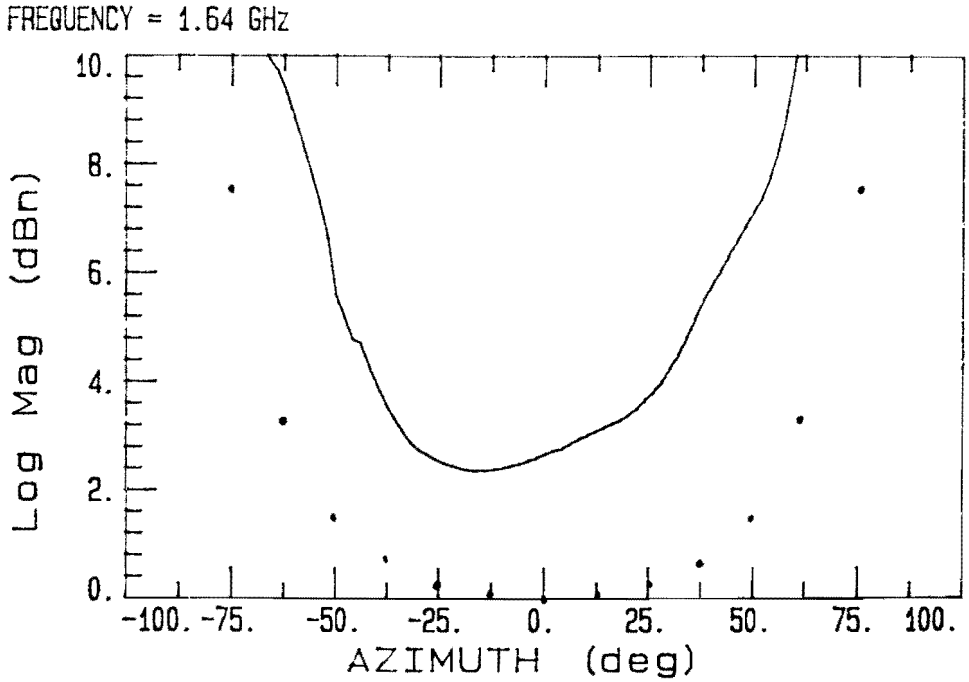

Fig. H.19 : Axial ratio pattern of the circularly polarized circular stacked microstrip antenna in plane $\phi=0^{\circ}$ calculated : • ; measured : -

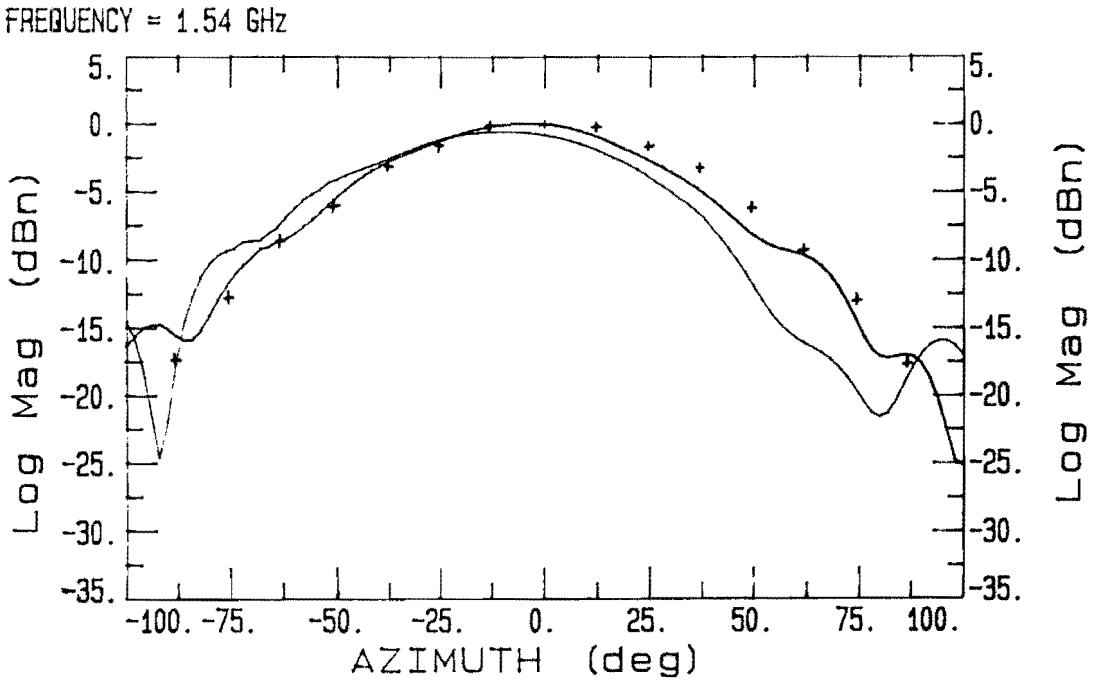

Fig. H.20 : Radiation patterns of the circularly polarized circular ring stacked microstrip antenna in plane $\phi=0^{\circ}$ calculated : + ; measured : –

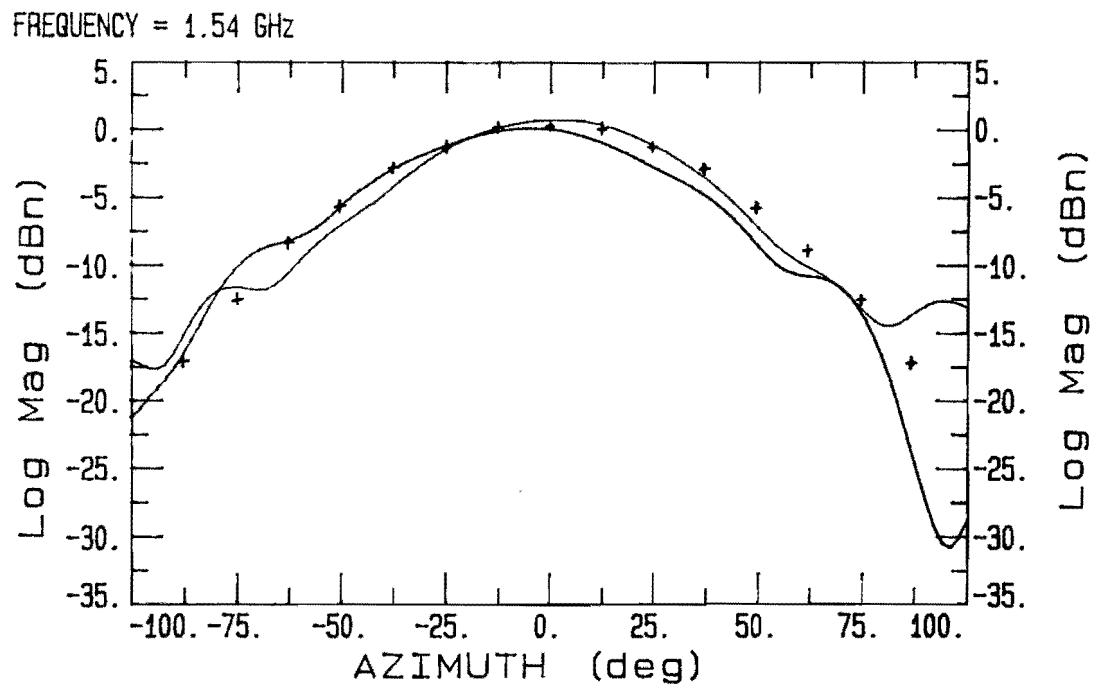

Fig. H.21 : Radiation patterns of the circularly polarized circular ring stacked microstrip antenna in plane $\phi=45^{\circ}$ calculated : + ; measured : –

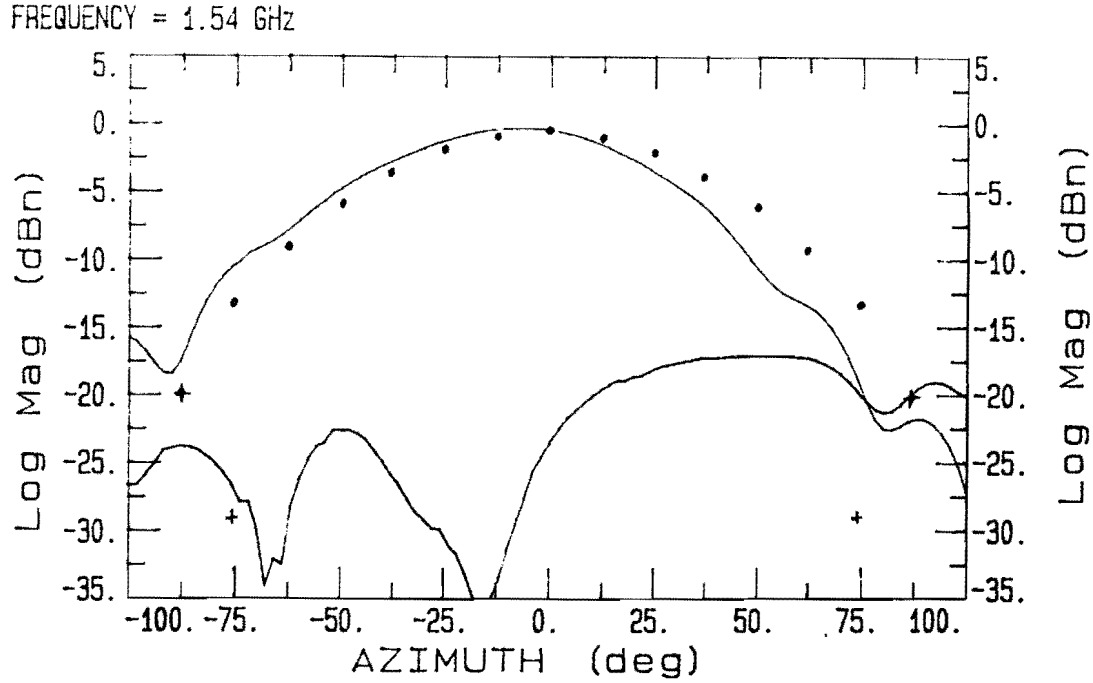

Fig. H.22 : Co- and cross-polarization patterns of the circularly polarized circular ring stacked microstrip antenna in plane $\phi=0^{\circ}$
co polarization : calculated : • ; measured : -
cross polarization : calculated : + ; measured : —

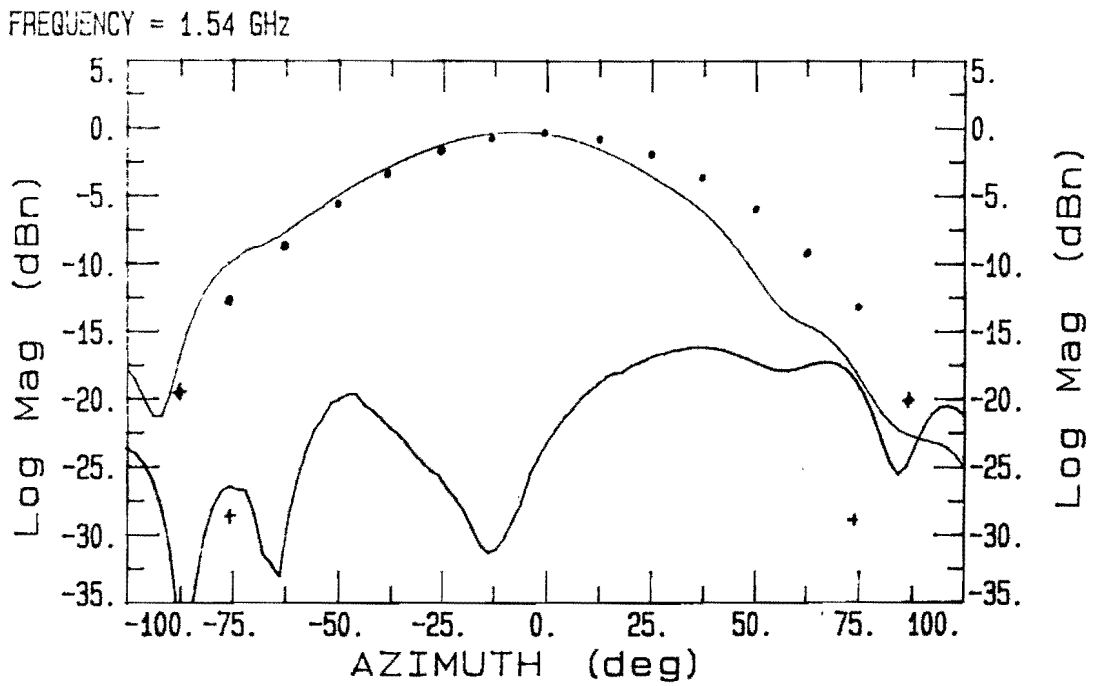

Fig. H.23 : Co- and cross-polarization patterns of the circularly polarized circular ring stacked microstrip antenna in plane $\phi=45^{\circ}$
co polarization : calculated : • ; measured : -
cross polarization : calculated : + ; measured : —

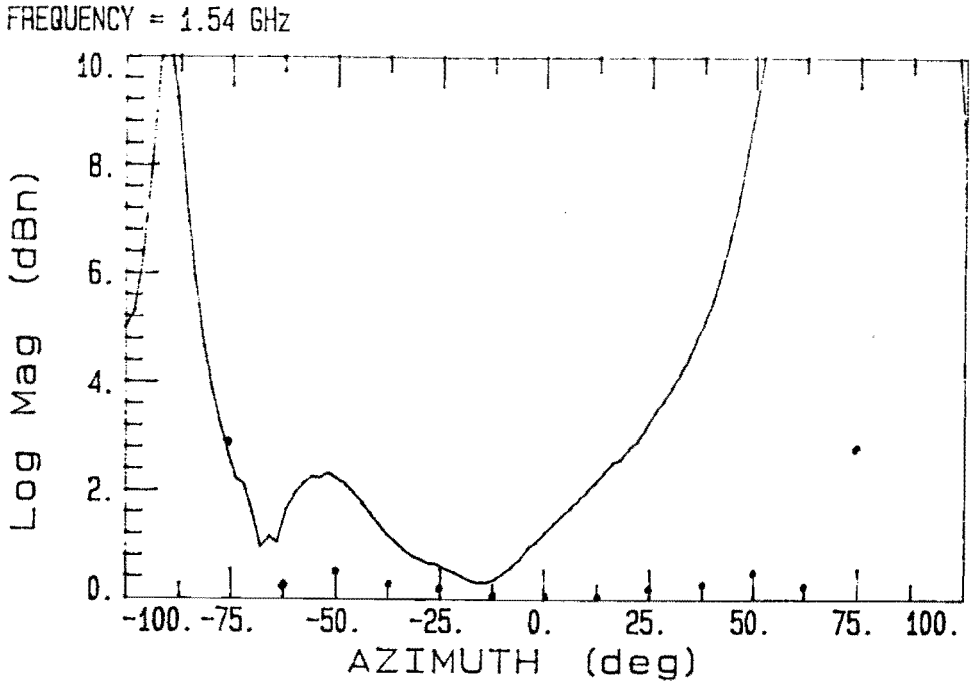

Fig. H.24 : Axial ratio pattern of the circularly polarized circular ring stacked microstrip antenna in plane $\phi=0^{\circ}$ calculated : • ; measured : -

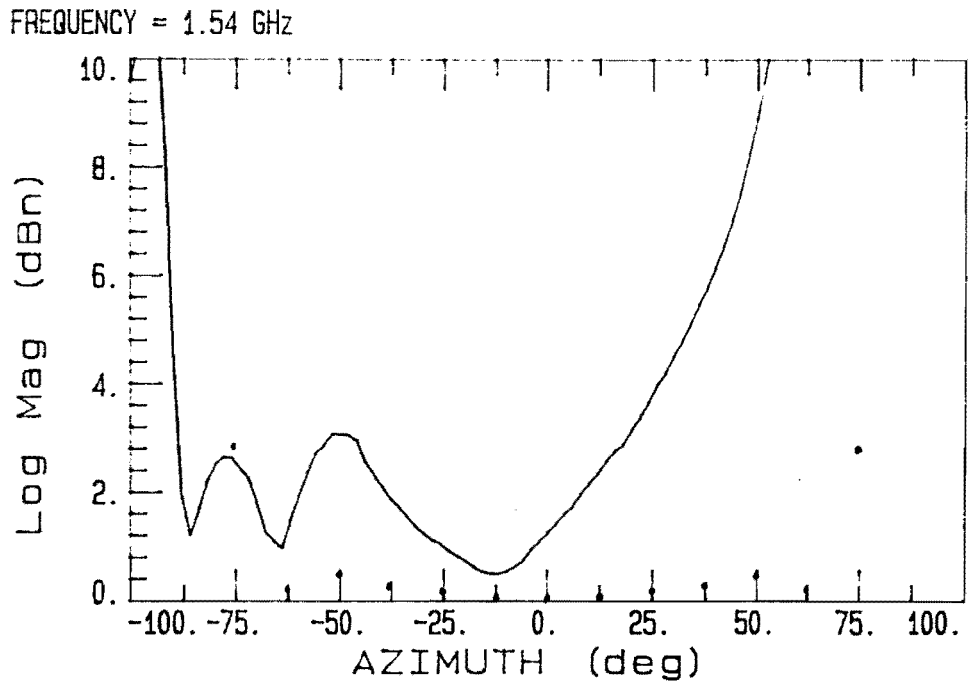

Fig. H.25 : Axial ratio pattern of the circularly polarized circular ring stacked microstrip antenna in plane $\phi=45^{\circ}$ calculated : • ; measured : -